NACA TN No. 1546

NATIONAL ADVISORY COMMITTEE FOR AERONAUTICS

TECHNICAL NOTE

No. 1546

AERODYNAMIC CHARACTERISTICS OF 24 NACA 16-SERIES AIRFOILS AT MACH NUMBERS BETWEEN 0.3 AND 0.8

By W. F. Lindsey, D. B. Stevenson, and Bernard N. Daley

Langley Aeronautical Laboratory
Langley Field, Va.

Washington
September 1948

NATIONAL ADVISORY COMMITTEE FOR AERONAUTICS

TECHNICAL NOTE NO. 1546

AERODYNAMIC CHARACTERISTICS OF 24 NACA 16-SERIES AIRFOILS AT MACH NUMBERS BETWEEN 0.3 AND 0.8

By W. F. Lindsey, D. B. Stevenson, and Bernard N. Daley

SUMMARY

An investigation has been conducted to determine the aerodynamic characteristics of a group of NACA 16-series airfoils related in camber and thickness over a Mach number range from 0.3 to approximately 0.8. The results obtained from the present investigation were combined with the data of 12 NACA 16-series airfoils obtained under the same conditions and previously reported in NACA Rep. No. 763. All the currently available force-test data for NACA 16-series airfoils obtained under the same test conditions in the Langley 24-inch high-speed tunnel are presented.

INTRODUCTION

The NACA 16-series airfoils were derived (reference 1) for use at high speeds, particularly for propeller applications. The variations in design camber and thickness ratio, covered in reference 1, were not of sufficient scope to meet all the requirements of propeller design. A test program was formulated, therefore, whereby the aerodynamic characteristics would be obtained for some of the airfoils of reference 1 over an extended angular range, as well as for 12 additional airfoils of the same series. The results of this investigation combined with the data of reference 1 are presented herein uncorrected for tunnel-wall constriction effects. The magnitude of the constriction effect on Mach number at supercritical speeds is approximately 2 percent of the uncorrected value and does not affect the validity of the conclusions.

SYMBOLS

α	angle of attack, degrees
c_l	section lift coefficient
c_{l_i}	design section lift coefficient (incompressible potential flow)

c_{l_o}	section lift coefficient at M = 0 (experimental values were obtained by extrapolating from M = 0.3 to M = 0 by Glauert's method)
c_d	section drag coefficient
$c_{m_{c/4}}$	section pitching-moment coefficient about quarter-chord axis
l/d	lift-drag ratio
M	stream Mach number
M_{cr}	critical Mach number; Mach number at which speed of sound is attained locally as on airfoil
$P_{o_{max}}$	maximum incompressible pressure coefficient
t/c	thickness-chord ratio, percent
x	airfoil station, fractions of chord
y	airfoil ordinate, fractions of chord measured normal to camber line

APPARATUS AND TESTS

Force measurements of lift, drag, and pitching moment were made in the Langley 24-inch high-speed tunnel (described in reference 2) on a series of airfoils having NACA 16-series profiles. The thickness-chord ratios of the airfoils tested ranged from 6 to 30 percent and the design lift coefficients ranged from 0 to 1.0. The specific airfoils for which force measurements were made in this investigation are given in table I and are differentiated from those airfoils reported in reference 1.

The models were made of duralumin and had a chord of 5 inches. Each model spanned the 24-inch test section and passed through holes cut in flexible brass end plates that preserved the contour of the tunnel walls. The holes were the same shape as, but slightly larger than, the model. The ends of the model were secured in a balance of the type described in reference 3.

The lift, drag, and pitching-moment coefficients were measured at angles of attack corresponding at low Mach numbers to a lift-coefficient range from 0 to approximately 1.0. These data were obtained for a Mach

number range from 0.3 to approximately 0.8. The corresponding Reynolds number range extended approximately from 0.85×10^6 to 2×10^6. Drag coefficients for several of the airfoils were obtained by the wake-survey method. The wake-survey measurements were generally limited to an angle of attack of 0° or the design angle.

Critical Mach numbers at low angles of attack were estimated by means of small total-pressure tubes mounted on the upper surface of the airfoils. The tubes were generally located at the 75-percent-chord station and 2 to 3 percent chord above the airfoil surface. The Mach number at which the measured total pressure decreased approximately 0.02 percent was taken as an estimate of the critical Mach number.

NACA 16-SERIES AIRFOILS

The NACA 16-series airfoils are designated by a five-digit number (except for the case in which the design lift coefficient is equal to or more than 1.0). The first digit represents the series classification. The second digit indicates at design conditions the distance in tenths of chord from the leading edge to the position of minimum pressure. The third digit, first digit following the dash, indicates the amount of camber expressed in terms of design lift coefficient in tenths. The last two digits together express the thickness in percent chord.

The thickness distribution of the NACA 16-series airfoils was developed (reference 1) to produce a shape having very low induced velocities and thus having high critical Mach numbers. The ordinates for the basic or symmetrical profile of the NACA 16-series airfoils can be obtained from the following equations:

$$\pm y_1 = 0.01\frac{t}{c}\left(0.989665x_1^{1/2} - 0.239250x_1 - 0.041000x_1^{2} - 0.559400x_1^{3}\right)$$

and

$$\pm y_2 = 0.01\frac{t}{c}\left[0.010000 + 2.325000\left(1 - x_2\right) - 3.420000\left(1 - x_2\right)^2 + 1.460000\left(1 - x_2\right)^3\right]$$

where y is the ordinate in fractions of the chord measured normal to the camber line and x is the station in fractions of the chord.

Subscripts 1 and 2 pertain to the region ahead of and behind the maximum thickness location, respectively (for example, $x_1 \leqq 0.5$ and $x_2 \geqq 0.5$).

The leading-edge radius expressed in percentage of the chord is

$$\text{L.E. radius} = 0.004897^2\left(\frac{t}{c}\right)^2$$

The ordinates for a 9-percent-thick airfoil are presented in table II.

The camber line for the NACA 16-series airfoils was derived (reference 1) to have essentially a uniform chordwise loading. This camber line, designated the $a = 1$ mean line in reference 4, can be expressed in equation form as

$$y_c = -0.079577c_{l_i}\left[x \log_e x + (1 - x)\log_e(1 - x)\right]$$

$$\frac{dy_c}{dx} = -0.079577c_{l_i}\left[\log_e x - \log_e(1 - x)\right]$$

where y_c is the mean-line ordinate in fractions of chord and x is the station in fractions of the chord.

The ordinates and slopes of the camber line for NACA 16-series airfoils are presented in table II. It may be noted that the slope of the leading-edge radius as given in table II differs from that given in the corresponding table of reference 1. Since the slope of the leading-edge radius is determined by the slope of the camber line, the value specified for the leading-edge radius depends upon the chordwise station x at which the camber-line slope is obtained. The slope specified in reference 1 corresponded to the 0-percent-chord station and fairing difficulties were later encountered at the leading edge of highly cambered thick airfoils. The slope specified in table II corresponds to the 0.5-percent-chord station. The leading-edge radius must be as specified but the slope of the leading-edge radius does not appear to be rigidly fixed, probably as a result of the approximations made in determining the extremities of the camber line. (See reference 1.)

PRECISION

The errors to which the data were subject can be classified as accidental and systematic. The accidental errors arose from inaccuracies in model installation, in calibrations of air stream and balance, and in the reduction of the test records. The accidental errors evaluated from an inspection of the test data are as follows:

c_l	± 0.005
c_d	± 0.0005
$c_{m_{c/4}}$	± 0.002
α, deg	± 0.1

The largest systematic error to which the data were subject arose from leakage of air through the (3/64 inch) gaps at the junctures of airfoils and tunnel wall. The corrections were first determined by tests on an NACA 0012 airfoil with various end gaps; these corrections were applied to the data of reference 1. Tests to determine the correction were extended for the present investigation to include not only airfoils of various thickness-chord ratios but also a large angle-of-attack range. The tests of the NACA 16-series airfoils cambered for a design lift coefficient of 0.3 and having thickness-chord ratios from 6 to 21 percent were made. The angle-of-attack range corresponded to the range presented herein for those airfoils.

Investigation of the end-leakage effects showed that the correction to drag coefficient depended not only on Mach number and lift coefficient but also on thickness-chord ratio. The investigation further indicated that camber might have an effect on the angle-of-attack correction since the tests on the cambered airfoils showed only a shift in angle of zero lift (see also fig. 10 of reference 2); whereas the tests on a symmetrical airfoil (reference 1) indicated that the correction was a function of lift coefficient. The maximum difference between the two corrections did not exceed 0.3°.

The corrections for end leakage as determined by the tests on NACA 16-series airfoils were considered to be more reliable than those used in reference 1 because of the greater range of the test. The corrections were applied not only to the 12 additional airfoils but also to the 12 airfoils reported in reference 1. Differences in the aerodynamic characteristics for airfoils in this paper and in reference 1 are primarily a result of the change in the end-leakage corrections.

A comparison of drag coefficients obtained from wake surveys and from force-test data corrected for end leakage is shown in figure 1. At low design lift coefficients the differences are approximately of

the same magnitude as the accidental errors. At high design lift coefficients the differences increase and thereby indicate that the applied leakage correction might be too small in that lift-coefficient range. The wake-survey drag coefficients, however, do not increase as rapidly with design lift coefficient as would be expected, especially at high values of c_{l_i}.

The remaining systematic errors associated with these data arise from wind-tunnel wall interference. The correction for this effect as determined by the method of reference 5 may be subject to error at supercritical Mach numbers. The method, however, should give an estimate of the magnitude of the errors involved. An estimate of the error can be obtained from figure 2 which shows a comparison between basic aerodynamic data for the NACA 16-309 airfoil corrected and uncorrected for tunnel-wall effects. An examination of figure 2 indicates that the correction is generally small and, therefore, has not been applied to the results presented herein. A further examination indicates that at the highest Mach numbers the correction appears to have the greatest effect on Mach number. Thus, in the application of the data in a design problem, the approximately 2-percent correction for Mach number could have a large effect.

The choking phenomenon is an additional effect of tunnel walls that enters into the problem of wind-tunnel testing at high subsonic Mach numbers. At the choking Mach numbers sonic velocities extend from model to tunnel wall, and the static pressure is lower behind the model than in the undisturbed region upstream of the model; thus, large gradients in static pressure can be produced. The resulting flow past the model is unlike any free-air condition, and data obtained at and near choking Mach numbers are, therefore, of questionable value. Data near the choking Mach number are, consequently, omitted from this paper with the exception of a few conditions shown in figure 3. The arrows at the zero-lift axes (fig. 3) show the one-dimensional theoretical choking Mach number at design conditions for each of the airfoils and indicate how closely these basic data approach the choking speed. The data at the higher angles of attack generally do not approach their respective choking Mach numbers as closely as do the data near design conditions.

RESULTS

The variation in aerodynamic characteristics with Mach numbers at constant angles of attack for each of the NACA 16-series airfoils tested constitutes the basic data for the investigation and is presented in figure 3.

The data of figure 3 were cross-plotted to show the effects of variation of thickness-chord ratio and camber or design lift coefficient on the aerodynamic characteristics. The cross-plotted results are shown in figures 4 to 9.

The effect of camber on the variation of lift-drag ratio with lift coefficient for airfoils of 6-percent, 9-percent, 12-percent, and 15-percent thickness is presented in figures 10, 11, 12, and 13, respectively. The effect of thickness on lift-drag ratio for cambered airfoil having a design lift coefficient of 0.3 is presented in figure 14.

The theoretically derived maximum negative pressure coefficients (reference 4) for NACA 16-series airfoils are presented in figure 15. Figure 16 permits the maximum negative pressure coefficients in an incompressible or low-speed flow to be transcribed to critical Mach numbers in accordance with von Kármán-Tsien's relation (reference 6). A comparison between the theoretically derived and the experimentally determined critical Mach numbers is given in figure 17. The measured critical Mach numbers at several stations on an untwisted propeller tip are compared in figure 18 with the values estimated from two-dimensional flow.

A comparison is made in figure 19 between the critical Mach number and the Mach number for lift break and maximum lift-drag ratio. The effects of thickness and camber on the Mach numbers for lift break and drag rise are presented in figure 20.

A tabulation of the airfoils investigated and the figure numbers containing the pertinent test data are given in table I.

DISCUSSION

Subcritical

Lift.- The NACA 16-series airfoils at the design angle of attack of 0° and at low Mach numbers do not produce experimental lift coefficients of the same value as the design lift coefficients. The difference can be attributed primarily to viscosity in the real flow and its modifying effect on the theoretically predicted influence of the camber line, especially over the rear of the model.

At low Mach numbers and at an angle of attack of 0°, figures 4 to 9 showed that the experimental lift coefficients decreased from 85 percent of the design lift coefficient for airfoils of 6-percent thickness to 38 percent of the design lift coefficient for airfoils of 21-percent thickness. The variation with thickness for airfoils between 6-percent and 21-percent thickness can be approximated by

the relation $\frac{c_l}{c_{l_i}} = 100 - \left(\frac{t}{c}\right)^{1.35}$ (all values in percent). Cambered airfoils $\left(c_{l_i} = 0.1 \text{ and } 0.5\right)$ having a thickness of 30 percent chord (figs. 7 and 9) produced negative lift coefficients at an angle of attack of 0°. These negative lift coefficients were about −20 percent of the design lift coefficient.

The negative lift coefficients of the 30-percent-thick airfoils were produced as a result of either separation on the upper surface of the airfoil or a greater chordwise extent of separation on the upper surface than on the lower and less curved surface. The separation effects were illustrated by an unpublished investigation of the flow past thick airfoils.

The lift characteristics of many of the airfoils (figs. 4 to 9) at angles of attack between 2° and 8° exhibited a break or region of reduced slopes over an angular range of 2° to 3°. At angles of attack beyond this region of reduced slope, the slopes increased but generally did not reach the values produced near an angle of attack of 0°. Figures 4 to 9 illustrated that the break became more pronounced as either the design lift coefficient or the thickness-chord ratio was increased. The thickness-chord ratio, however, had a greater effect than camber. (Compare figs. 4 to 6 with figs. 7 to 9.)

The forward movement of the center of pressure and the rapid increase in drag, which occurred simultaneously with the break in the lift curve, indicated that transition moved rapidly forward or that laminar separation occurred. Since compressibility has the same effect on adverse pressure gradients as increases in thickness, this assumption is further substantiated by the effect of compressibility on the breaks in the curves inasmuch as increases in the Mach number of the flow generally tended to emphasize the abruptness of the change in aerodynamic characteristics.

Figure 4 shows at a Mach number of 0.30 that the lift-curve slope near design angle of attack generally increased with design lift coefficient for 9-percent-thick airfoils. For thicker airfoils, the change in lift-curve slope with design lift coefficient became very small. Increasing the thickness-chord ratio of an airfoil of given design lift coefficient, however, resulted in a decrease in lift-curve slope.

Pitching-moment coefficients.- Thin-airfoil theory (summarized in reference 4) has shown that the effect of increasing the camber of airfoils having approximately uniform chord loading, such as the NACA 16-series, is to produce a large increase in the negative pitching-moment coefficient. The theory has also shown that the effect of angle

of attack is independent of camber and, therefore, increasing the design lift coefficient would have no effect on $\frac{\partial c_{m_{c/4}}}{\partial c_l}$. The data in figures 4 to 6 are in agreement with the thin-airfoil theory. Increases in thickness-chord ratio (especially above 12 percent), however, produced a forward movement of the center of pressure and a positive increase in $\frac{\partial c_{m_{c/4}}}{\partial c_l}$ (figs. 7 to 9). This effect of thickness is probably a result of the adverse effect of viscosity on the loading near the trailing edge of the thicker airfoils. The effect of compressibility was to produce a large rearward movement of the center of pressure without noticeably affecting $\frac{\partial c_{m_{c/4}}}{\partial c_l}$.

Drag.- The drag data presented in the form of polars indicate that the change in minimum drag coefficient with design lift coefficient is small at low Mach numbers for thickness-chord ratios of 9 percent (fig. 4). This change increases with thickness (figs. 5 and 6), but at a sufficiently slow rate that for airfoils of 15-percent thickness at low Mach numbers the maximum lift-drag ratio increases with design lift. (See also figs. 10 to 13.) Increases in Mach number above a value of approximately 0.60 caused the maximum lift-drag ratio to occur at progressively lower lift coefficients and at lower design lift coefficients (figs. 10 to 13). This effect, illustrated by figures 10(c) to 10(f) and figures 11(c) to 11(f), is a result of an increase in induced velocities associated with an increase in design lift and is the normally expected effect of compressibility.

The maximum lift-drag ratio for a given airfoil at low Mach numbers (figs. 10 to 13) generally occurred at a lift coefficient approximately 0.1 to 0.2 greater than the design value. Pressure-distribution data (unpublished) has shown at low Mach numbers that the shape of the pressure distribution for an NACA 16-212 airfoil at an angle of attack of 2° corresponded more closely to the theoretical or design distribution than did the distribution obtained at 0°. Consequently, in that speed range the airfoil could be expected to be more efficient at an angle of attack slightly greater than the design angle of attack of 0°.

The general decrease in the lift-drag ratio with increases in thickness-chord ratio shown in figure 14 results from the observed and expected increase in drag coefficient and some decrease in lift coefficient. As the Mach number increased, the effect of thickness on lift-drag ratio was magnified in accordance with the usual effects of compressibility on the aerodynamic characteristics.

Critical Mach Number

The critical Mach number is that value of the Mach number of the undisturbed stream at which sonic velocities are attained locally within the flow field. Experimental investigations in two-dimensional flows have shown that the adverse effects of compressibility, such as the drop in lift coefficient, rapid rise in drag coefficient, and abrupt changes in moment coefficient, do not occur until the critical Mach number has been reached or exceeded.

The Mach number at which abrupt changes in aerodynamic characteristics occur in a two-dimensional flow cannot at present be reliably predicted. There is, however, the generalization that the Mach number for the force break is equal to or greater than the critical Mach number. Thus, as a first step in the high-speed application of airfoils, the critical Mach numbers should be known.

The theoretical critical Mach number of a body can be estimated from the maximum theoretical negative pressure coefficient (fig. 15 and reference 4) by using some method of estimating the effect of compressibility on the pressure coefficient (fig. 16). The maximum negative pressure coefficient may also be obtained from the following empirical equation (within ±2 percent for design lift coefficients from 0 to 1 and thickness-chord ratios from 6 to 21 percent chord):

$$-P_{o_{max}} = 0.01\frac{t}{c}\left(2.33 + 0.01\frac{t}{c}\right) + c_{l_1}\left(0.5 + 0.005\frac{t}{c} + 0.07c_{l_1}\right)$$

In order to evaluate the applicability of the theoretical critical Mach numbers, the theoretical values obtained from figures 15 and 16 were compared in figure 17(a) with the critical Mach number estimated from total-pressure measurements near the surface of the airfoils. A further comparison was made in figure 17(b) between theoretical critical Mach numbers (obtained from the methods of reference 4 and fig. 16) and the critical Mach numbers determined from pressure-distribution measurements. The experimental lift coefficients were extrapolated from $M = 0.3$ to $M = 0$ by Glauert's relation given in reference 7. The comparisons presented illustrated that for NACA 16-series airfoils the critical Mach numbers obtained from the several specified sources were in reasonably good agreement.

The effects of thickness-chord ratio (fig. 17(c)) and design lift coefficient (fig. 17(d)) on the variations in critical Mach number with the low-speed (incompressible) lift coefficient were similar to and independent of each other. Increases in either variable increased the angle-of-attack or lift-coefficient range of high critical Mach numbers but were accompanied by a reduction in the maximum value of the critical Mach number.

Investigations in three-dimensional flows have shown a delay in the onset of the adverse effects from those predicted by two-dimensional tests or by section critical Mach numbers. The results of one three-dimensional investigation are presented in figure 18. Pressure-distribution measurements were made in the Langley 24-inch high-speed tunnel on an untwisted propeller blade having NACA 16-series airfoil sections. The untwisted propeller blade could also be considered to represent a semispan of an untwisted tapered wing having an aspect ratio of 6.7. The results, summarized in figure 18 for an angle of attack of 0°, showed that the critical Mach number for the outer stations was delayed approximately 0.05 beyond the value estimated from two-dimensional data. A delay of approximately 0.04 was obtained as far inboard as the 50-percent-semispan station. A more extensive investigation of the variation of the relieving effects with aspect ratio (unpublished) is in general agreement with this result.

Supercritical

Airplane high speeds are now in a range for which propellers would be forced to operate at supercritical speeds. The critical Mach number of an airfoil section is not an adequate index of section performance at supercritical speeds, and since no usable criterions are yet available to design optimum sections for supercritical operation, the supercritical-speed performance of available airfoil sections must be investigated experimentally. The data presented in figure 3 for airfoils of various thickness-chord ratios and cambers offer a good opportunity for studying the supercritical characteristics of NACA 16-series airfoils. The adverse effects of compressibility, which occur on airfoil characteristics at constant angles of attack as the Mach number is increased above the critical, are evidenced by a steep increase in drag, sudden decrease in lift, and abrupt change in pitching moment (fig. 3). These conditions have previously been referred to as shock stalling or compressibility stalling and more recently have been called force breaks. For this discussion, the lift break is defined as the point at which the rate of change of lift coefficient with Mach number is 0 or slightly negative, whereas the drag rise is determined as the point at which the rate of change of drag coefficient with Mach number is 0.1; both conditions are determined for constant angles of attack. The drag rise as defined is admittedly quite arbitrary because early increases in drag resulting from effects of compressibility on the boundary layer are neglected. The effect is such that in some cases, particularly at moderately high angles of attack, the total increase in drag is large before a rate of change of drag coefficient with Mach number of 0.1 is attained (for example, see fig. 3(d) at $\alpha = 7.77^{\circ}$); any other definition of the drag rise, however, would be equally arbitrary.

In order to provide a comparison between the conditions at the critical speed and at the Mach number of the lift break, figure 19

has been prepared. It can be seen that at lift coefficients near the design condition, the Mach number for lift break is only slightly greater than the critical Mach number; with increasing lift coefficient, however, the lift-break Mach number exceeded the critical Mach number by an increasing increment. The Mach numbers of lift break and drag rise for the various NACA 16-series airfoils (presented in fig. 20) decrease with increase in thickness from approximately 0.8 for thickness-chord ratios of 6 percent to 0.7 for thickness-chord ratios of 15 percent. For applications in which very high Mach numbers will be encountered, the thickness-chord ratios should be confined to the lower values (that is, 9 percent and less) to assure high force-break Mach numbers. In addition to the effect of thickness, figure 20 also shows that an increase in camber of the thinner airfoil sections generally decreases the force-break Mach numbers. A more significant effect of camber, however, is the fact that for moderate lift coefficients, the maximum force-break Mach number is obtained with an airfoil having a design camber that is less than the value corresponding to the operating lift coefficient. The trend toward decrease in the optimum camber was expected at speeds near the lift break for these airfoils, since other data (reference 8) have indicated that the aerodynamic characteristics of cambered sections are generally inferior to those of symmetrical sections at very high supercritical Mach numbers. A related inferiority of the cambered airfoils is their change in the angle of zero lift that occurs at high Mach numbers. The change is a function of the airfoil camber or design lift coefficient. As a result, the adverse changes in angle of attack required to maintain a fixed lift coefficient decreased as the design camber was reduced.

Figure 19 shows that the maximum lift-drag ratios obtainable at the lift-break conditions generally occur at section lift coefficients as much as 0.3 greater than the design lift coefficient. In order to obtain high values of lift-drag ratio at the highest possible Mach number, it therefore appears that airfoils cambered for lift coefficients less than the desired operating lift coefficient (thus having a higher lift-break Mach number) would be preferable. For the thinner airfoils in figures 10 and 11, the higher cambered airfoils $\left(c_{l_i} \approx 0.5\right)$ are shown to be advantageous at Mach numbers less than 0.7. At the highest Mach numbers presented (that is, near the lift break), however, the airfoils having only slight camber $\left(c_{l_i} \approx 0.1\right)$ are shown to have the highest efficiencies. These airfoils of slight camber are also shown to maintain the best efficiency over a large operating lift-coefficient range $\left(c_l = 0 \text{ to } 0.5\right)$ which extends to values much higher than the design lift coefficient. Figures 10 and 11 also indicate that, at higher Mach numbers than those presented, the optimum design lift coefficient may be less than 0.1.

CONCLUDING REMARKS

The results of the investigation of 24 NACA 16-series airfoils related in camber and thickness over a Mach number range from 0.3 to approximately 0.8 indicate the following conclusions, the validity of which is not affected by neglecting tunnel-wall effects:

1. For cambered NACA 16-series airfoils at low Mach numbers M and at an angle of attack of 0°, the ratio of the lift coefficient produced c_l to the design lift coefficient c_{l_i} was generally less than unity and varied with airfoil thickness-chord ratio t/c as follows (all values measured in percent): $\frac{c_l}{c_{l_i}} = 100 - \left(\frac{t}{c}\right)^{1.35}$.

2. The theoretical method of estimating the critical Mach number provided values which were in reasonably good agreement with experiment. In the lift-coefficient range for high critical Mach numbers, the Mach number for lift break was only slightly greater than the critical Mach number. With increasing lift coefficients, however, the lift-break Mach number exceeded the critical Mach number by an increasing increment.

3. The design camber resulting in best lift-drag ratio for a given lift coefficient decreased abruptly as the force-break Mach number was approached and exceeded. For example, the 6-percent-thick airfoil when cambered for a design lift coefficient of 0.1 produced the best lift-drag ratios at a Mach number of 0.80 and at all operating lift coefficients for which a comparison was possible $\left(c_l = 0 \text{ to } 0.5\right)$.

4. The adverse changes in angle of attack required to maintain a fixed lift coefficient decreased as the design camber was reduced.

Langley Aeronautical Laboratory
National Advisory Committee for Aeronautics
Langley Field, Va., December 19, 1947

REFERENCES

1. Stack, John: Tests of Airfoils Designed to Delay the Compressibility Burble. NACA Rep. No. 763, 1943.

2. Stack, John, Lindsey, W. F., and Littell, Robert E.: The Compressibility Burble and the Effect of Compressibility on Pressures and Forces Acting on an Airfoil. NACA Rep. No. 646, 1938.

3. Stack, John: The N.A.C.A. High-Speed Wind Tunnel and Tests of Six Propeller Sections. NACA Rep. No. 463, 1933.

4. Abbott, Ira H., von Doenhoff, Albert E., and Stivers, Louis S., Jr.: Summary of Airfoil Data. NACA ACR No. L5C05, 1945.

5. Allen, H. Julian, and Vincenti, Walter G.: The Wall Interference in a Two-Dimensional-Flow Wind Tunnel with Consideration of the Effect of Compressibility. NACA Rep. No. 782, 1944.

6. von Kármán, Th.: Compressibility Effects in Aerodynamics. Jour. Aero. Sci., vol. 8, no. 9, July 1941, pp. 337-356.

7. Glauert, H.: The Effect of Compressibility on the Lift of an Aerofoil. R. & M. No. 1135, British A.R.C., 1927. (Also, Proc. Roy. Soc. (London), ser. A, vol. 118, no. 779, March 1, 1928, pp. 113-119.)

8. Ferri, Antonio: Completed Tabulation in the United States of Tests of 24 Airfoils at High Mach Numbers. (Derived from Interrupted Work at Guidonia, Italy, in the 1.31- by 1.74-Foot High-Speed Tunnel.) NACA ACR No. L5E21, 1945.

TABLE I

INDEX FOR FIGURES CONTAINING TEST DATA

c_{l_1} / t/c (percent)	Figure numbers							
	0	0.1	0.2	0.3	0.4	0.5	0.7	1.0
6	[a]10 (Data from Langley rectangular high-speed tunnel	[b]3(b), 7 [a]10 [c]18(a) [d]19 (e)		[b]3(h), 8 [a]10, 14 [c]18(a), 18(c) [d]19		[b]3(n), 9 [a]10 [c]18(a) [d]19 (e)		
9	[b]3(a), 4 [a]11 [c]18(a), 18(d) [d]19 (e)	[b]3(c), 4, 7 [a]11 [c]18(a), 18(d) [d]20 (e)	[b]3(f), 4 [a]11 [c]18(a), 18(b), 18(d) [d]20 (e)	[b]3(i), 4, 8 [a]11, 14 [c]18(a), 18(c), 18(d) [d]19, 20	[b]3(m), 4 [a]11 [c]18(a)	[b]3(o), 4, 9 [a]11 [c]18(a), 18(d) [d]19, 20 (e)	[b]3(t), 4 [a]11 [c]18(a), 18(d) [d]19, 20 (e)	[b]3(w), 4 [a]11 [c]18(a) [d]19 (e)
12				[b]3(j), 5, 8 [a]12, 14 [c]18(a), 18(c) [d]19		[b]3(p), 5, 9 [a]12 [c]18(a) [d]19 (e)	[b]3(u), 5 [a]12 [c]18(a) [d]19	[b]3(x), 5 [a]12 [c]18(a) [d]19
15		[b]3(d), 6, 7 [c]18(a) [d]19	[b]3(g), 6 [a]13 [c]18(a) [d]19	[b]3(k), 6, 8 [a]13, 14 [c]18(a), 18(c) [d]19		[b]3(q), 6, 9 [a]13 [c]18(a) [d]19 (e)	[b]3(v), 6 [a]13 [c]18(a) [d]19	
21				[b]3(l), 8 [a]14 [c]18(a)		[b]3(r), 9 [c]18(a) (e)		
30		[b]3(e), 7 [c]18(a)				[b]3(s), 9 (e)		

[a]Lift-drag ratios.
[b]Aerodynamic characteristics.
[c]Critical Mach number.
[d]Force breaks.
[e]Reported in reference 1.

TABLE II

THICKNESS DISTRIBUTION AND MEAN-LINE CHARACTERISTICS FOR NACA 16-SERIES AIRFOILS

[All values in percent chord]

Station	NACA 16-009 ordinate[a]	Mean-line characteristics for $c_{l_i} = 1.0$[b]	
		Ordinate	Slope
0	0	0	0.62234
.6	.676	.295	.40665
1.25	.969	.535	.34771
2.5	1.354	.930	.29155
5	1.882	1.580	.23432
7.5	2.274	2.120	.19993
10	2.593	2.587	.17486
15	3.101	3.364	.13804
20	3.498	3.982	.11032
25	3.812	4.475	.08743
30	4.063	4.861	.06743
40	4.391	5.356	.03227
50	4.500	5.516	0
60	4.376	5.356	-.03227
70	3.952	4.861	-.06743
80	3.149	3.982	-.11032
90	1.888	2.587	-.17486
95	1.061	1.580	-.23432
100	.090	0	-.62234

L.E. radius = $0.3966\left(\frac{t}{c} \times \frac{1}{9}\right)^2$

Slope of L.E. radius through end of chord = $0.4212c_{l_i}$

[a]Values measured from and perpendicular to mean line; for other thicknesses multiply NACA 16-009 ordinates by $\left(\frac{t}{c} \times \frac{1}{9}\right)$.

[b]For other design lift coefficients multiply mean-line characteristics by desired value of c_{l_i}.

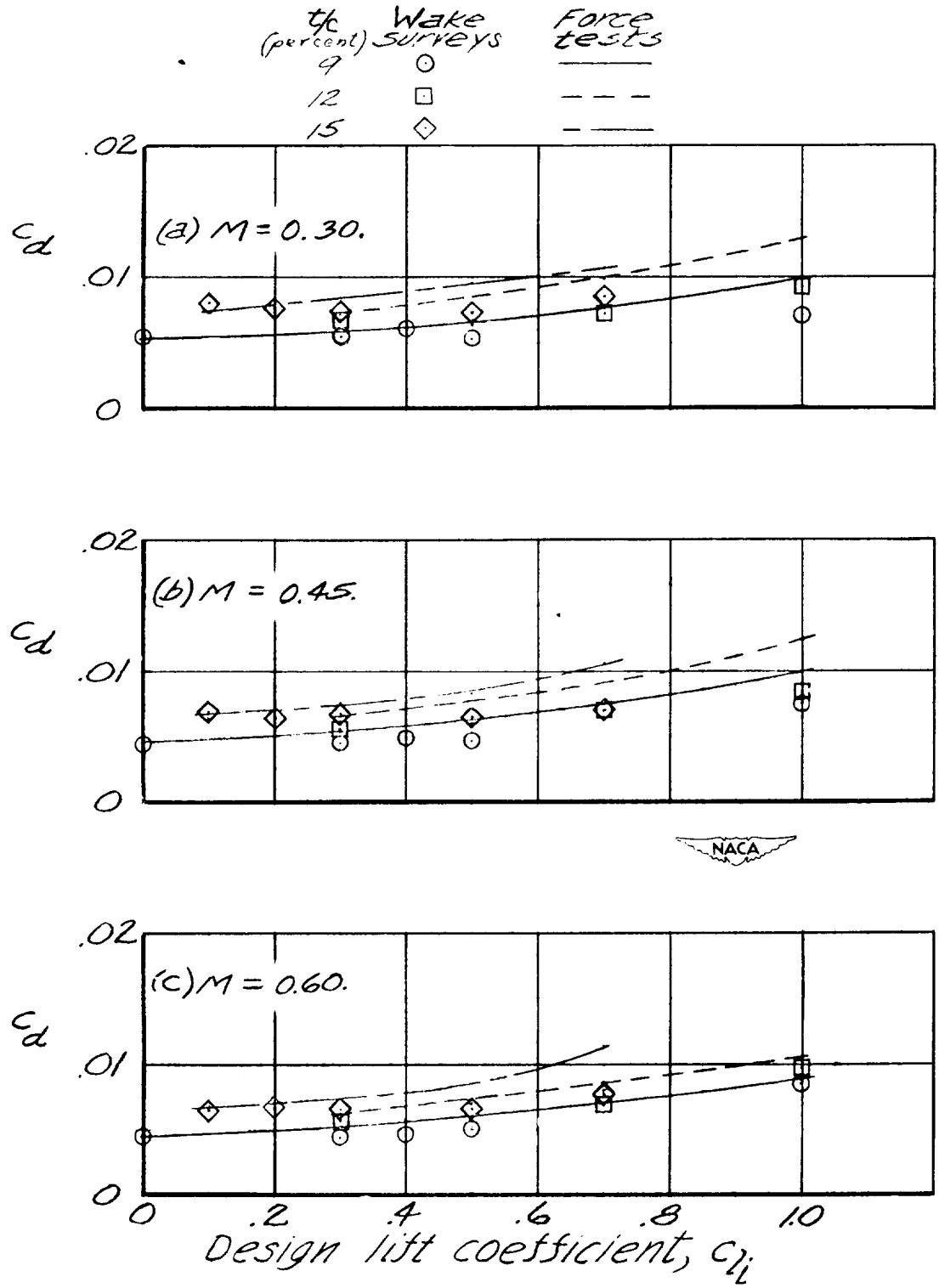

Figure 1.- Comparison of wake survey and force-test drag coefficients. $\alpha = -0.23°$.

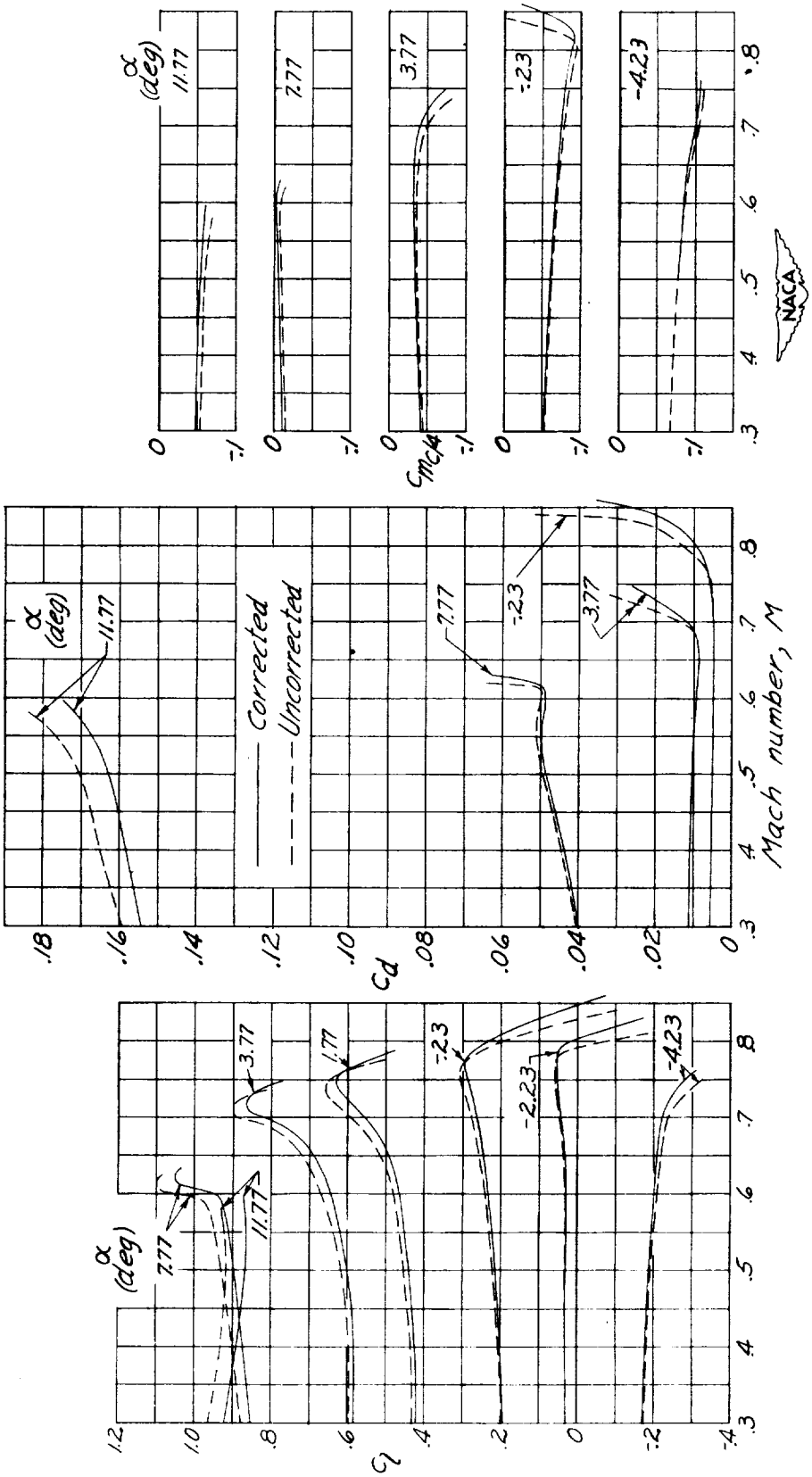

Figure 2.- A comparison of corrected and uncorrected data for the NACA 16-309 airfoil. (Corrections were determined by the method of reference 5.)

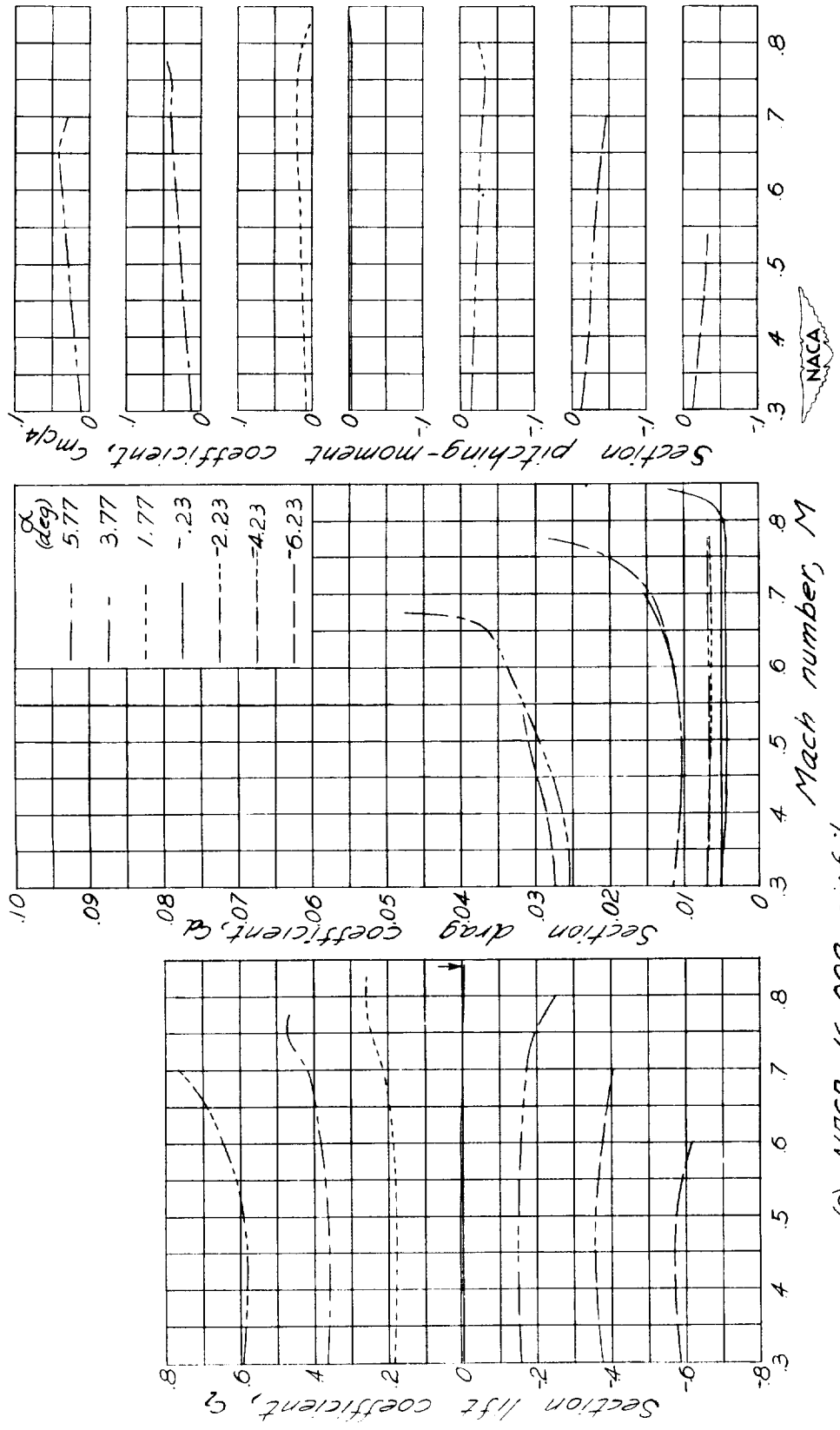

(a) NACA 16-009 airfoil.

Figure 3.- Variation of airfoil section characteristics with Mach number.

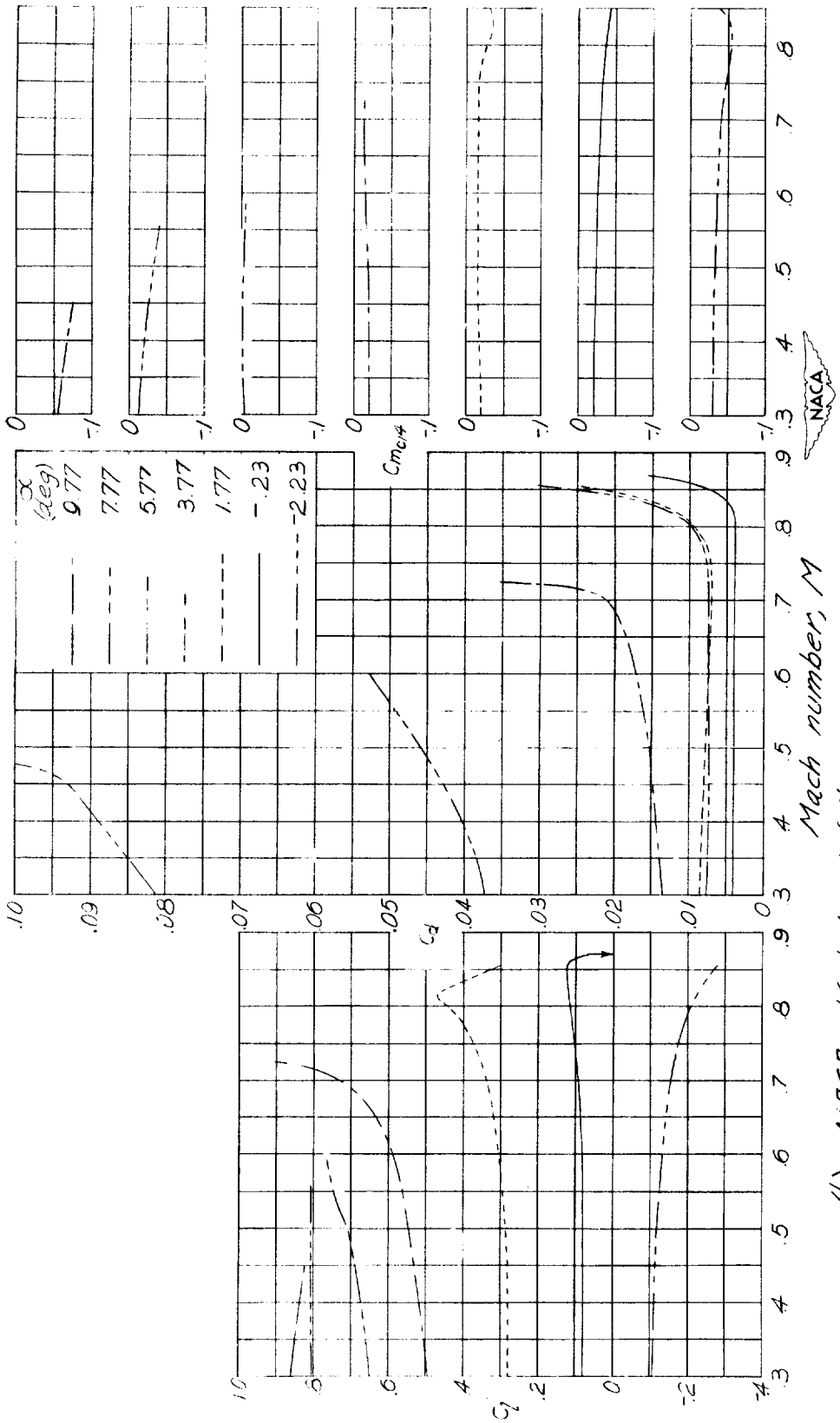

(b) NACA 16-106 airfoil.

Figure 3.- Continued.

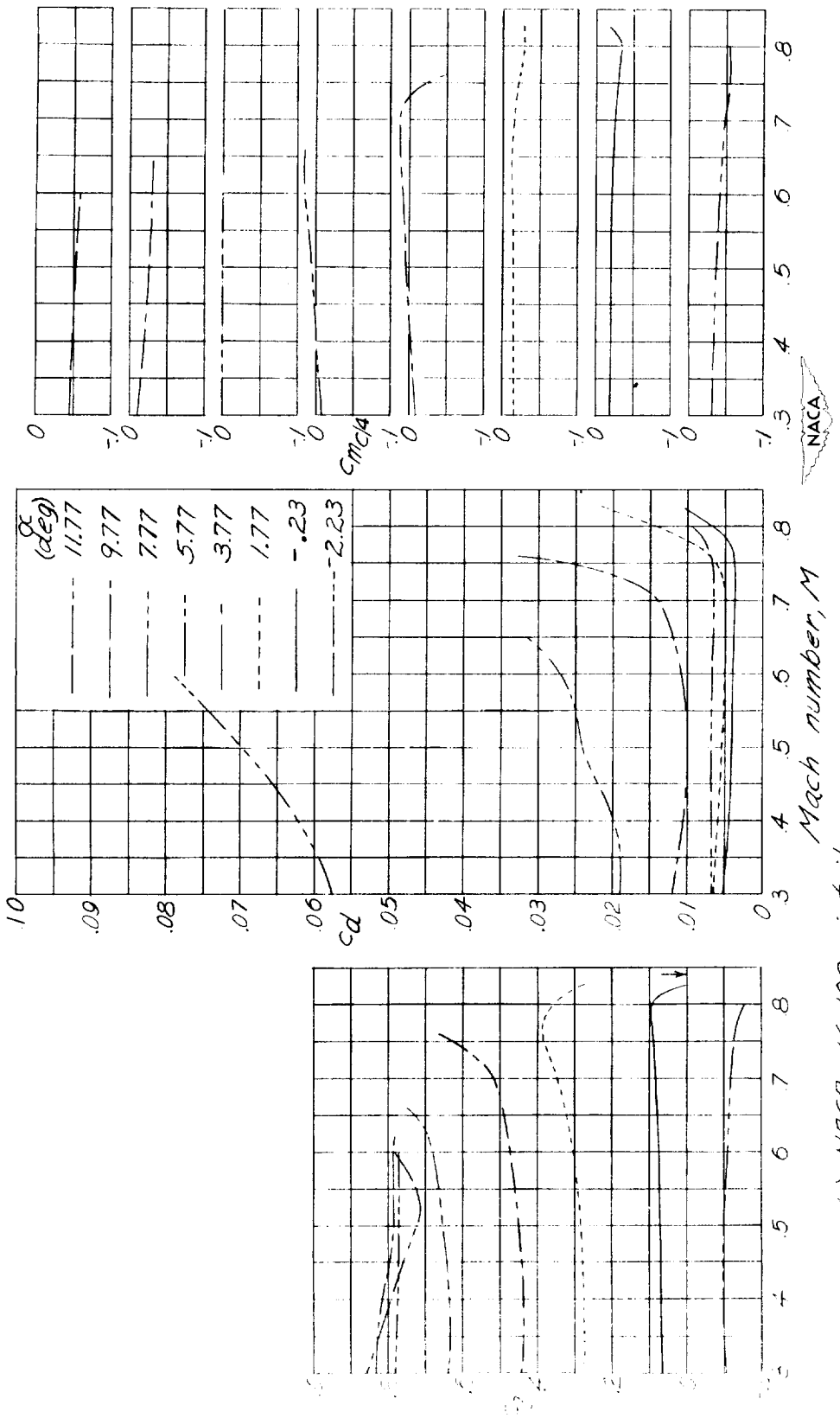

(c) NACA 16-109 airfoil.

Figure 3.- Continued.

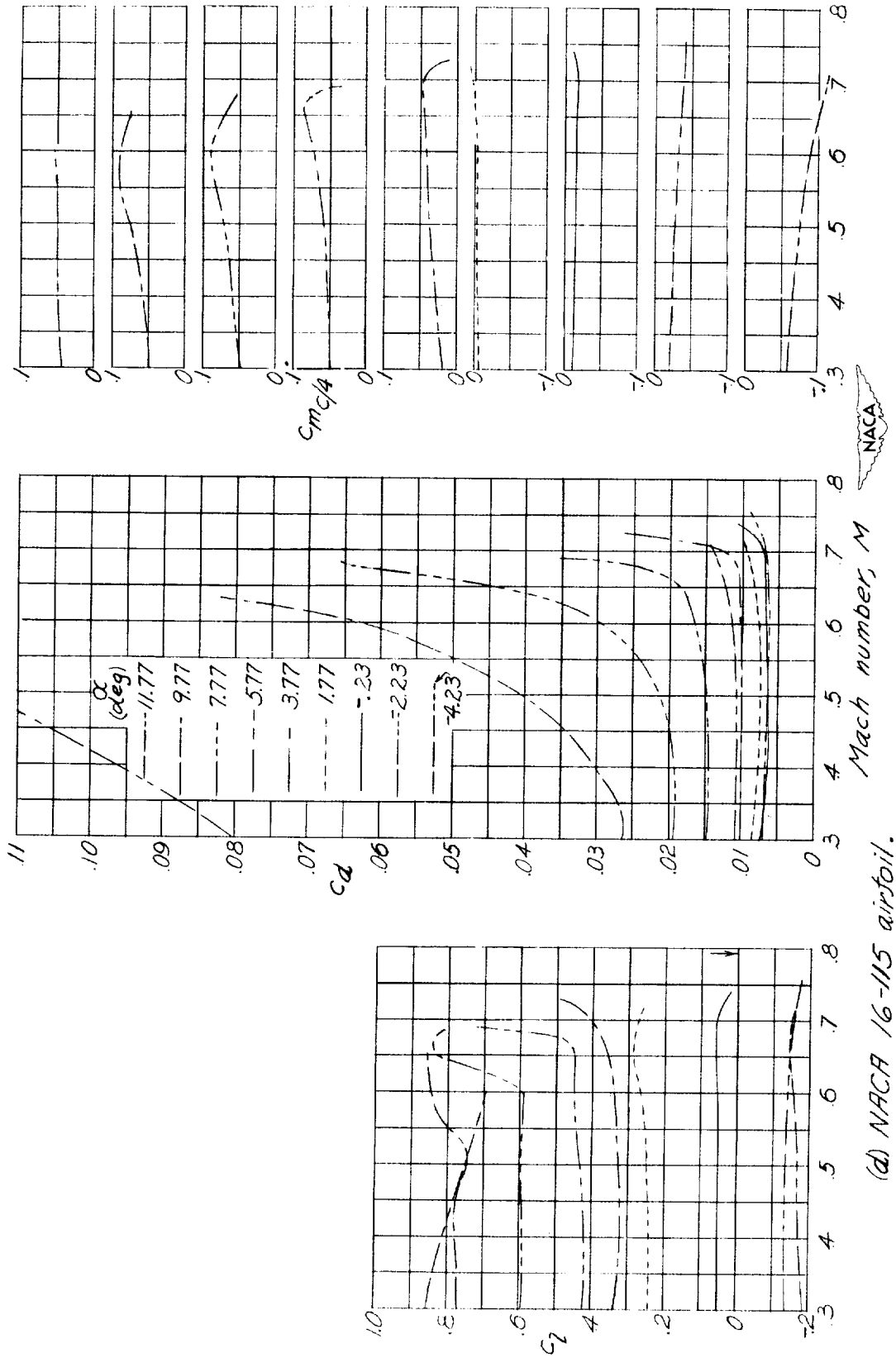

(d) NACA 16-115 airfoil.

Figure 3.- Continued.

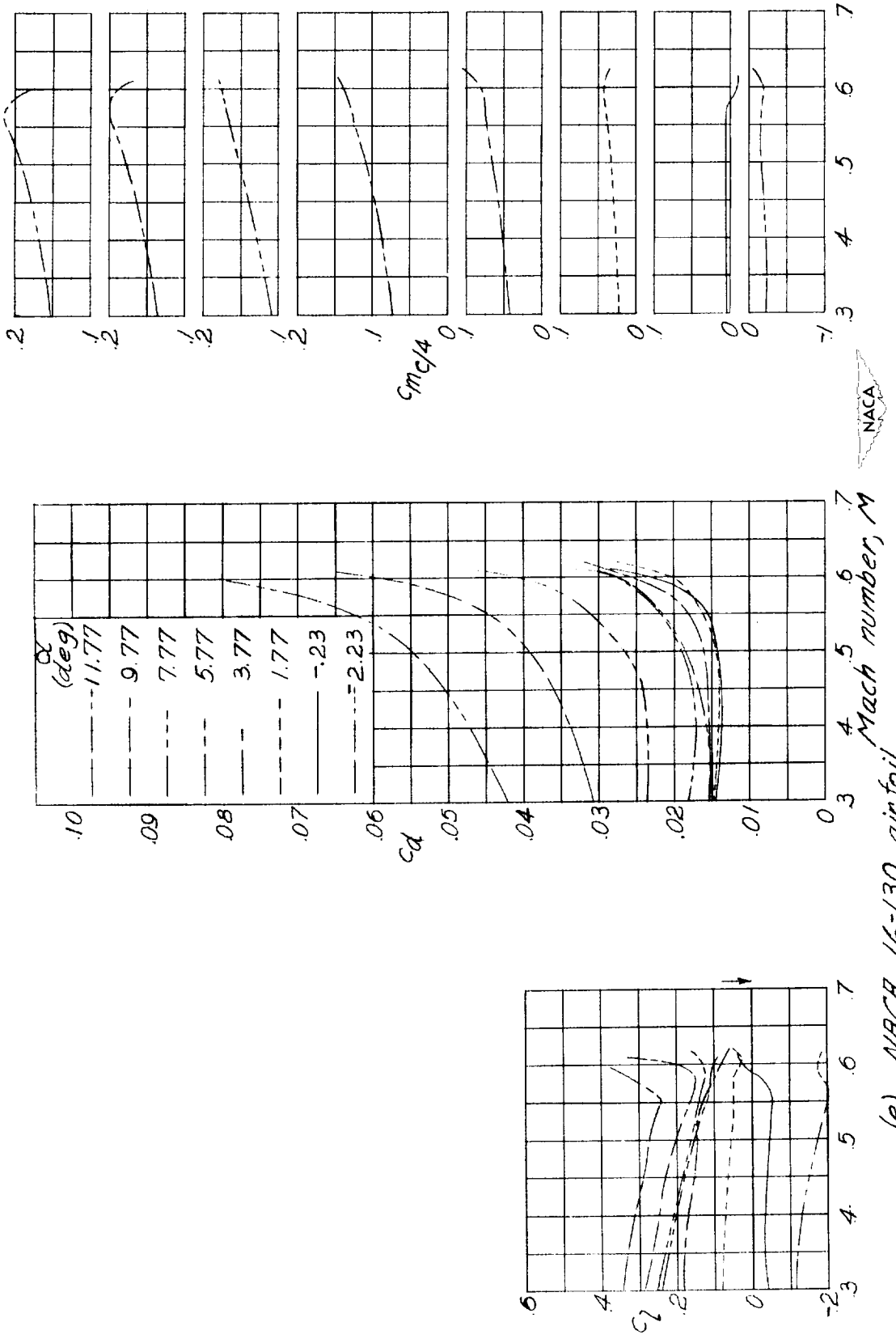

(e) NACA 16-130 airfoil.

Figure 3.- Continued.

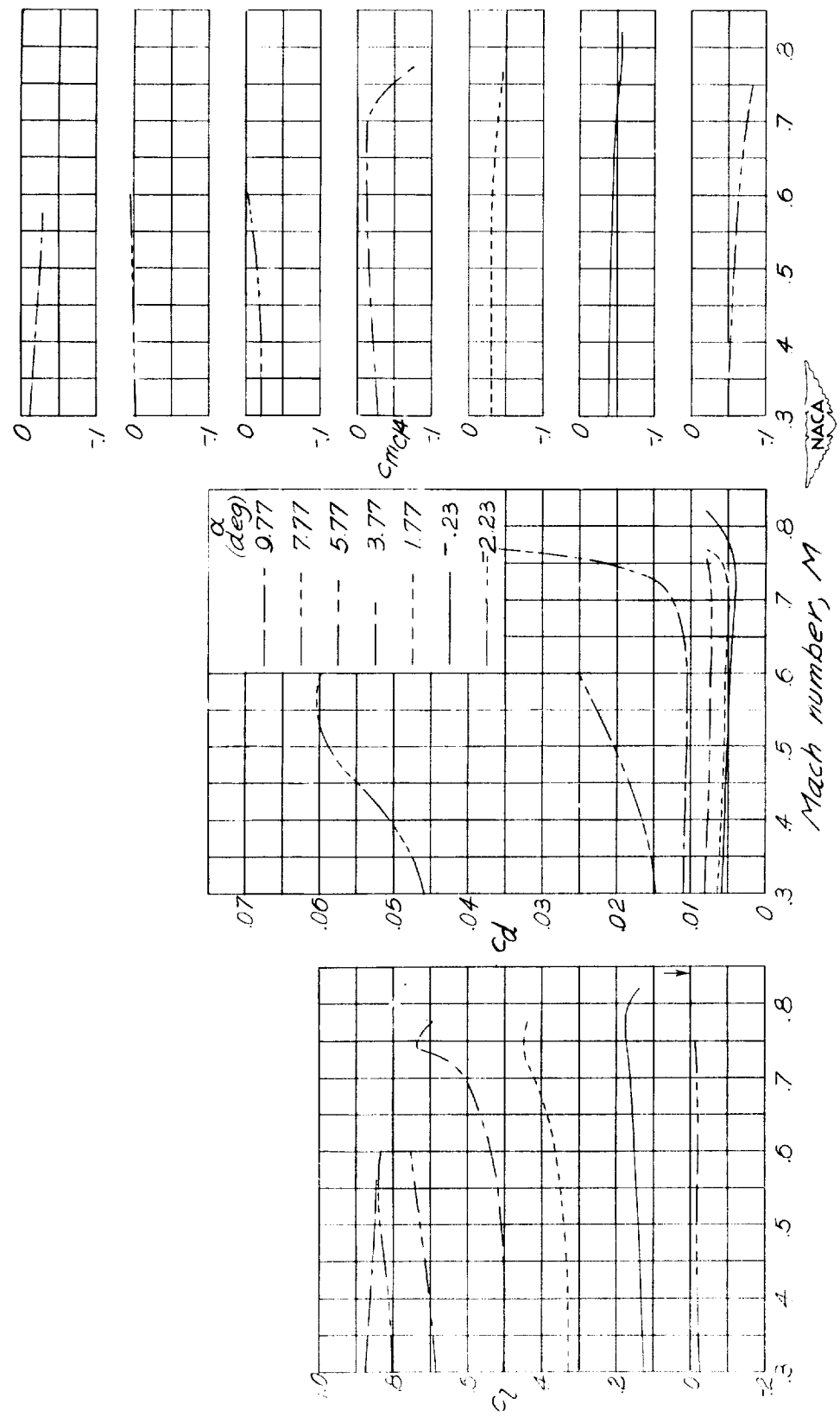

(f) NACA 16-209 airfoil.

Figure 3.- Continued.

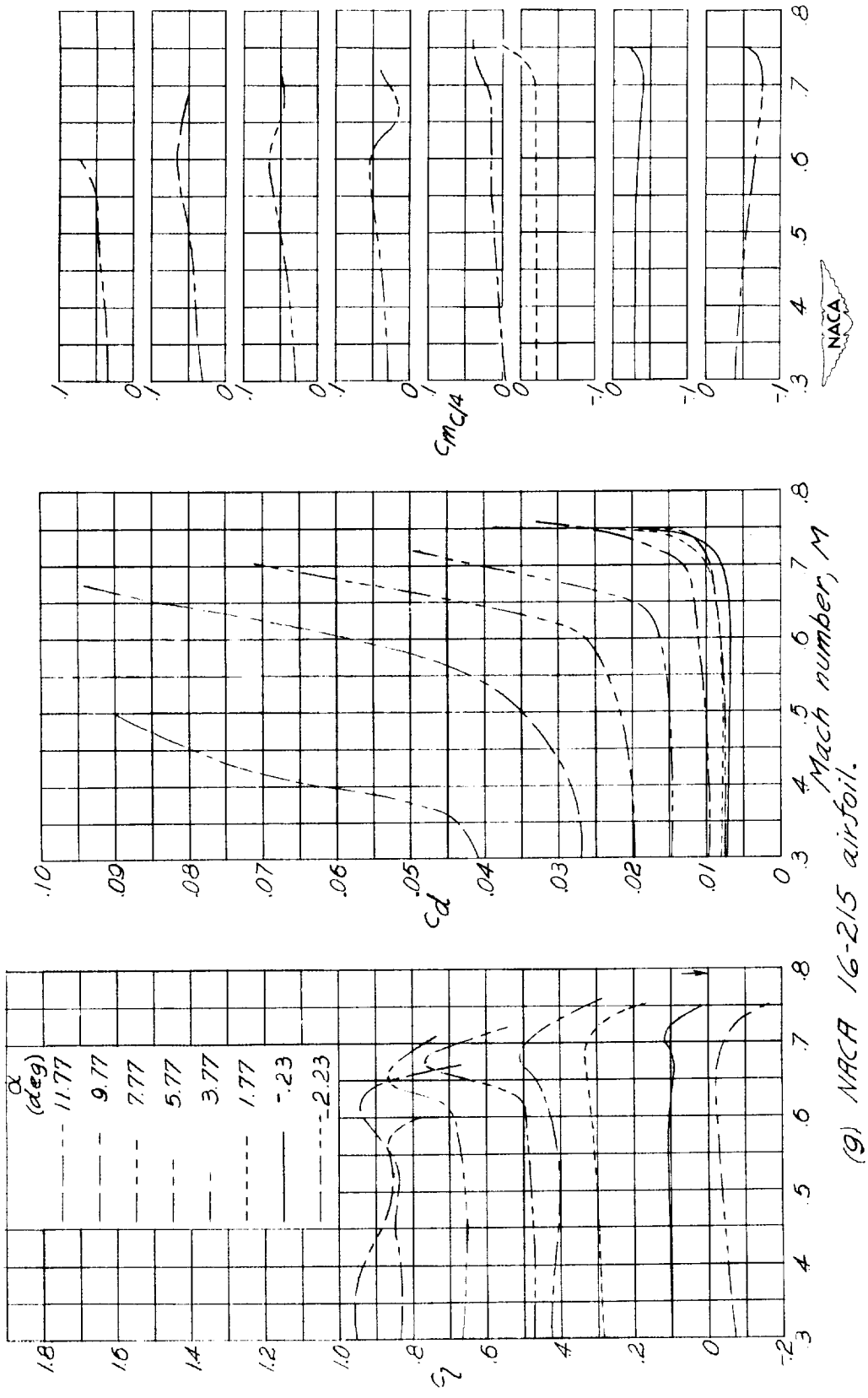

(g) NACA 16-215 airfoil.

Figure 3.- Continued.

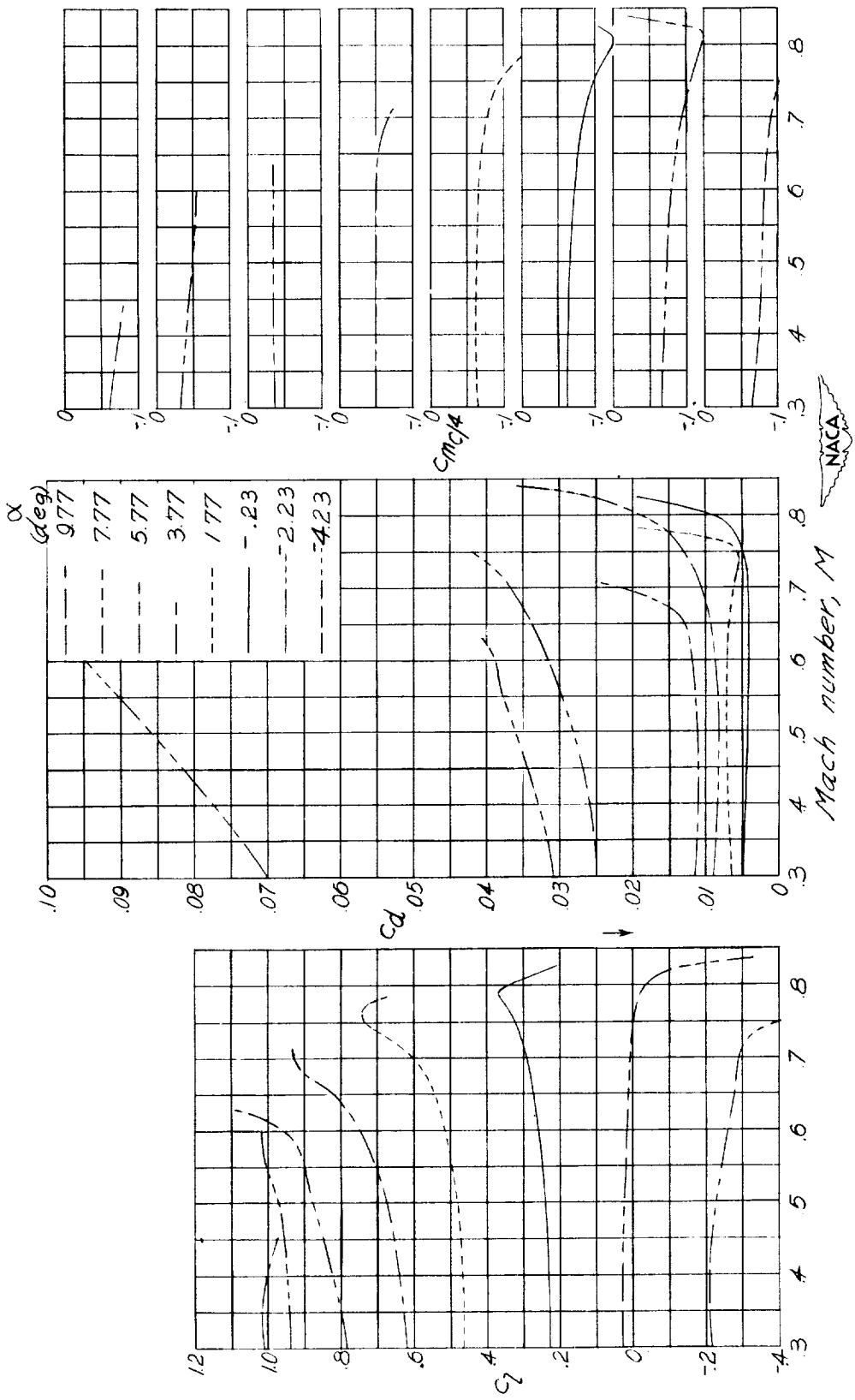

(b) NACA 16-306 airfoil.

Figure 3.- Continued.

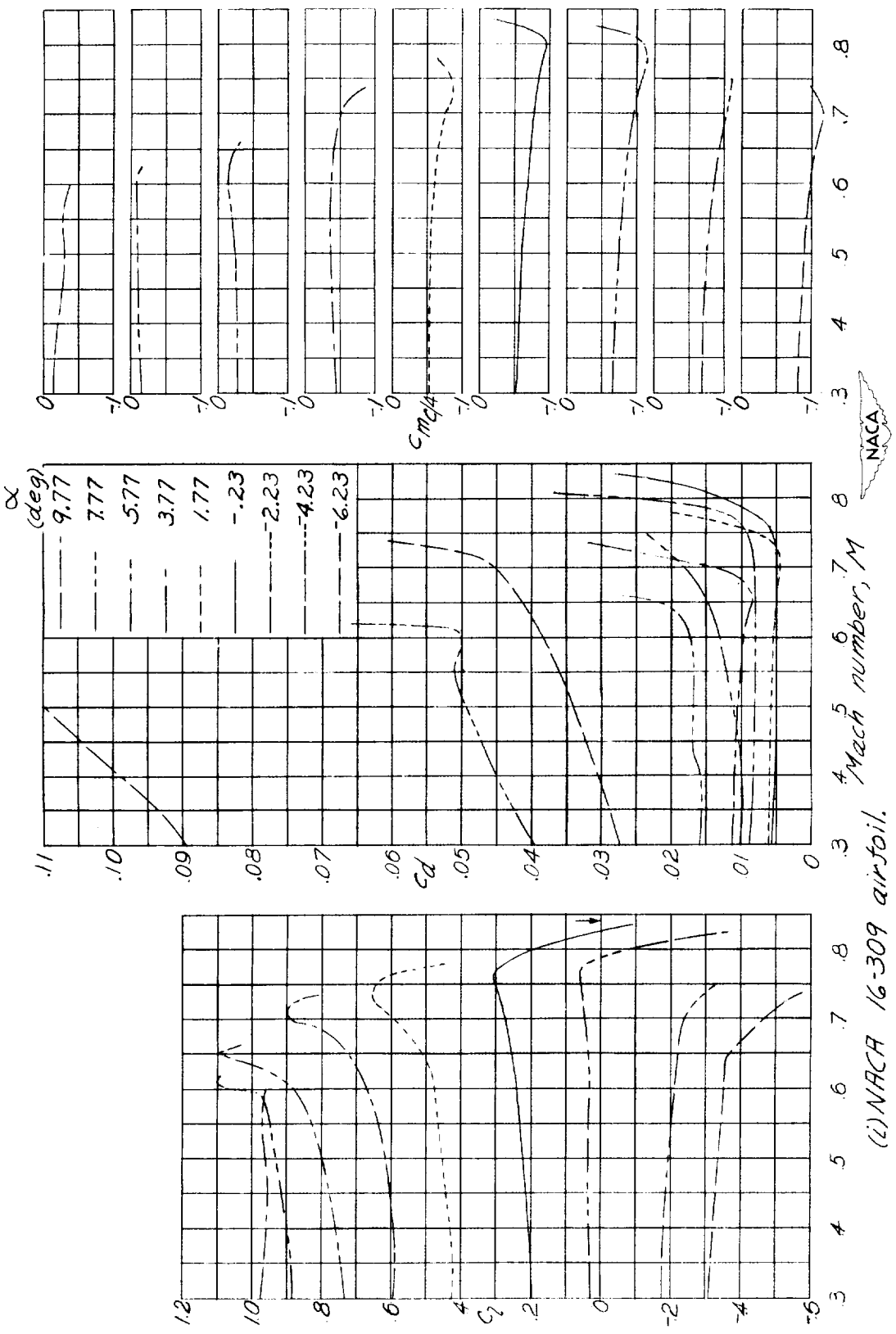

(i) NACA 16-309 airfoil.

Figure 3.- Continued.

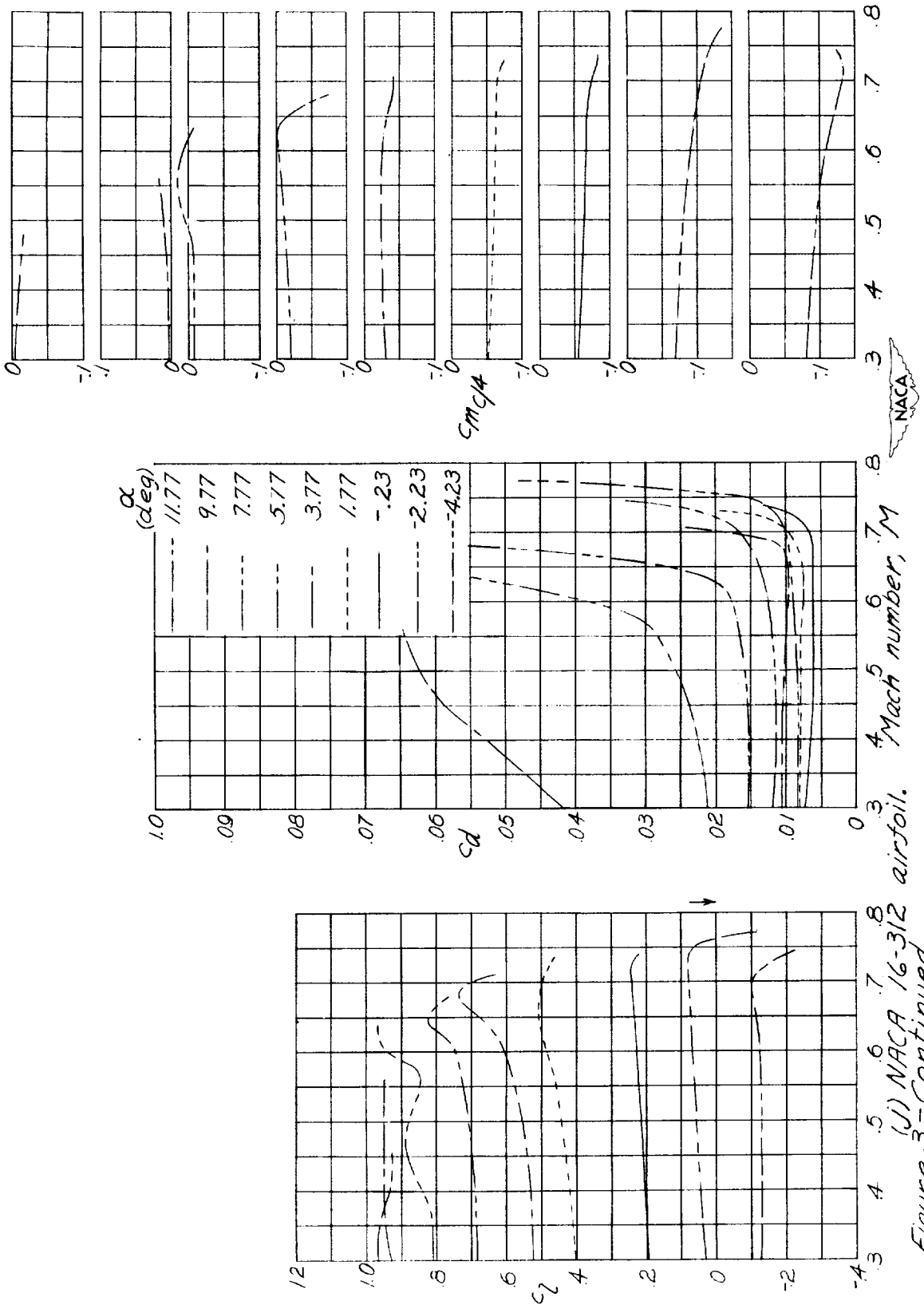

Figure 3.- Continued.
(j) NACA 16-312 airfoil.

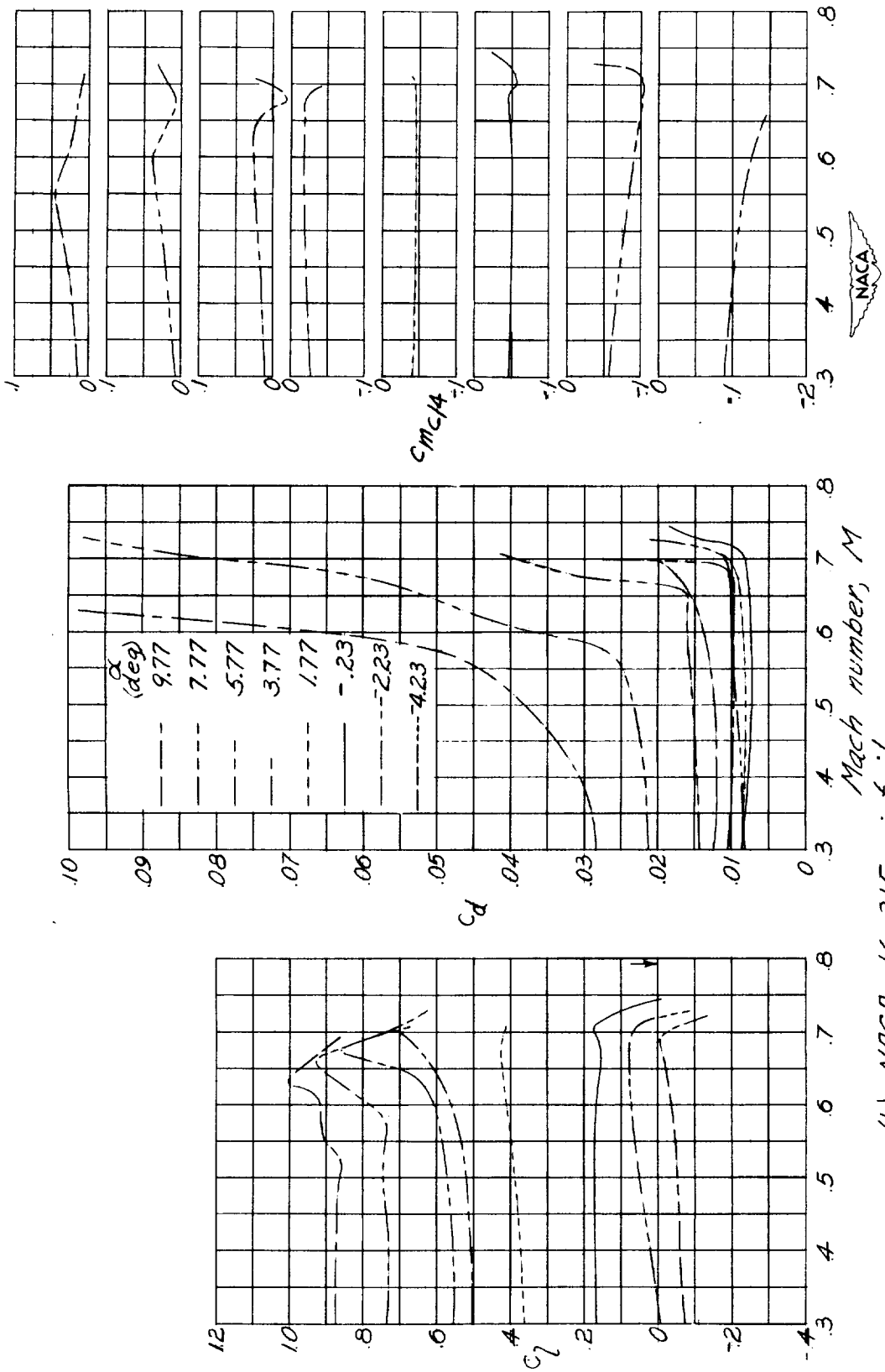

(k) NACA 16-315 airfoil.

Figure 3.- Continued.

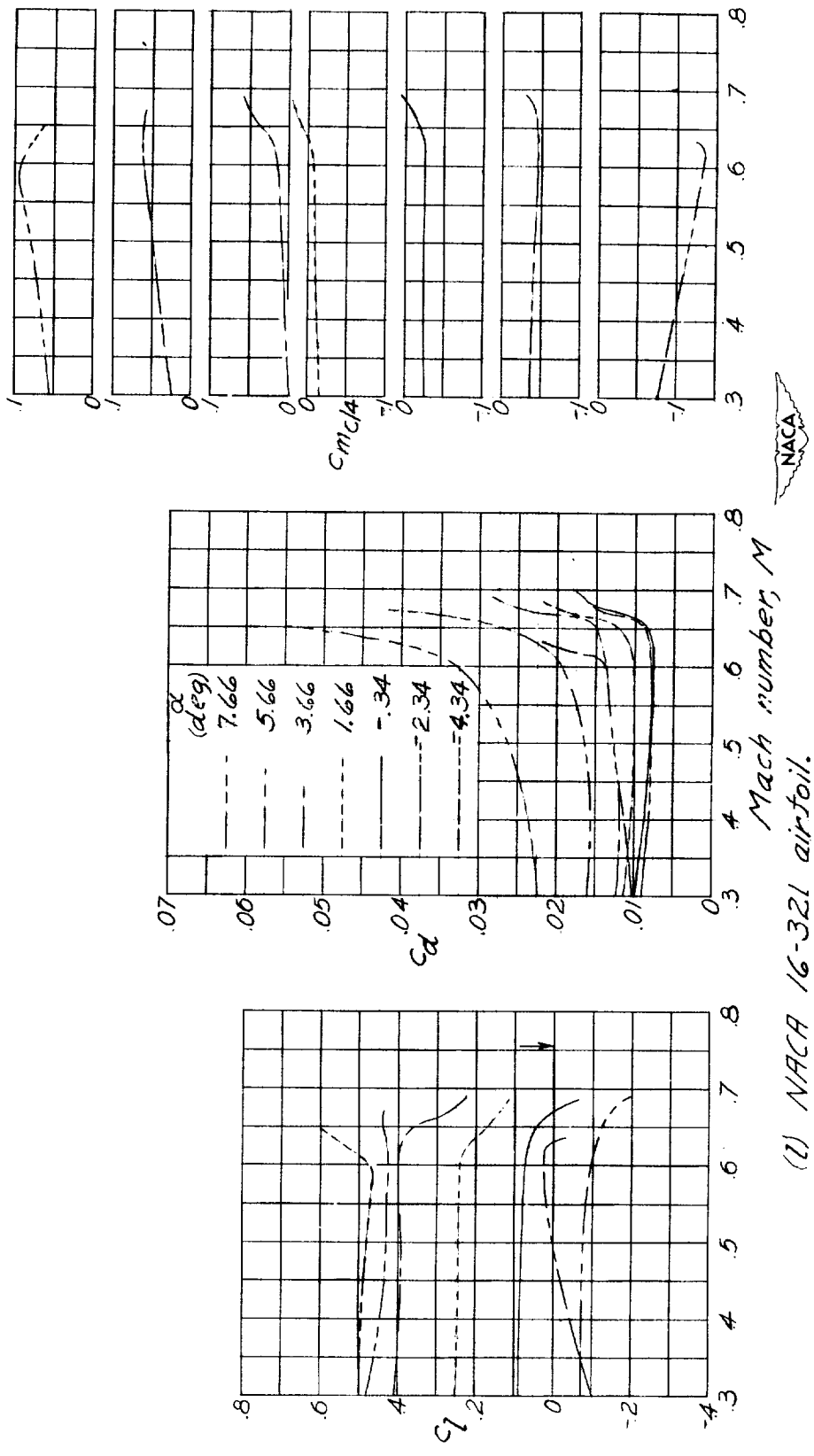

(l) NACA 16-321 airfoil.

Figure 3.- Continued.

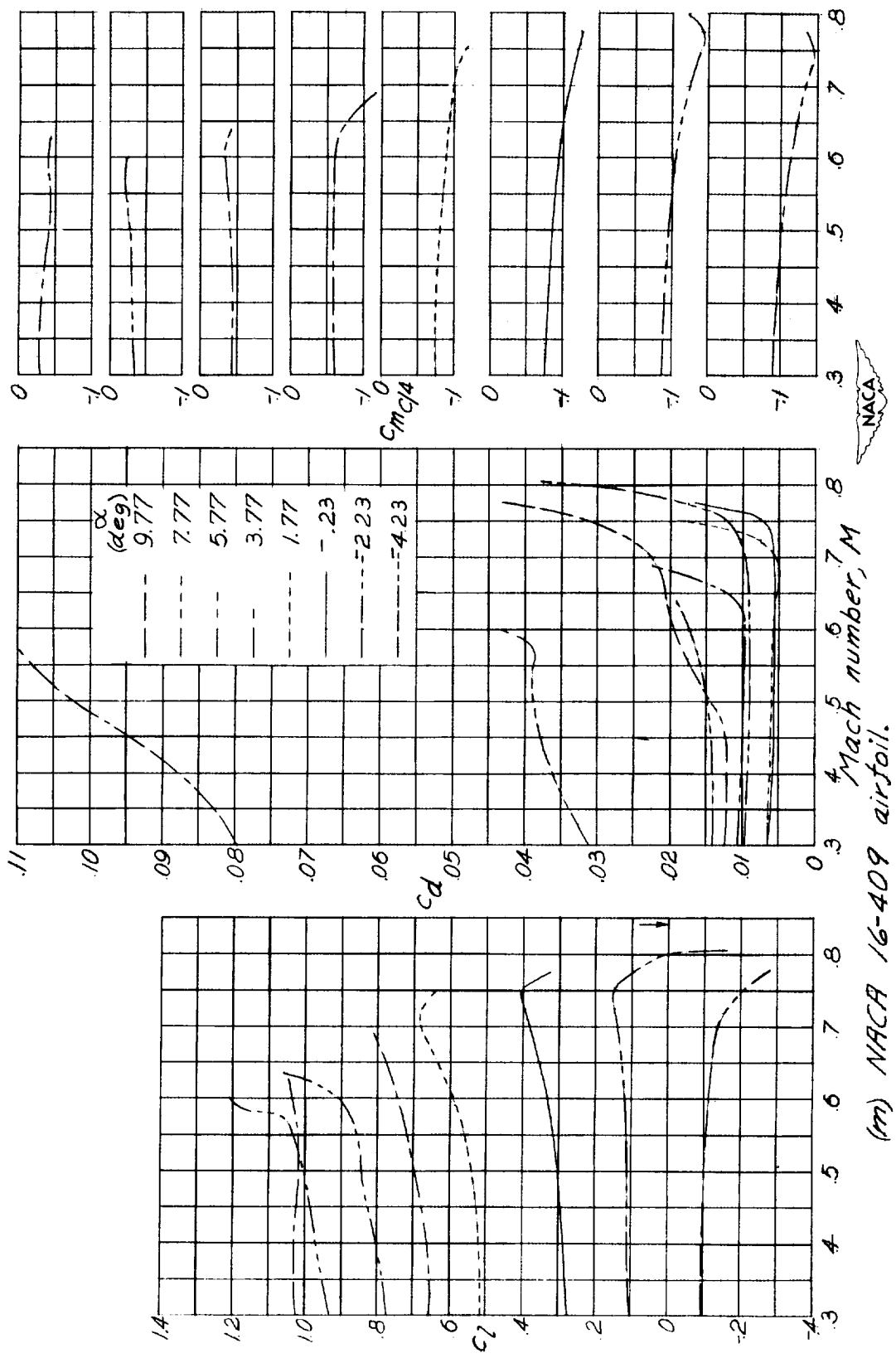

Figure 3.- Continued.

(m) NACA 16-409 airfoil.

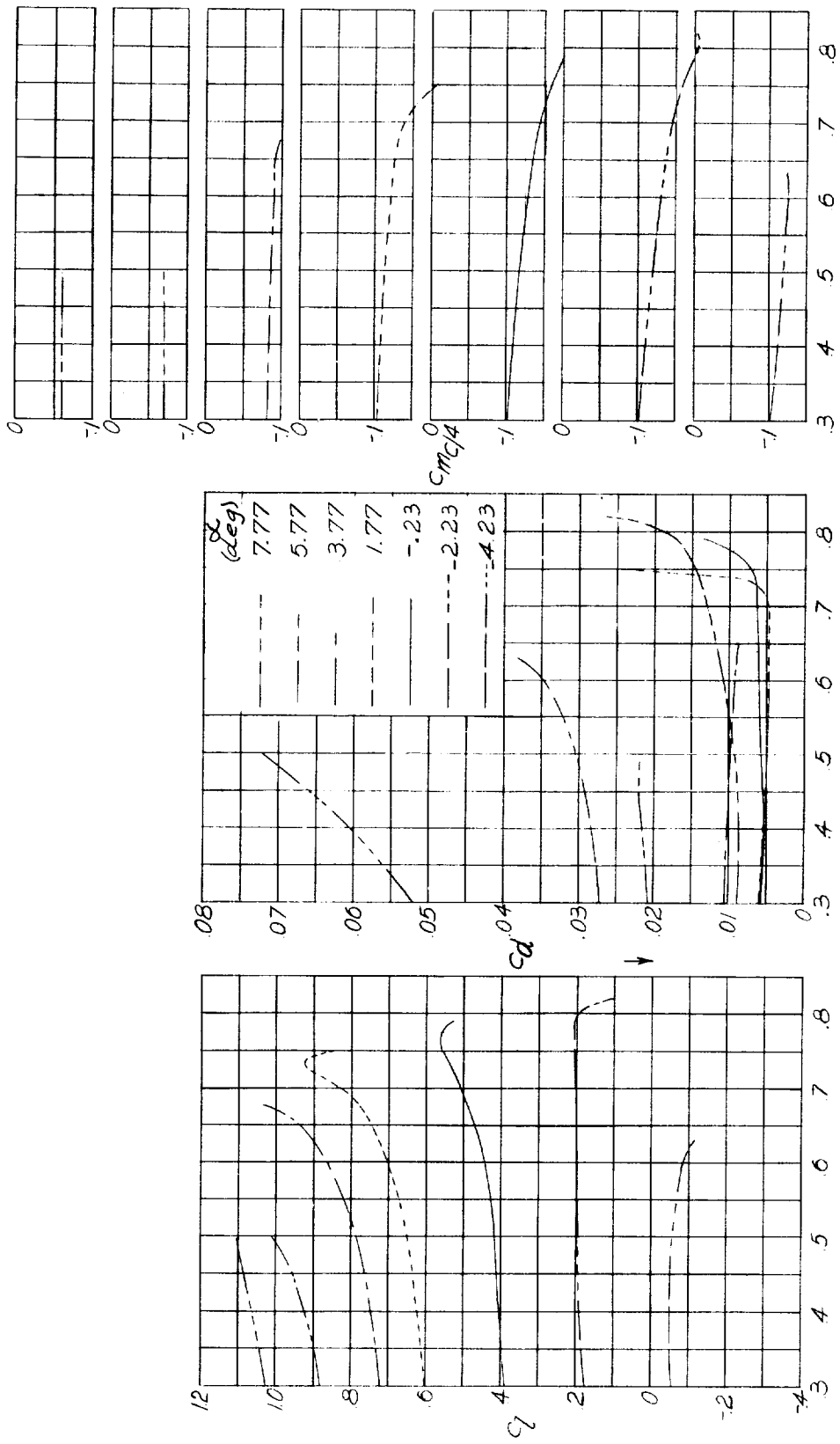

(n) NACA 16-506 airfoil.

Figure 3.- Continued.

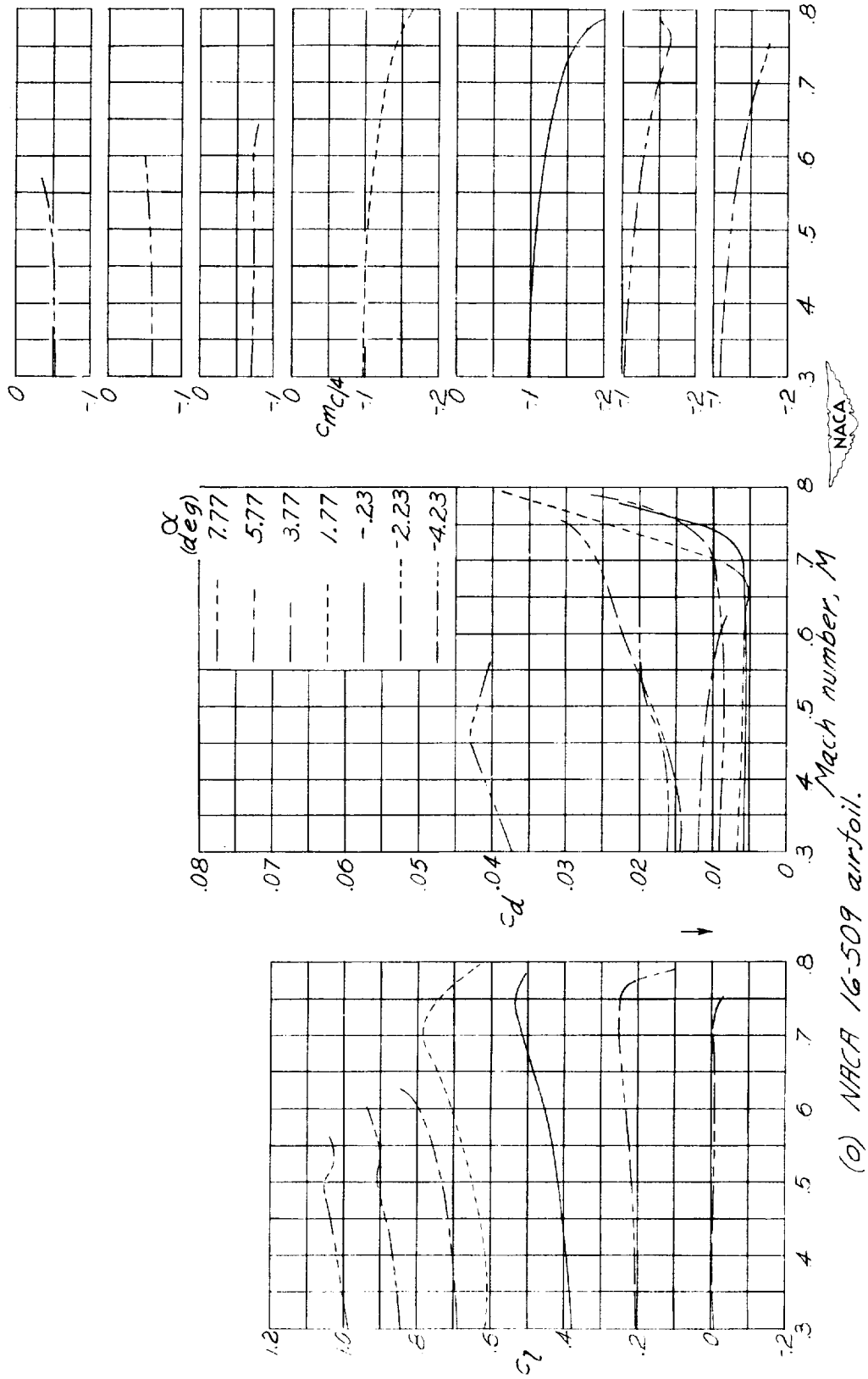

(o) NACA 16-509 airfoil.

Figure 3.- Continued.

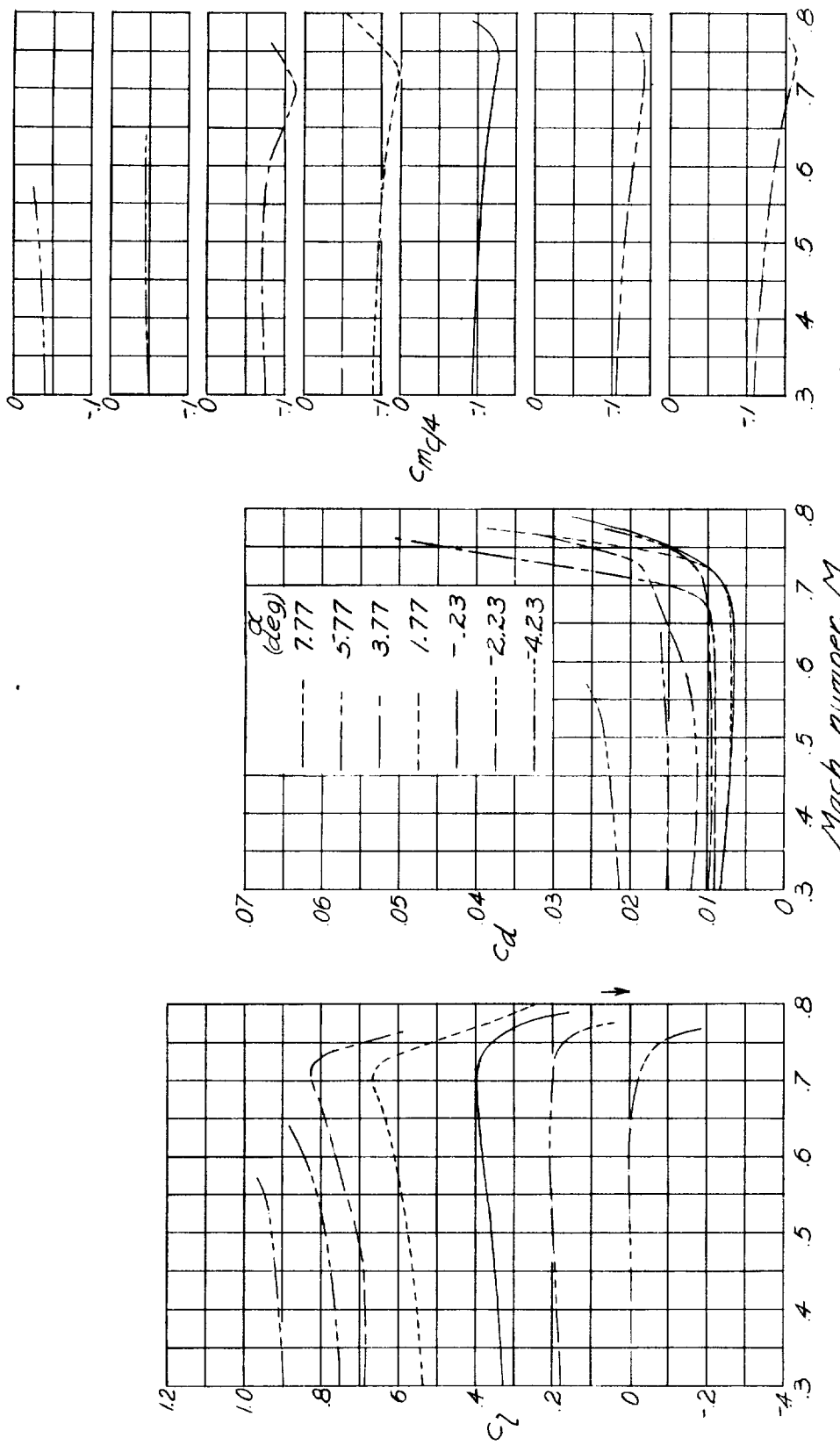

(d) NACA 16-512 airfoil.

Figure 3- Continued.

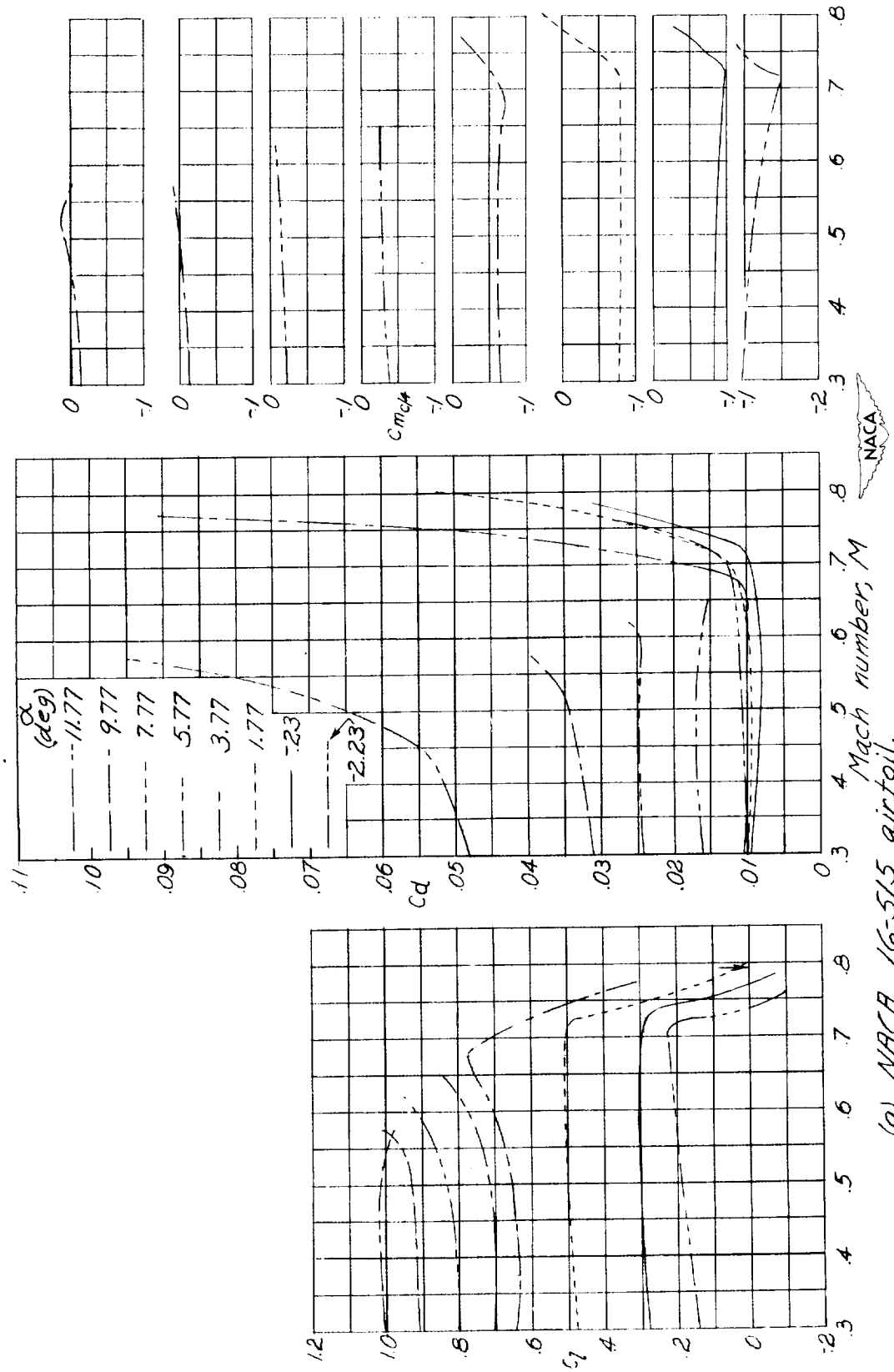

(g) NACA 16-515 airfoil.

Figure 3.- Continued.

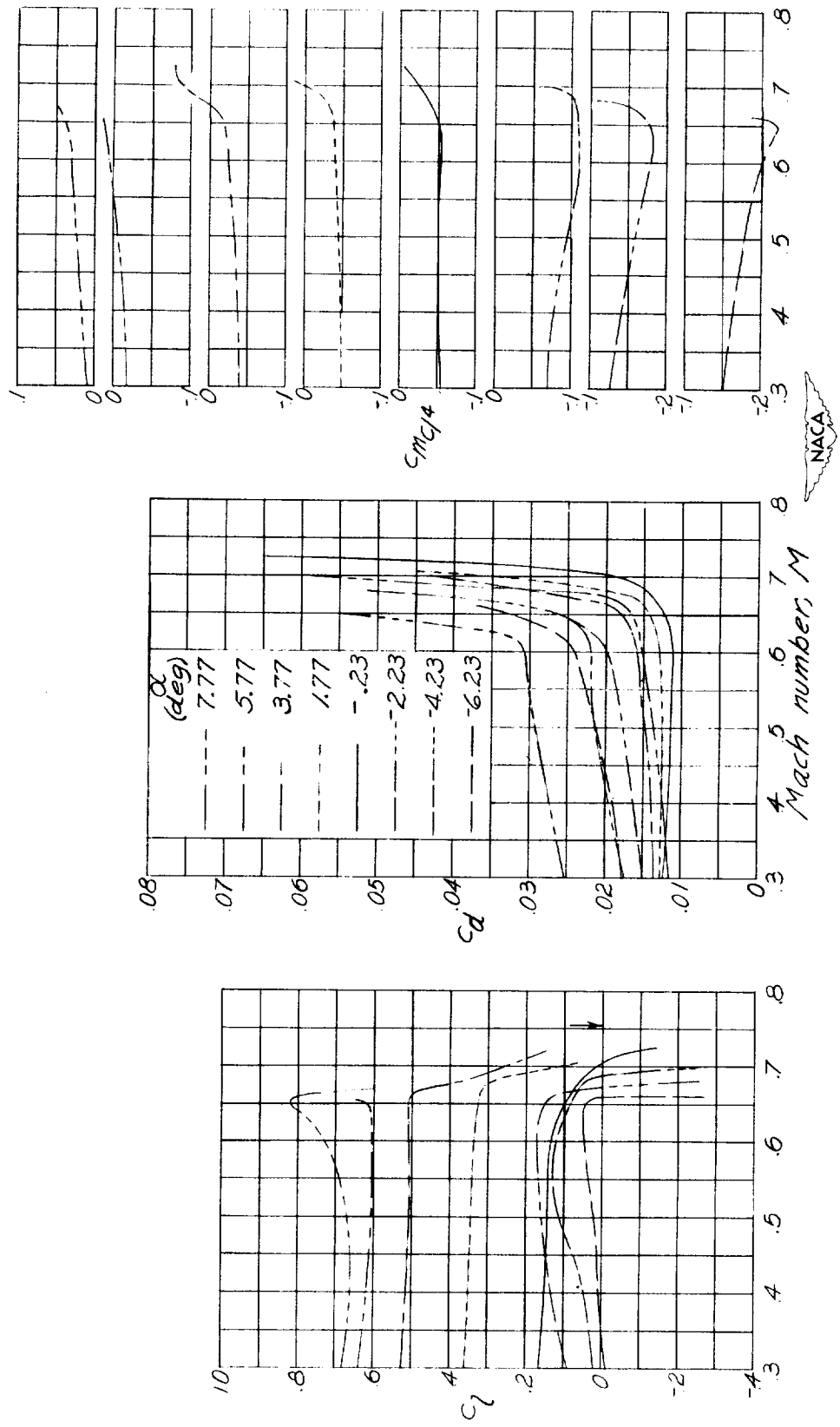

(r) NACA 16-521 airfoil.

Figure 3.- Continued.

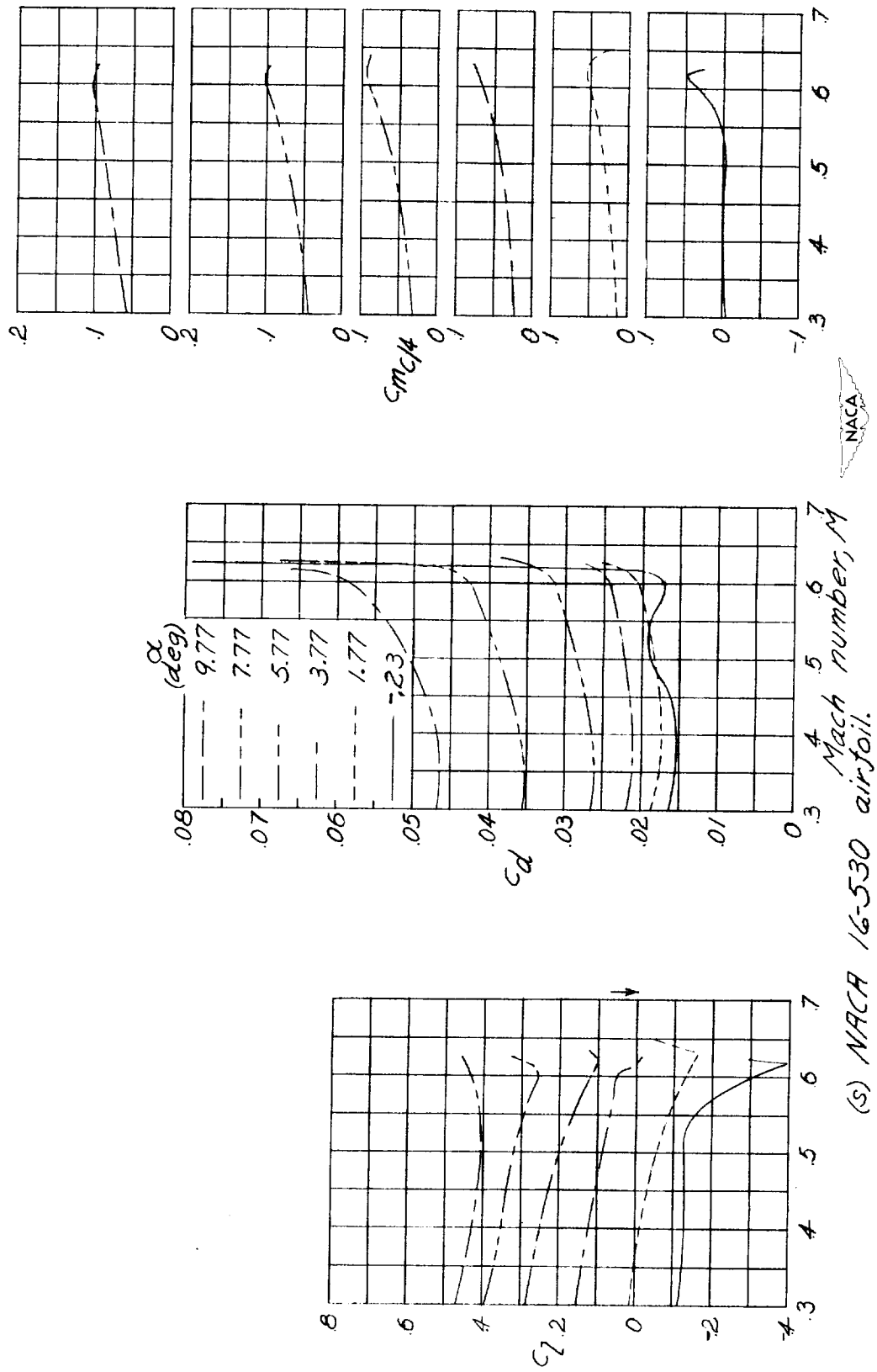

(s) NACA 16-530 airfoil.

Figure 3.- Continued.

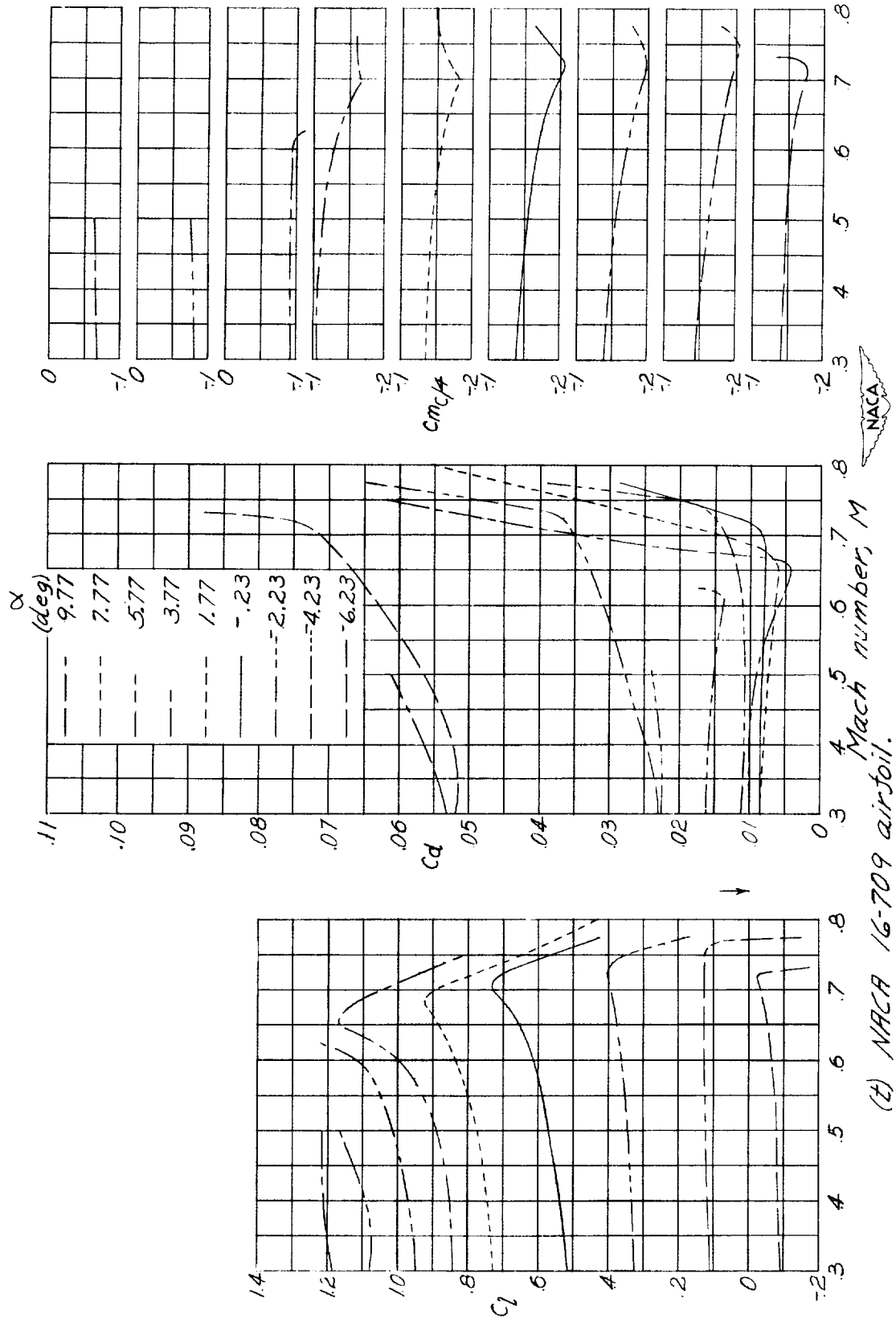

(t) NACA 16-709 airfoil.

Figure 3.- Continued.

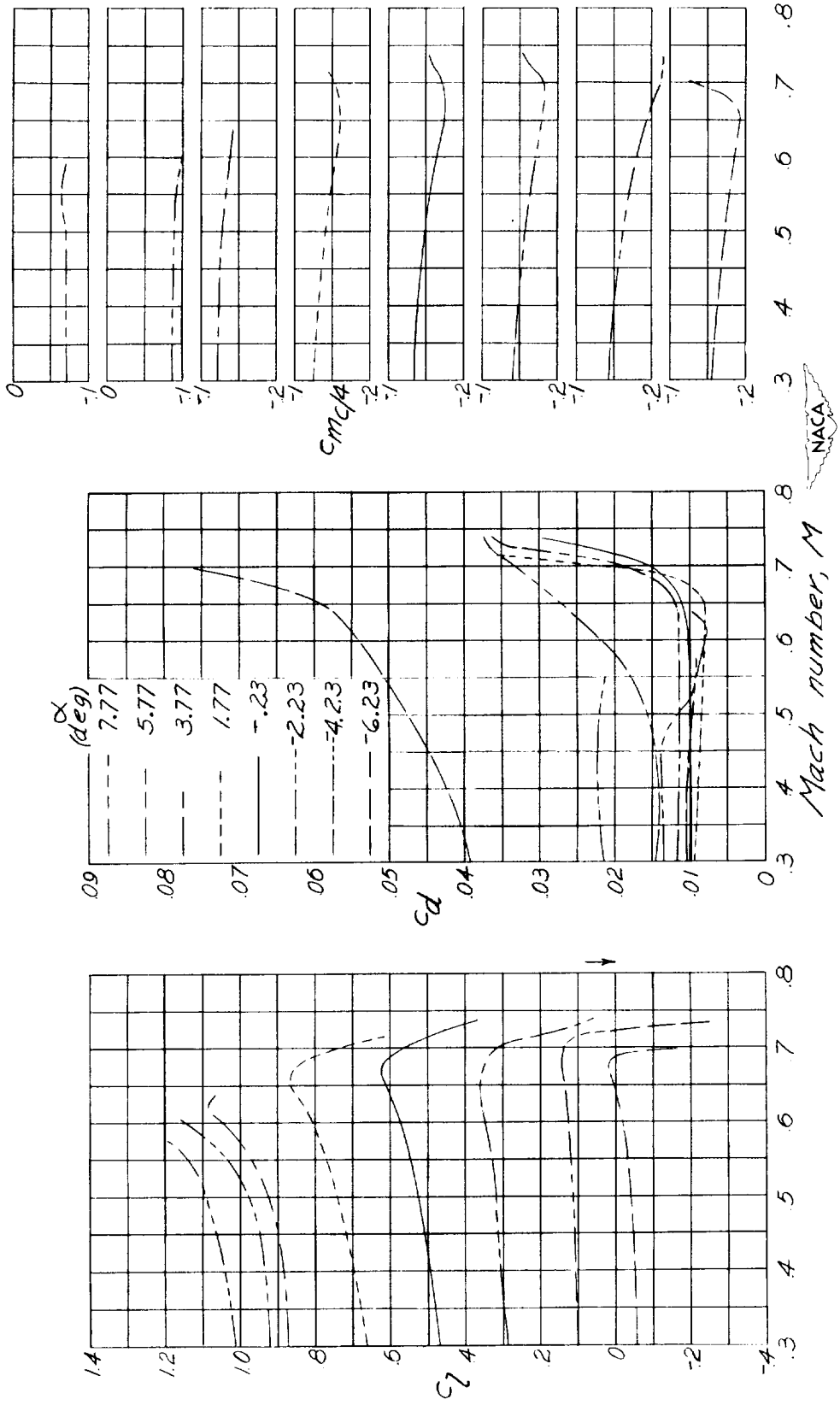

(u) NACA 16-712 airfoil.

Figure 3.- Continued.

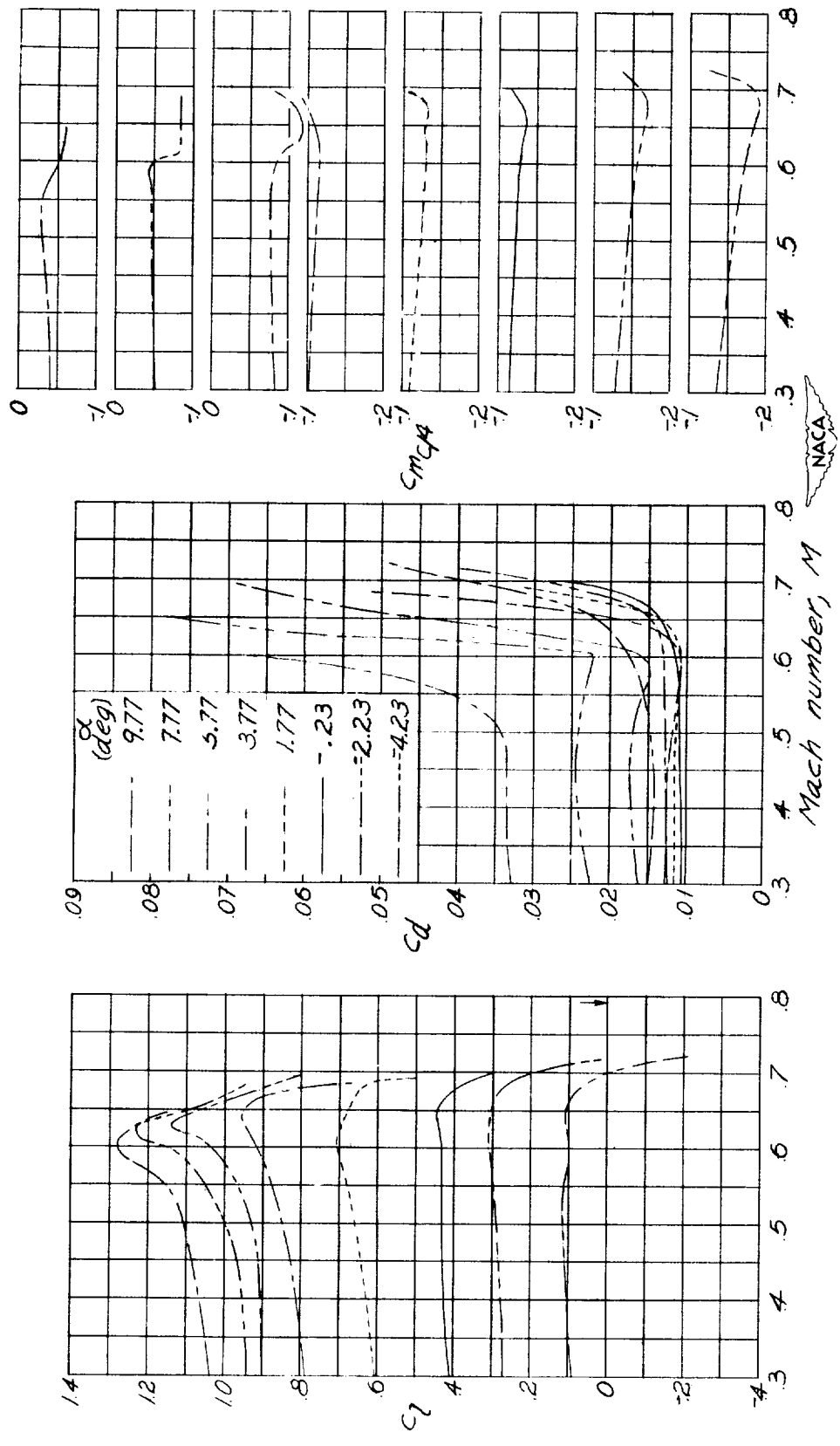

(a) NACA 16-715 airfoil.

Figure 3.- Continued.

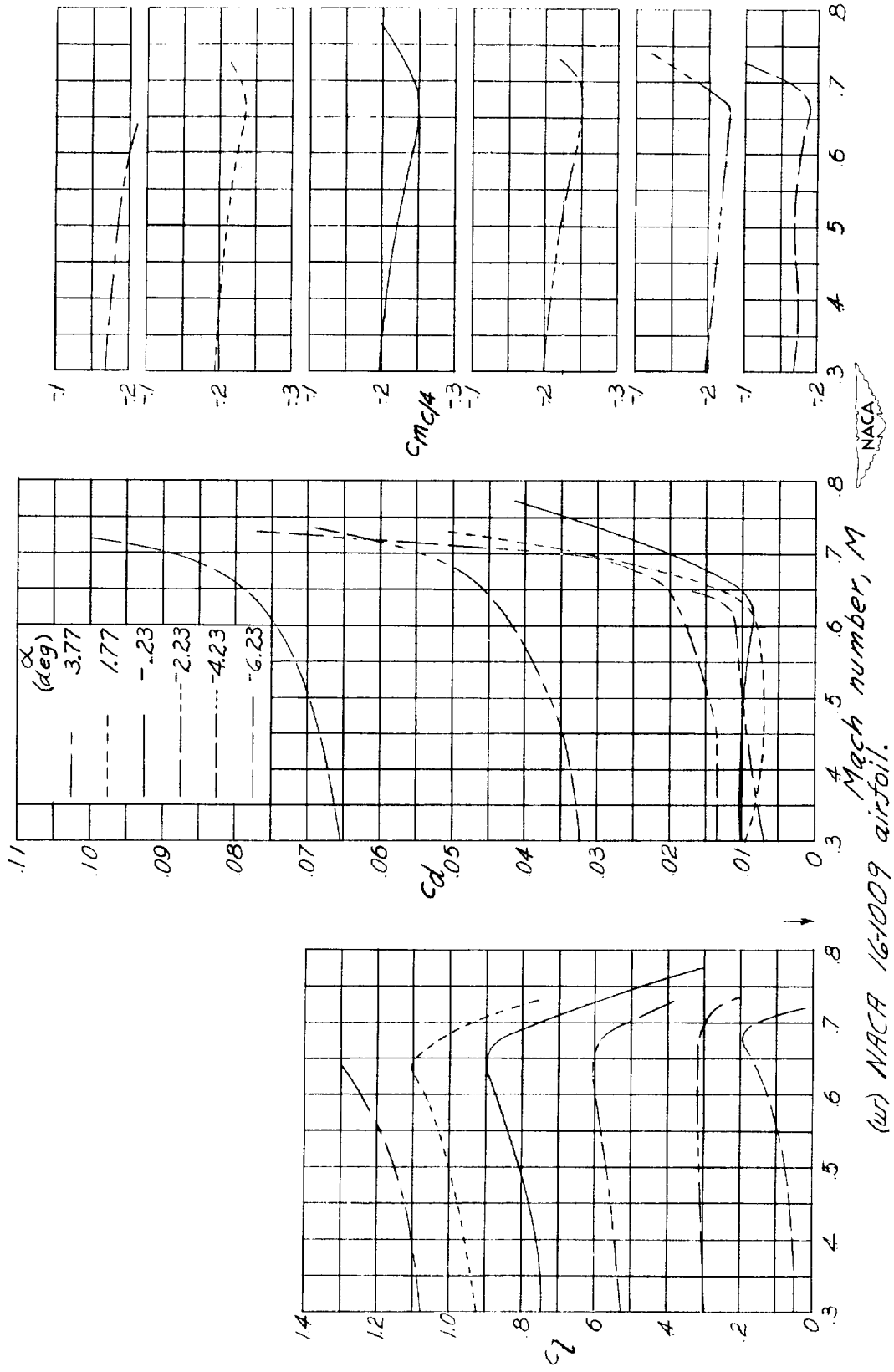

(w) NACA 16-1009 airfoil.

Figure 3.- Continued.

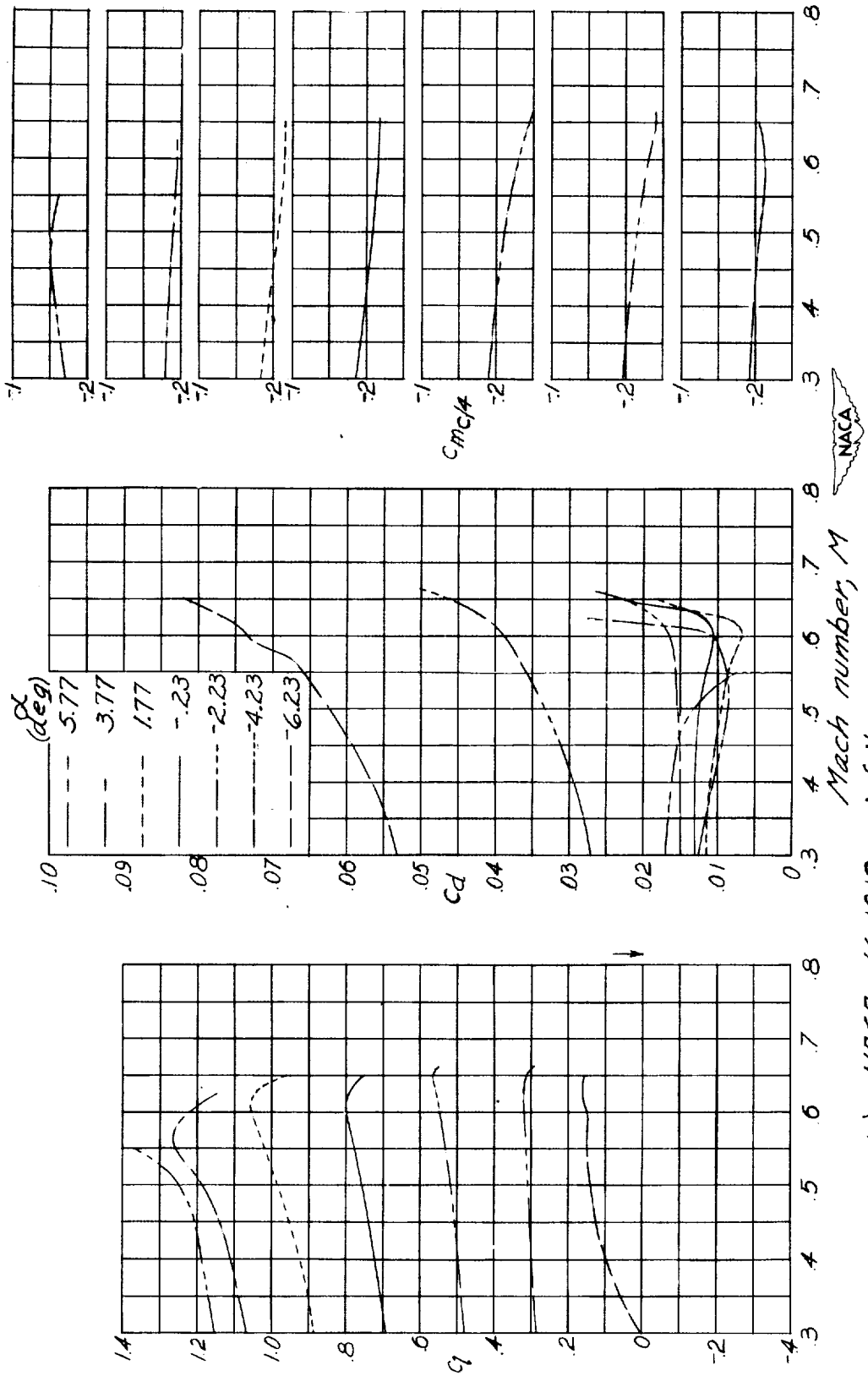

(x) NACA 16-1012 airfoil.

Figure 3.- Concluded.

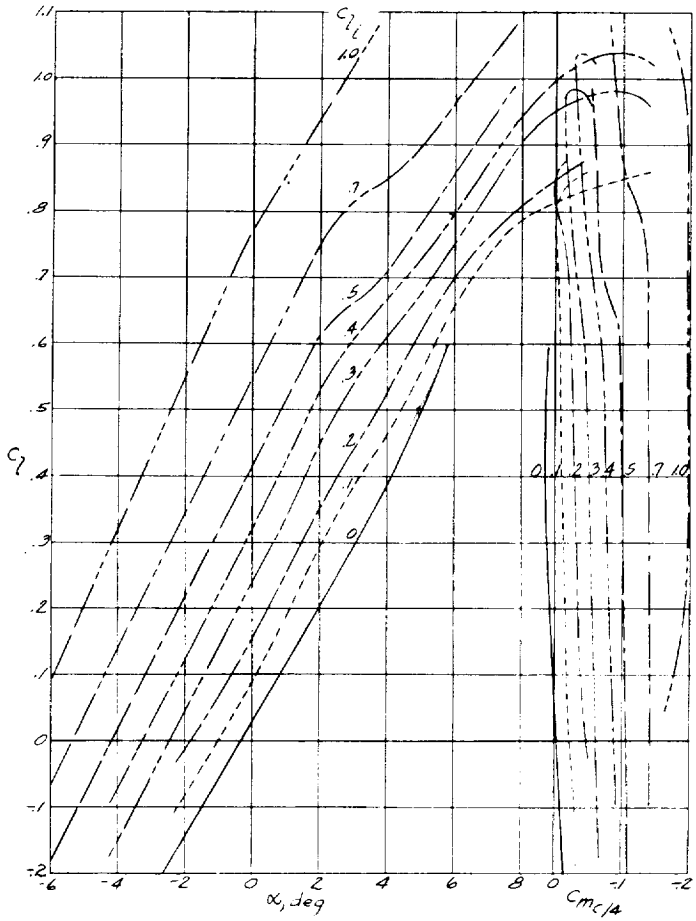

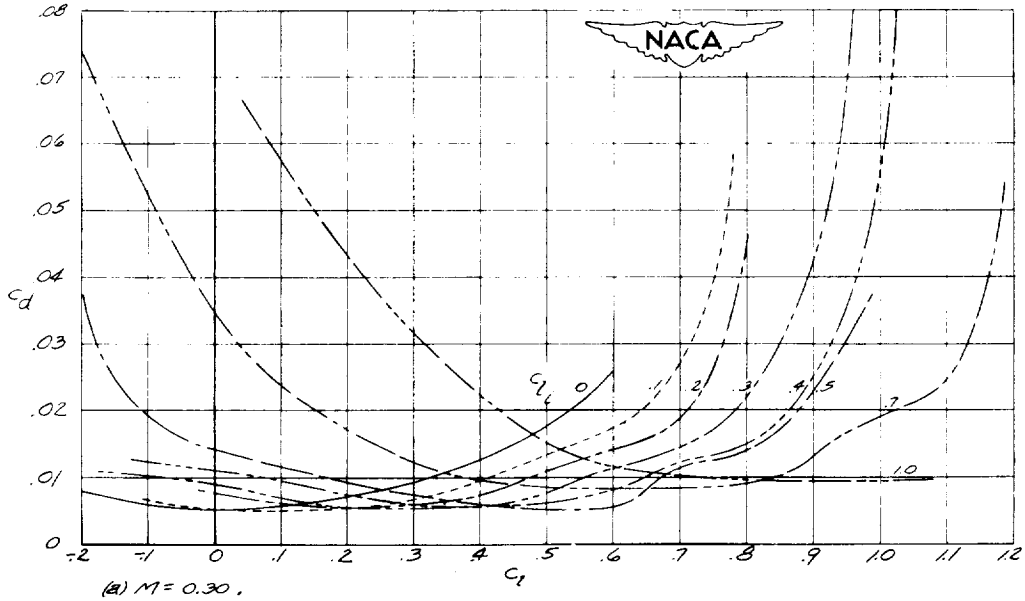

(a) $M = 0.30$.

Figure 4. - Aerodynamic characteristics of NACA 16-X09 airfoils.

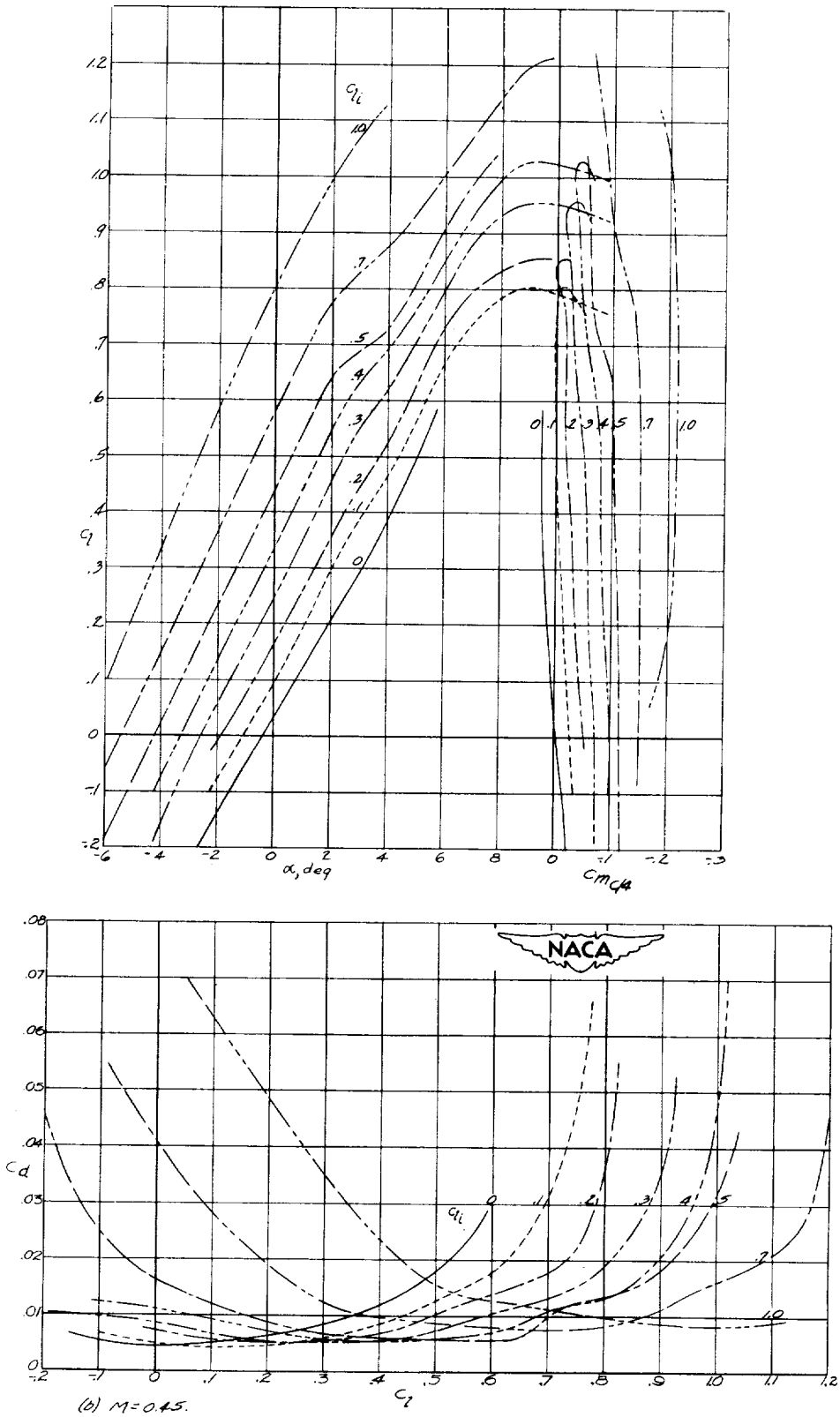

(b) M=0.45.

Figure 4. - Continued.

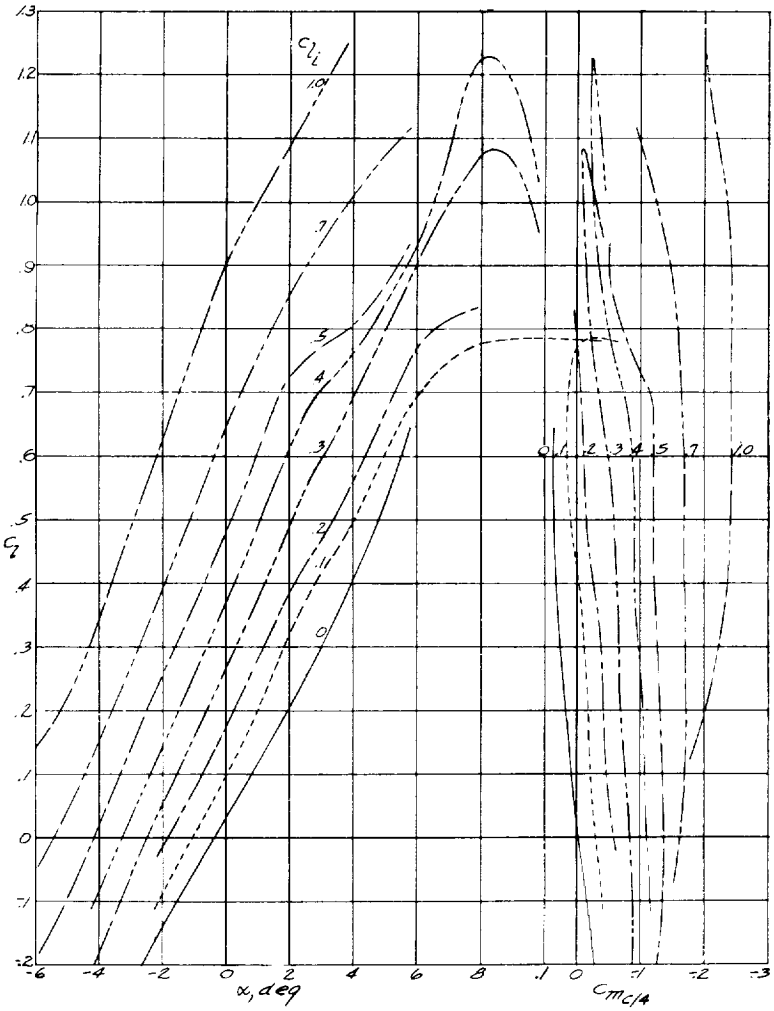

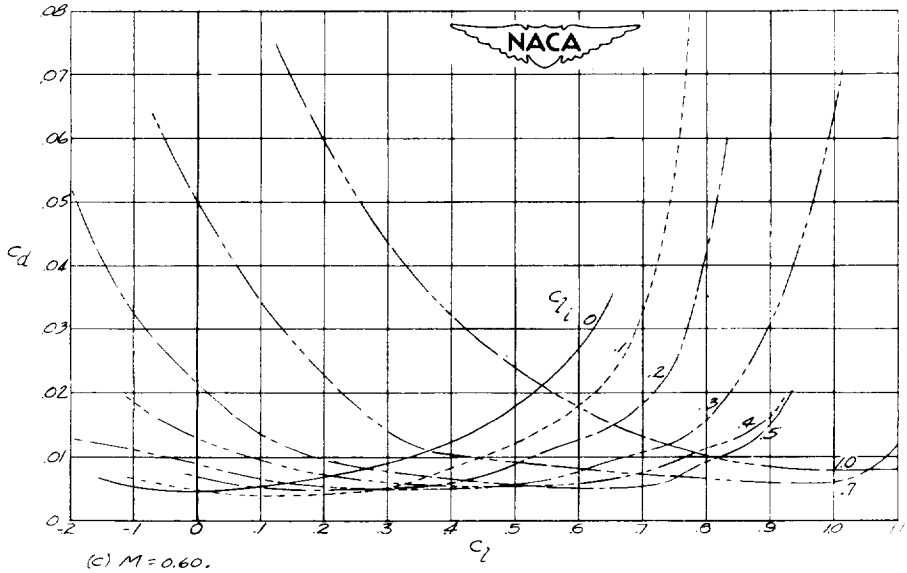

(c) $M = 0.60$.

Figure 4.- Continued.

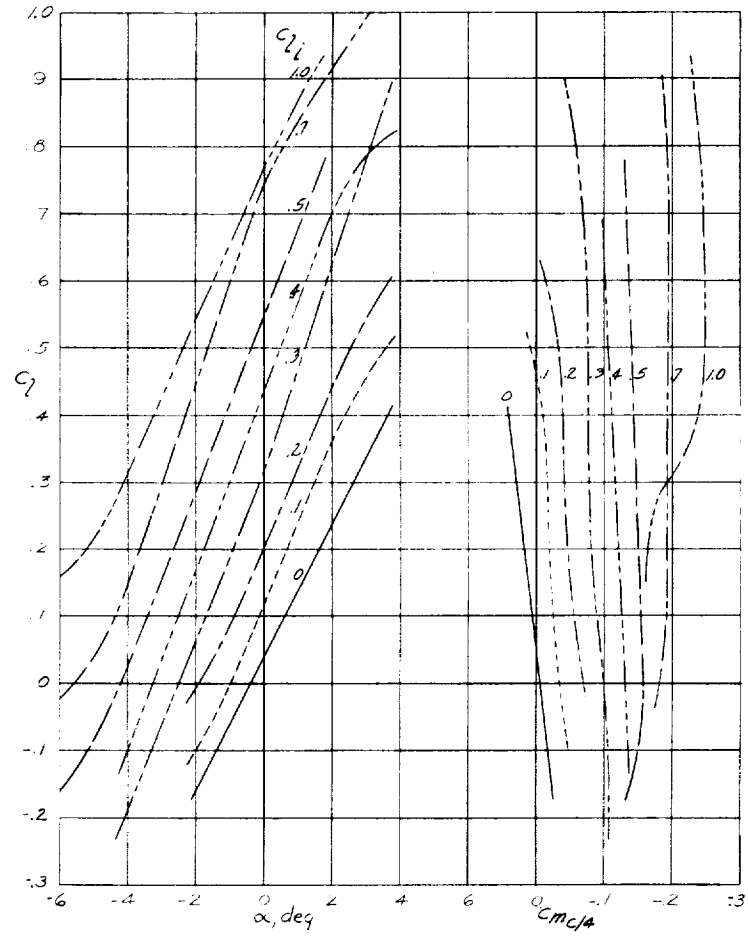

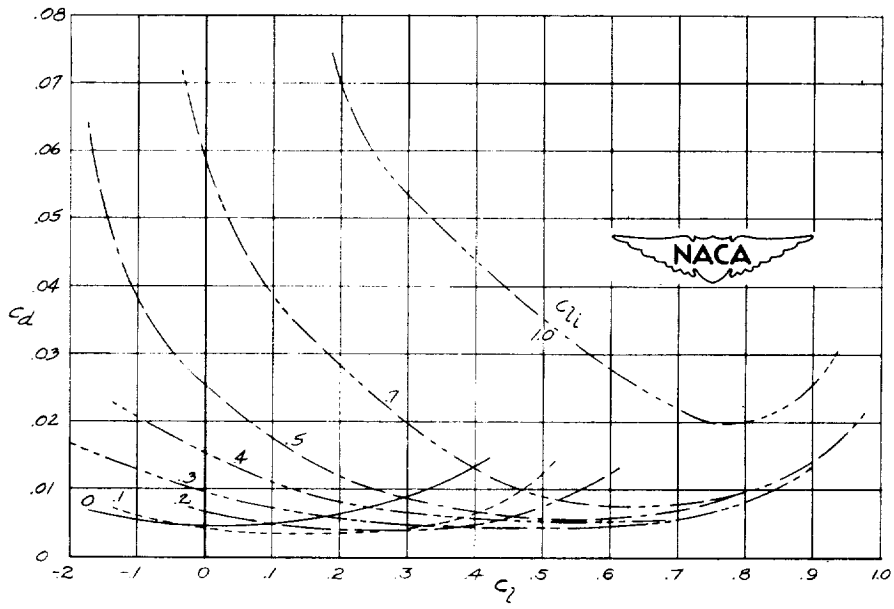

(d) $M = 0.70$.

Figure 4.- Continued.

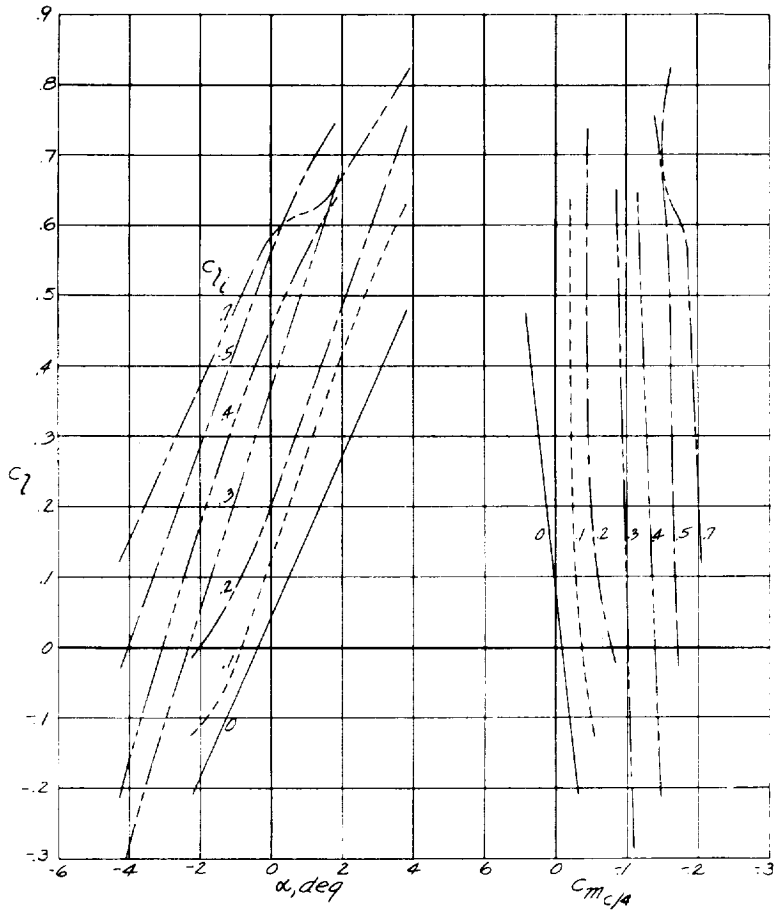

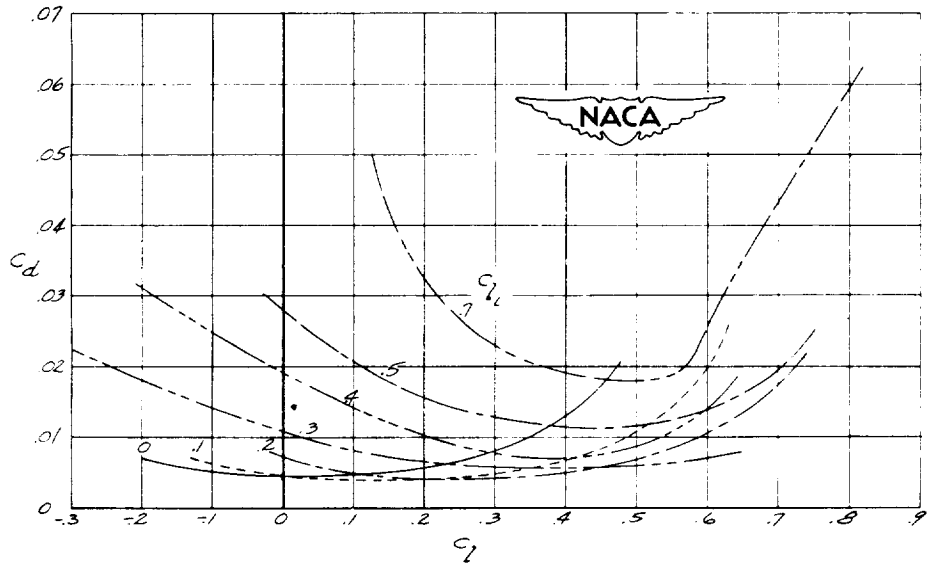

(e) $M = 0.75$.

Figure 4.—Continued.

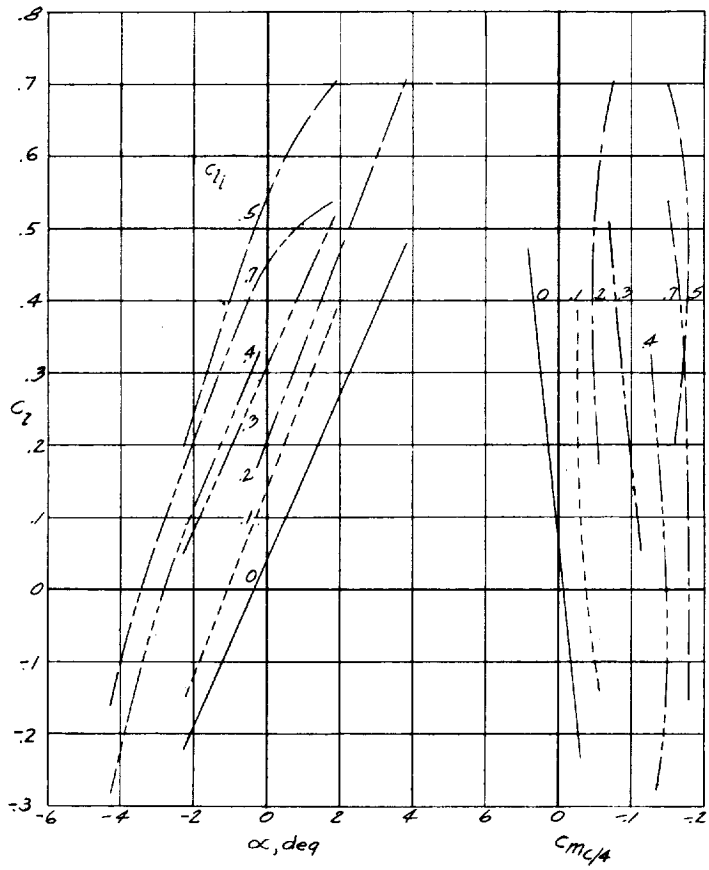

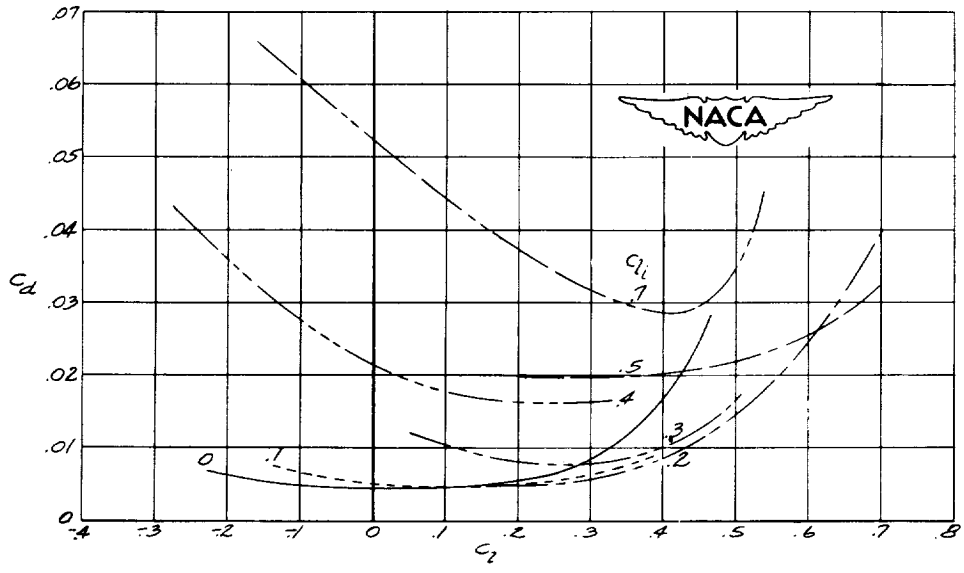

(f) $M = 0.775$.

Figure 4. - Concluded.

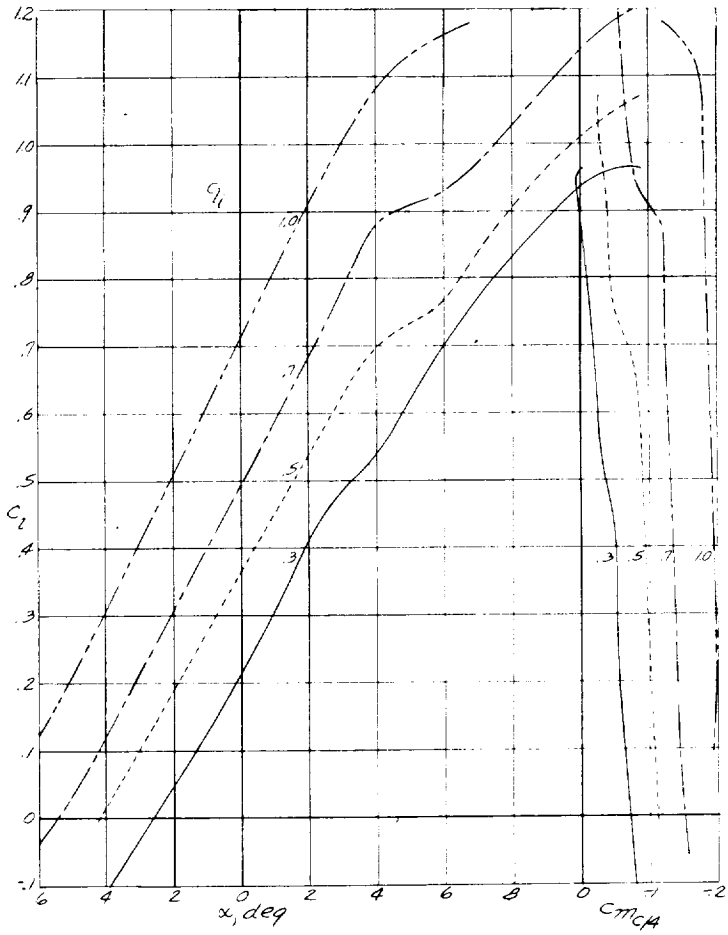

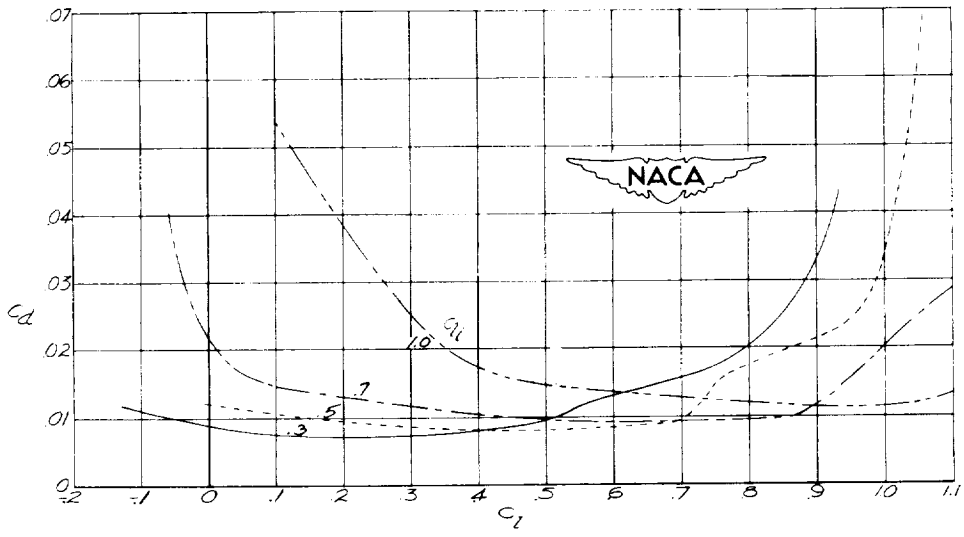

(a) $M = 0.30$.

Figure 5. – Aerodynamic characteristics of NACA 16-X12 airfoils.

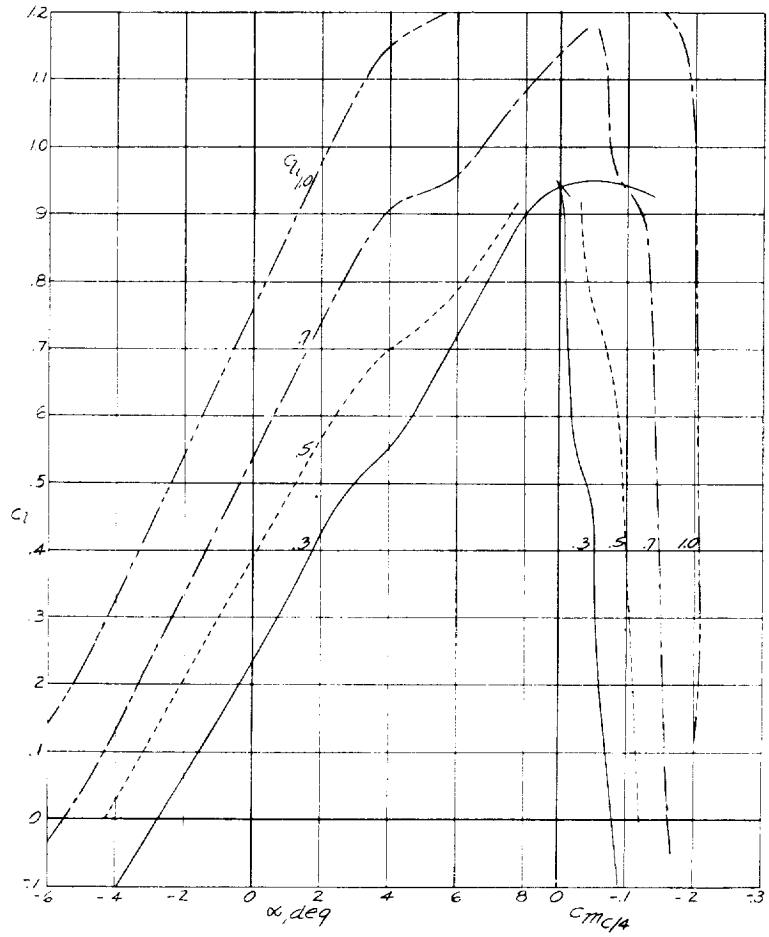

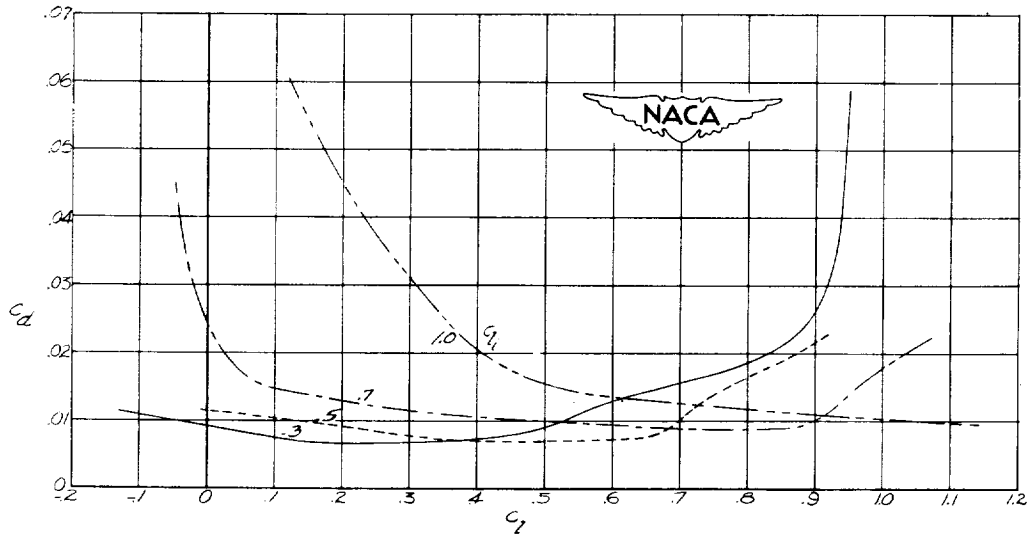

(b) $M = 0.45$.

Figure 5.- Continued.

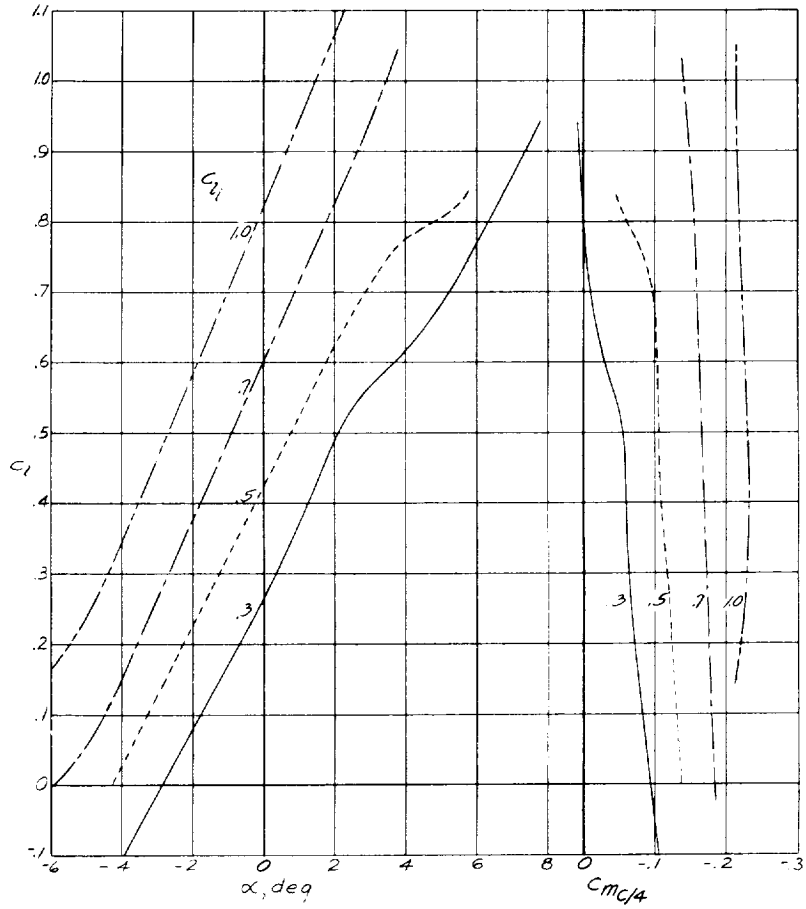

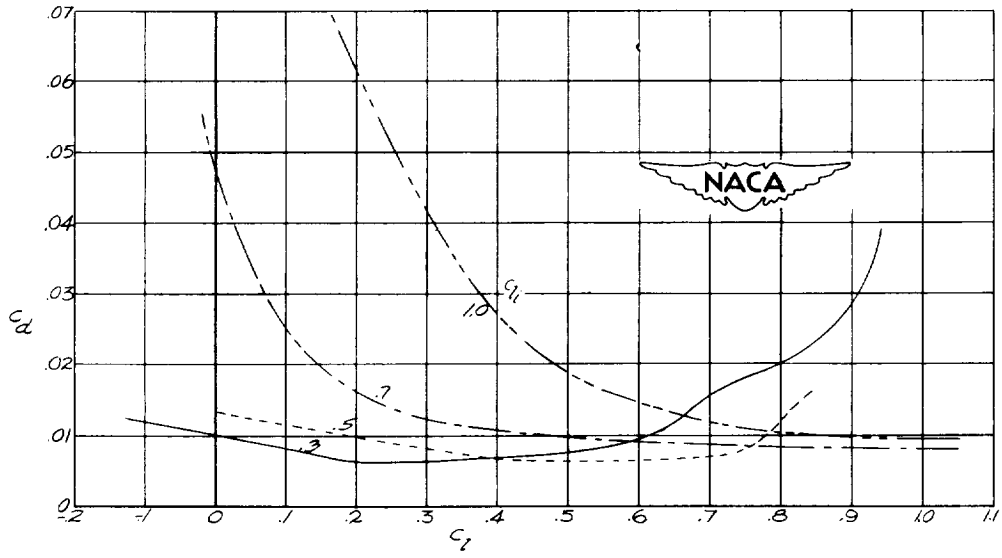

(c) $M = 0.60$.

Figure 5. - Continued.

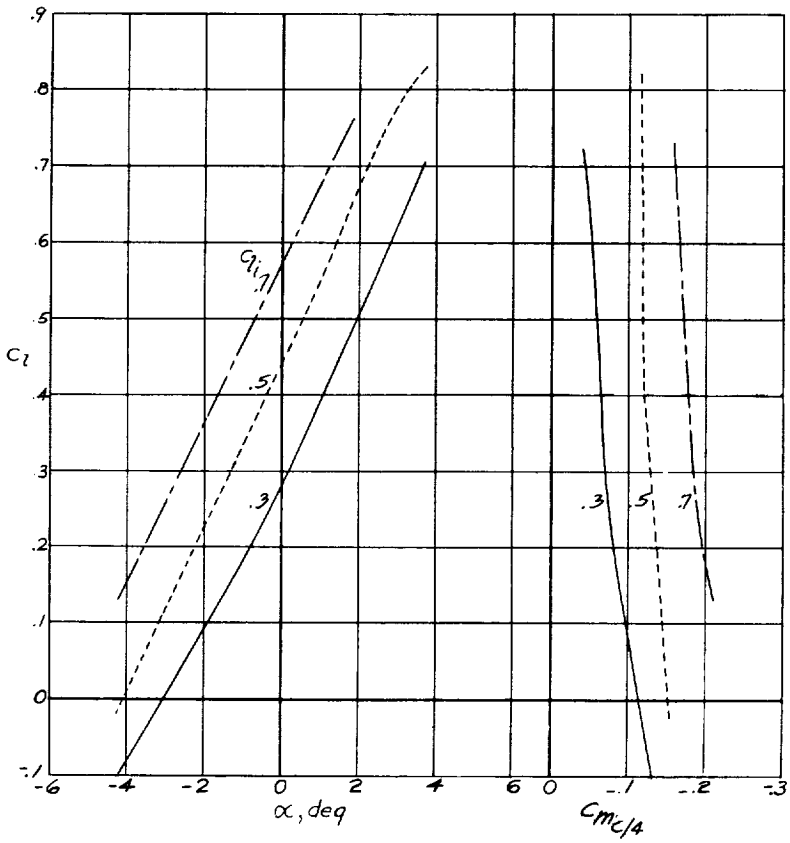

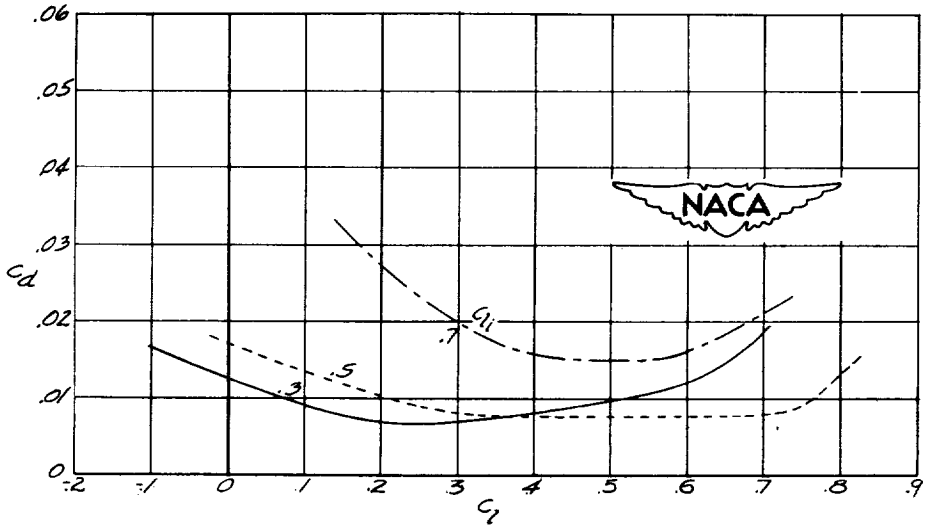

(d) $M = 0.70$.

Figure 5.- Concluded.

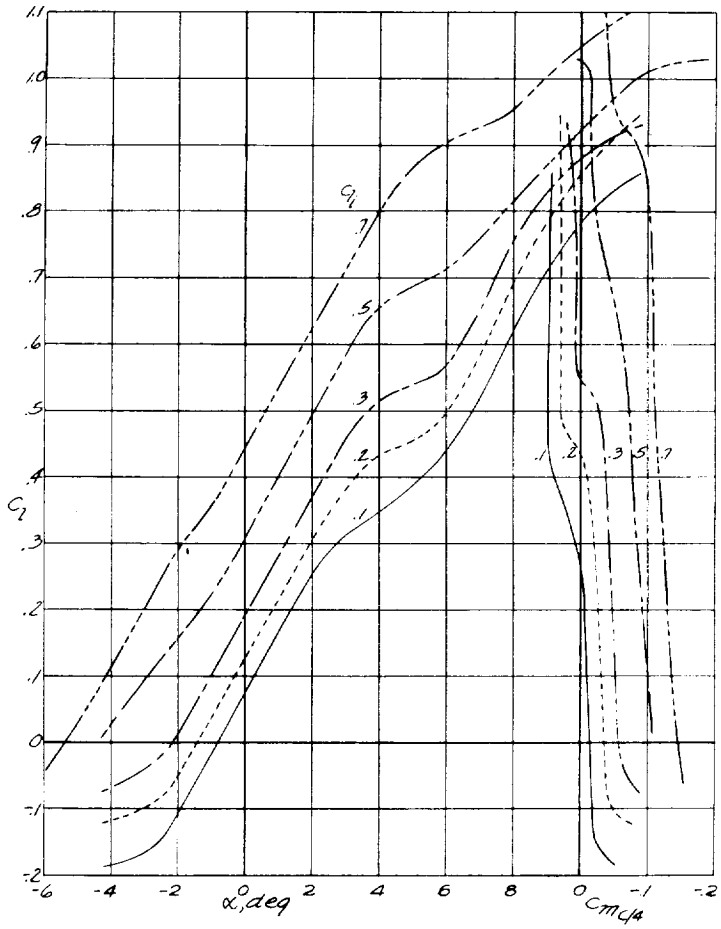

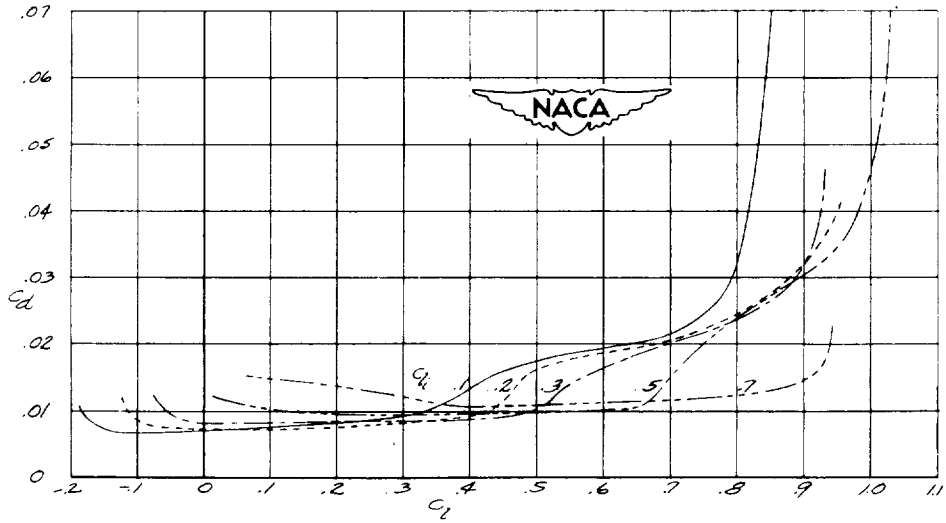

(a) $M = 0.30$.

Figure 6. - Aerodynamic characteristics of NACA 16-X15 air foils.

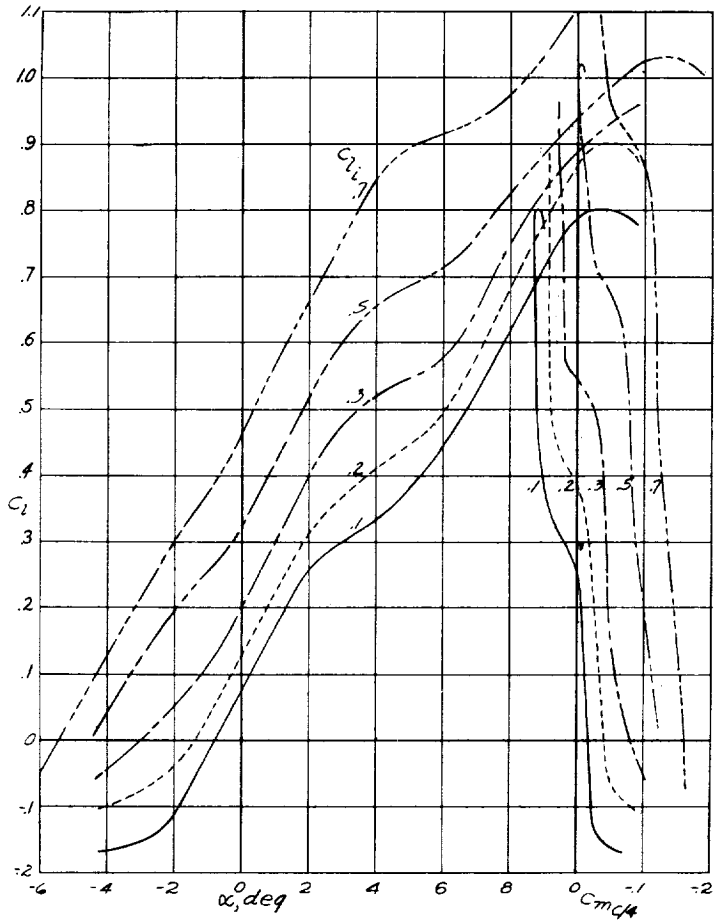

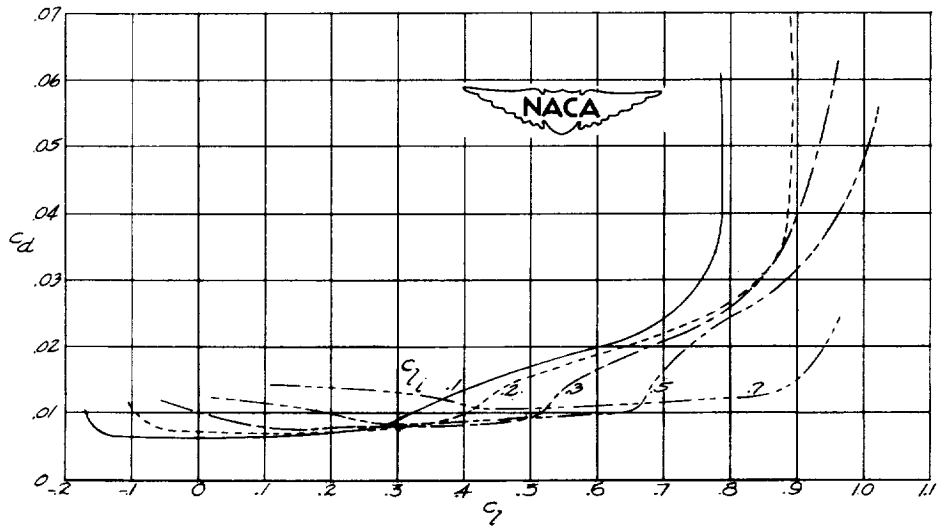

(b) $M = 0.45$.

Figure 6.- Continued.

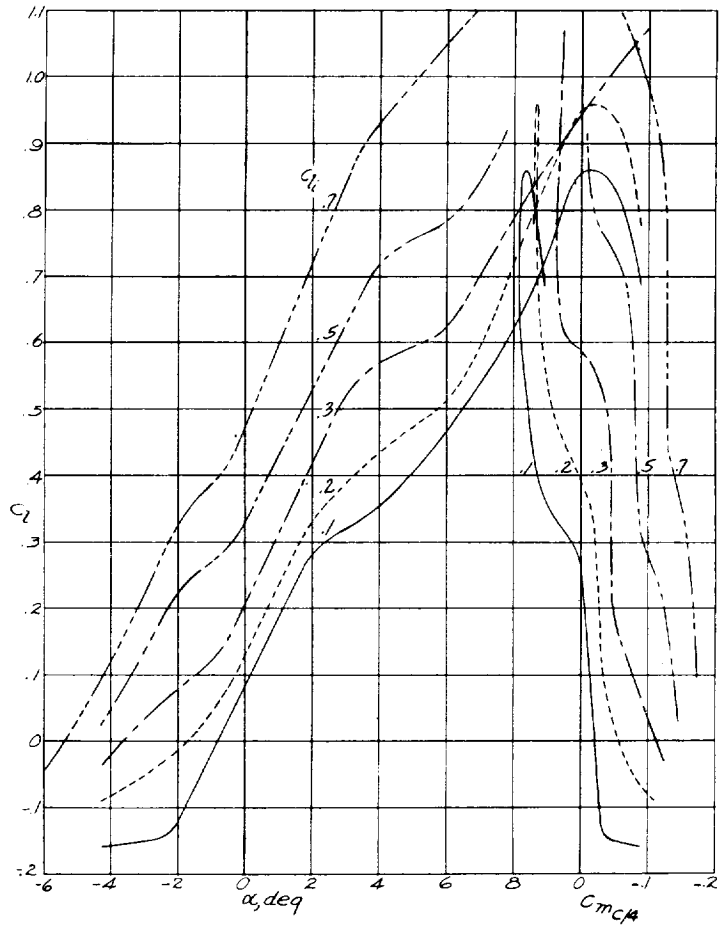

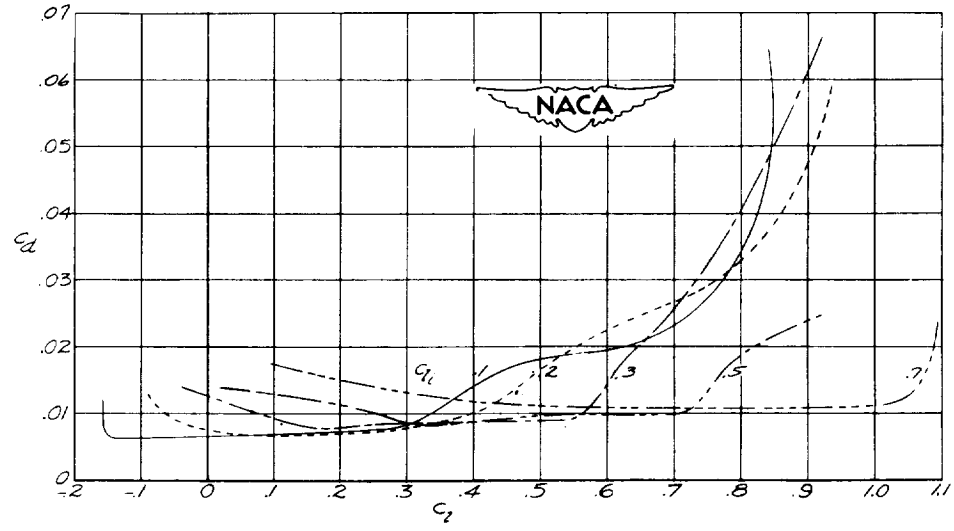

(c) $M = 0.60$.

Figure 6.- Continued.

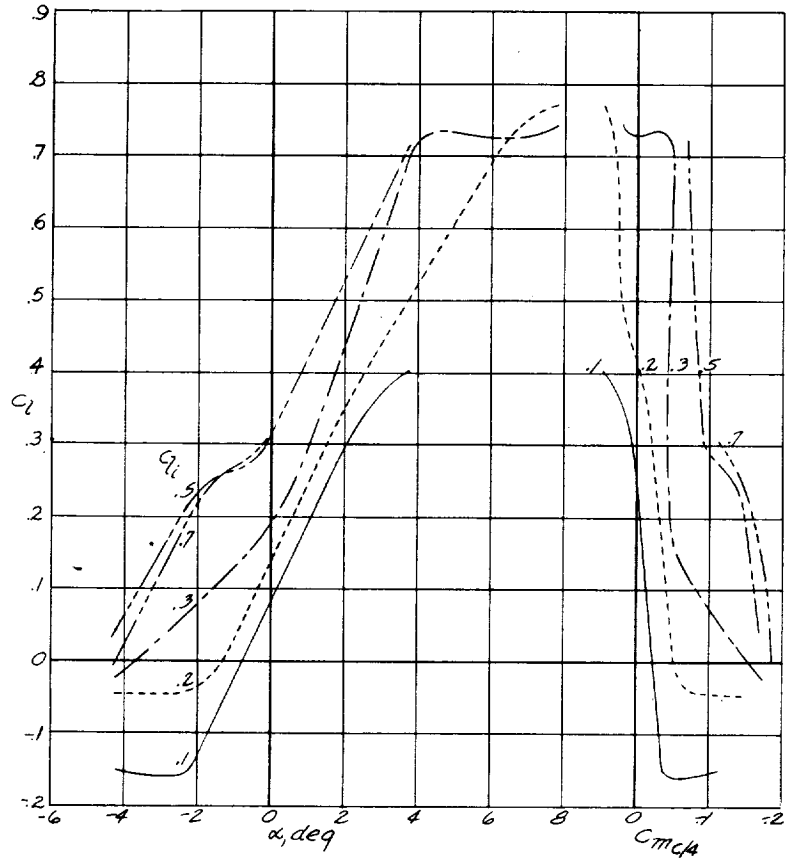

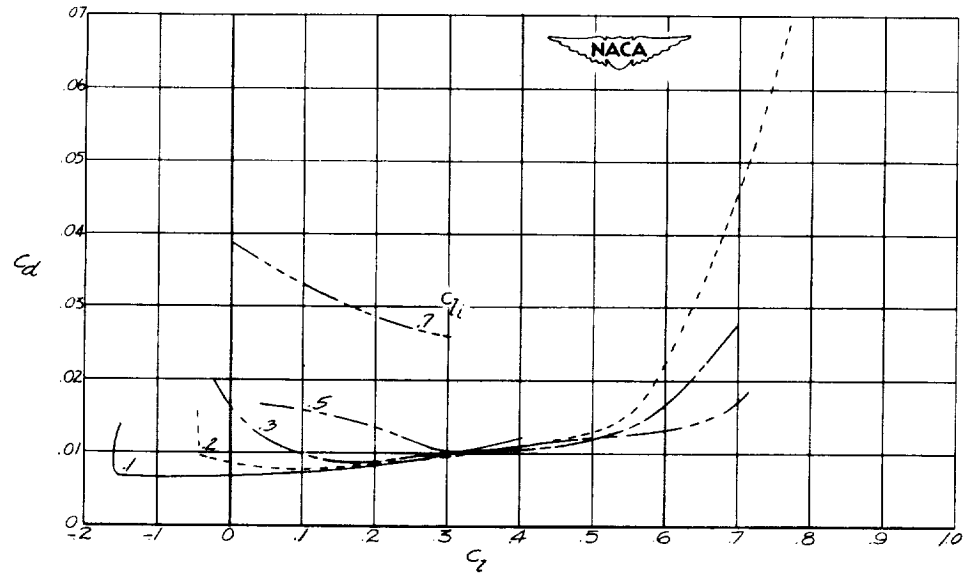

(d) $M = 0.70$.

Figure 6.- Concluded.

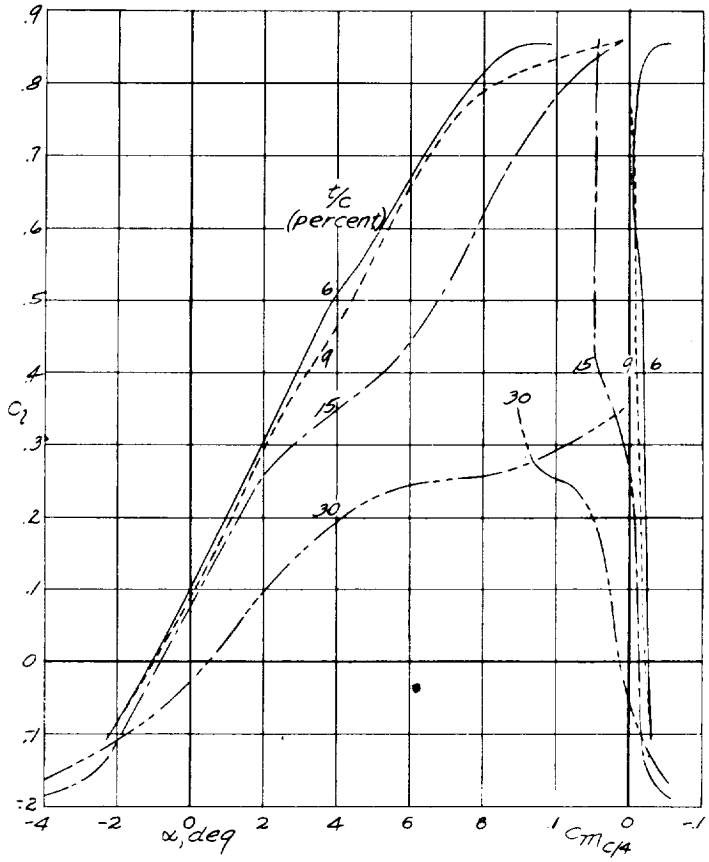

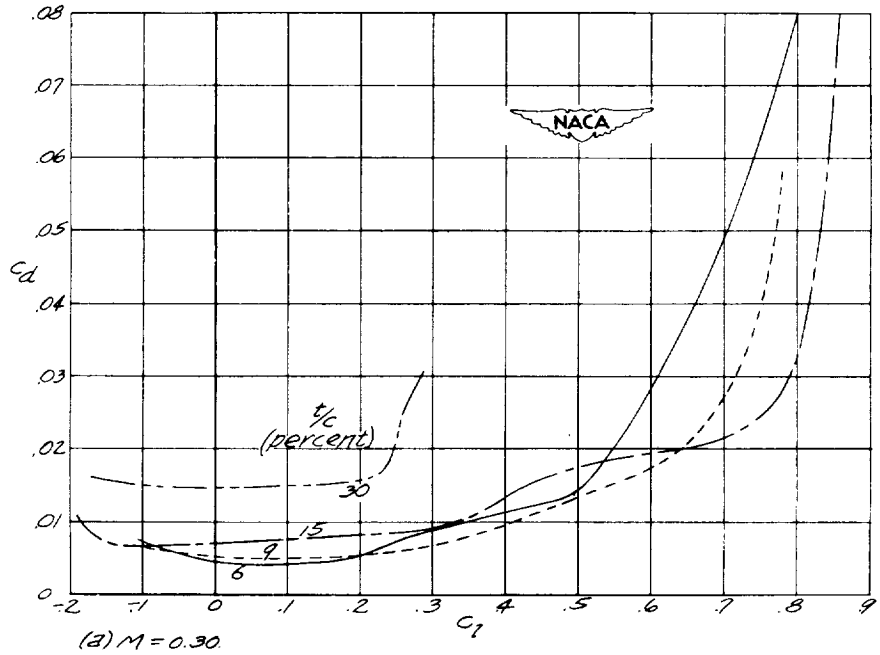

(a) $M = 0.30$.

Figure 7. – Aerodynamic characteristics of NACA 16-1xx airfoils

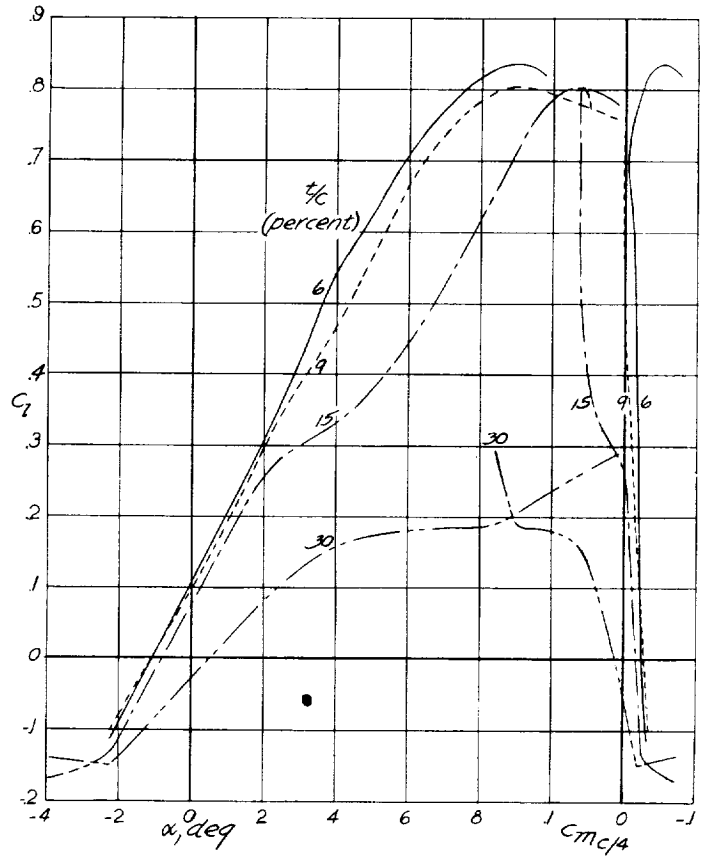

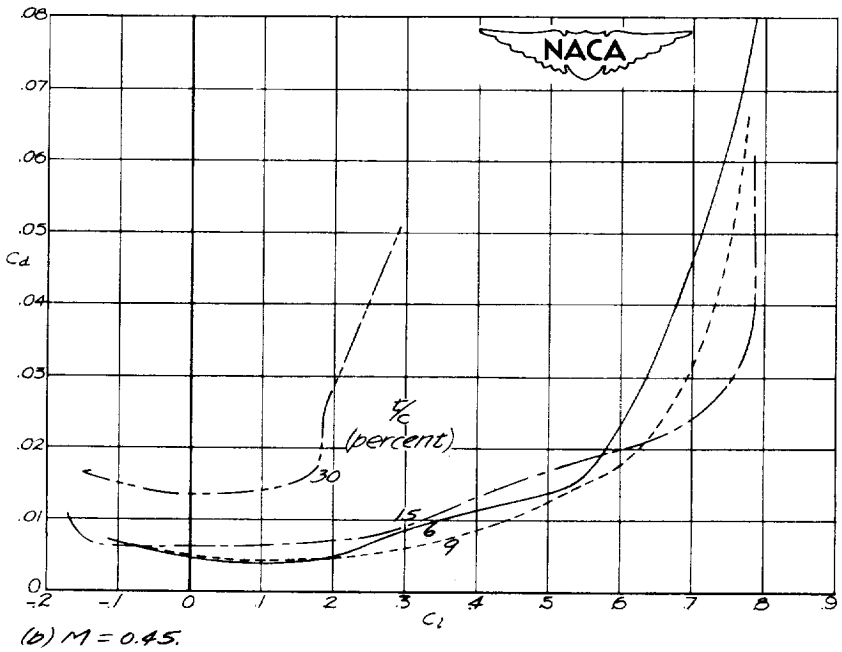

(b) $M = 0.45$.

Figure 7.- Continued.

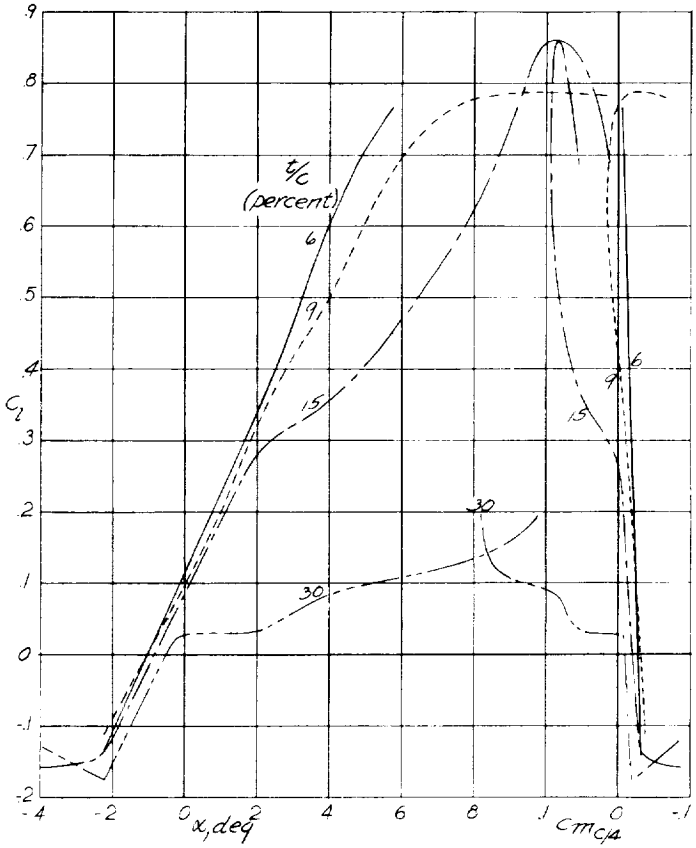

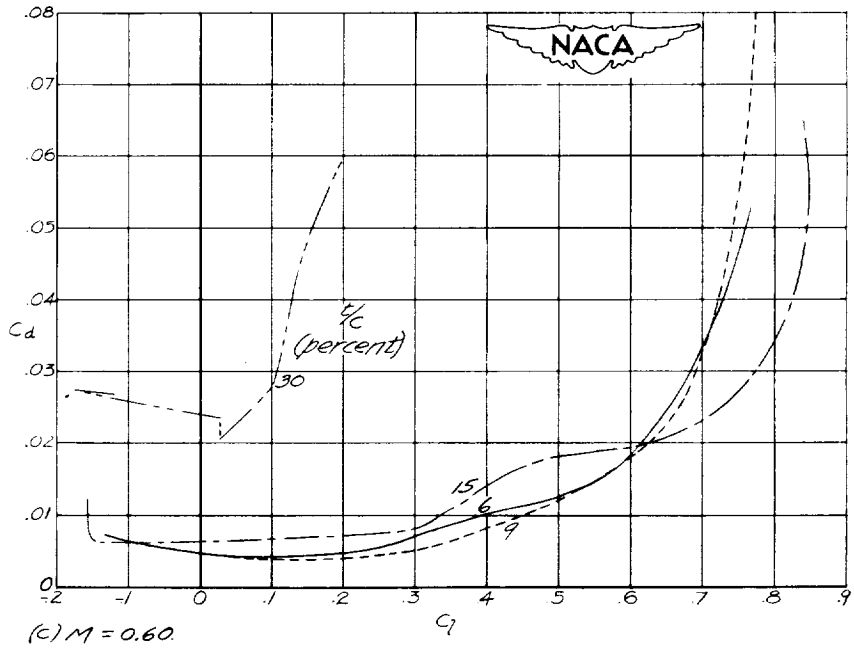

(c) $M = 0.60$.

Figure 7.- Continued.

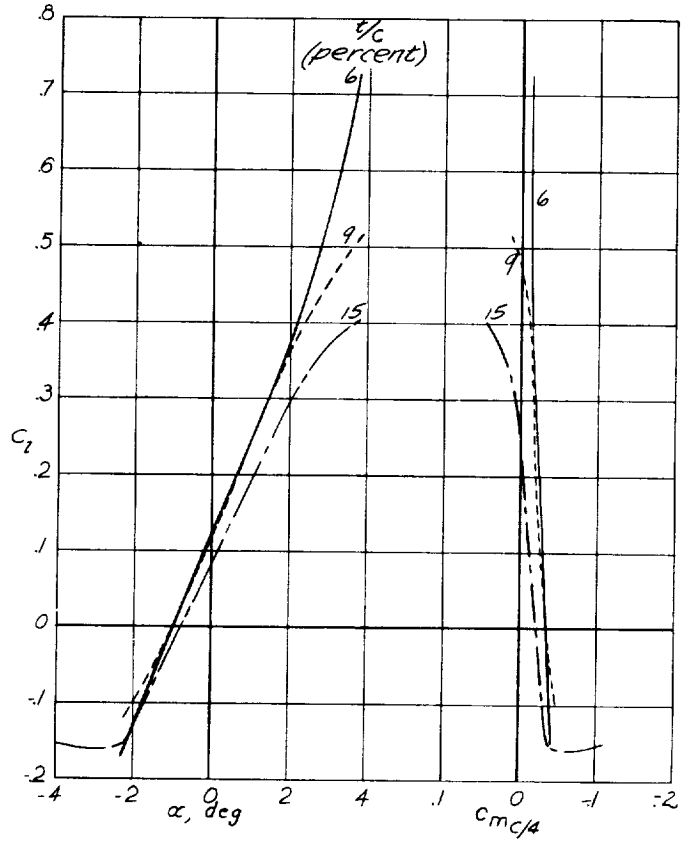

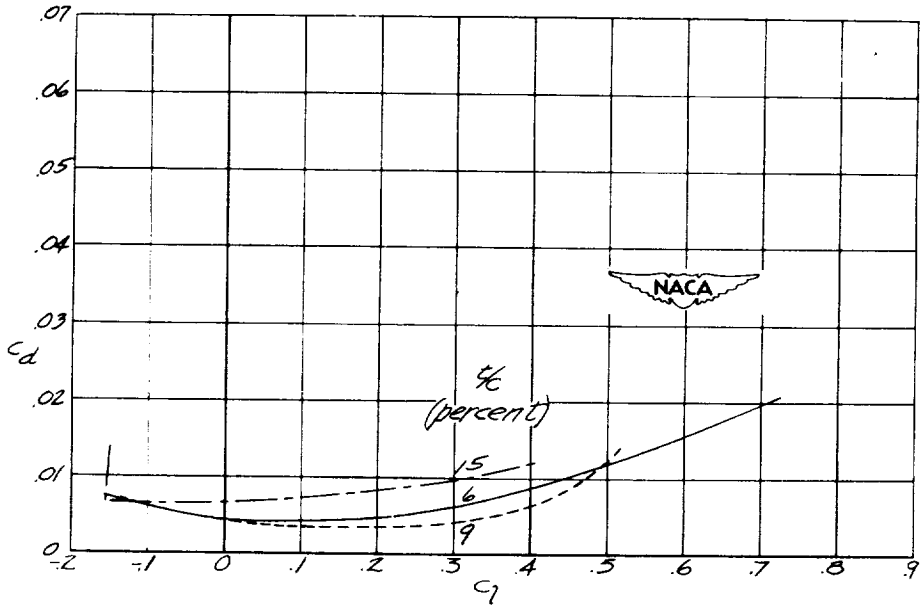

(d) $M = 0.70$.

Figure 7. – Continued.

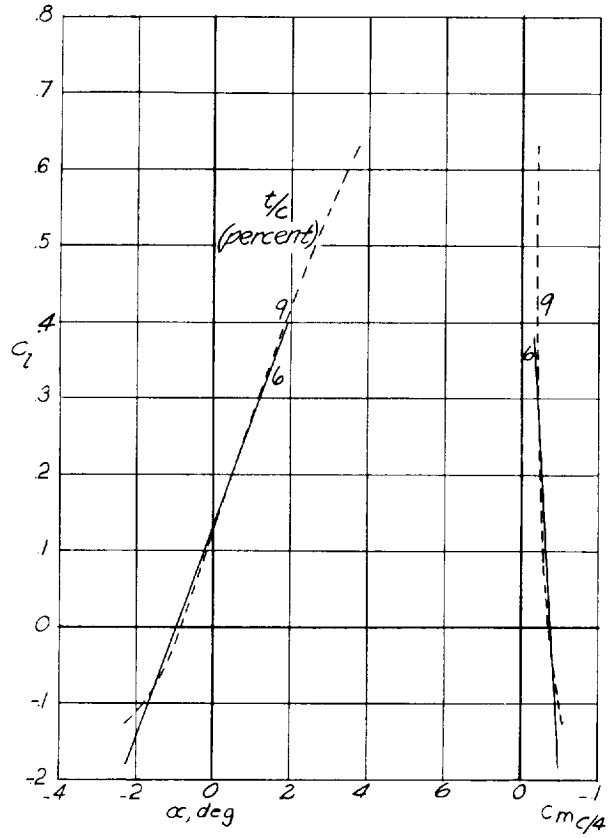

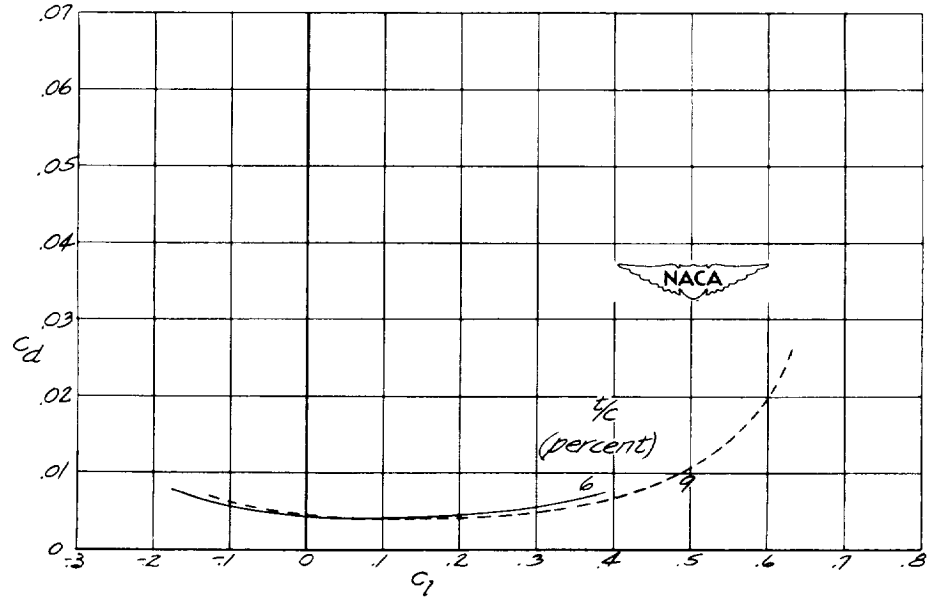

(e) $M = 0.75$.

Figure 7.- Continued.

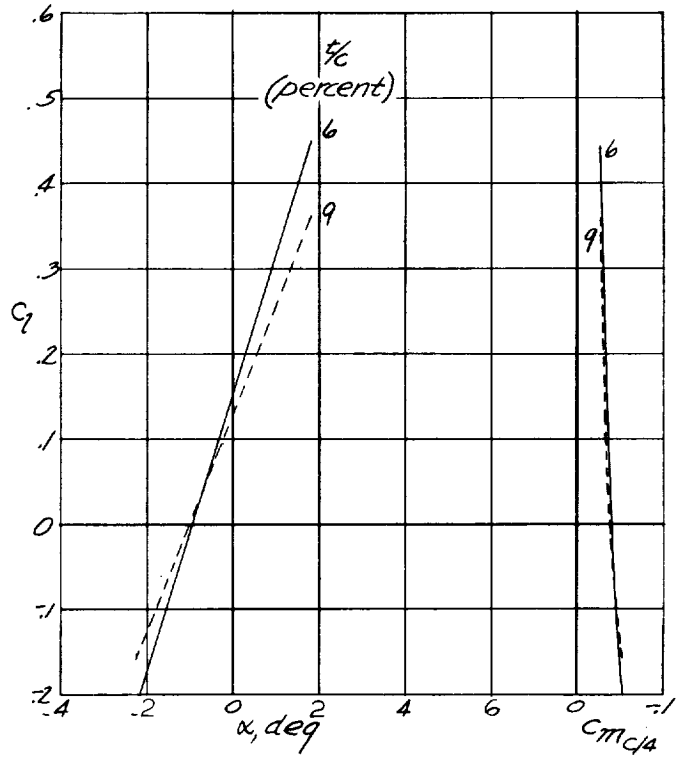

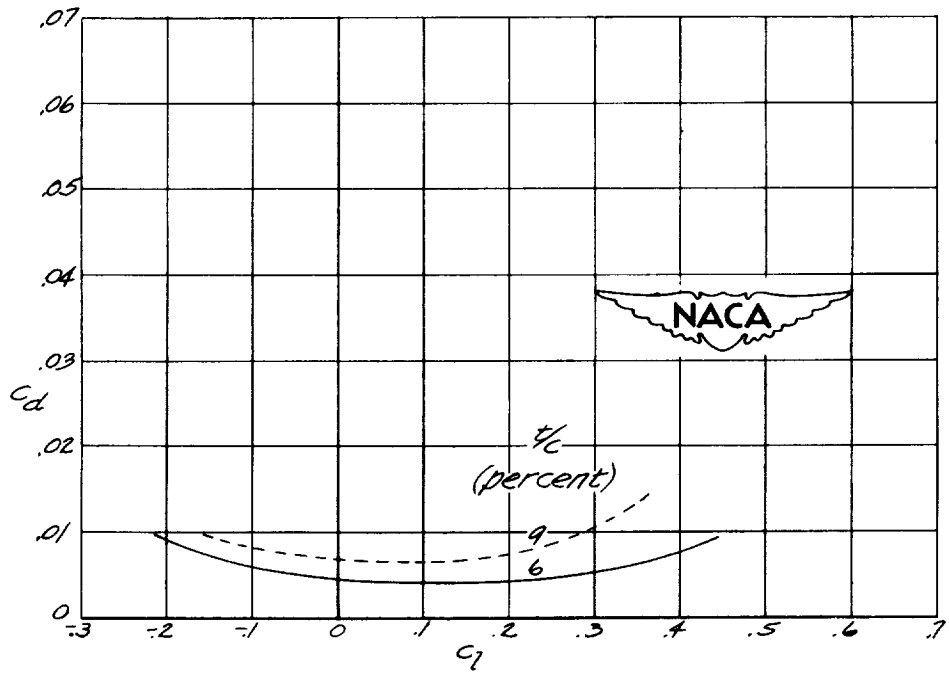

(f) $M = 0.80$.

Figure 7.- Concluded.

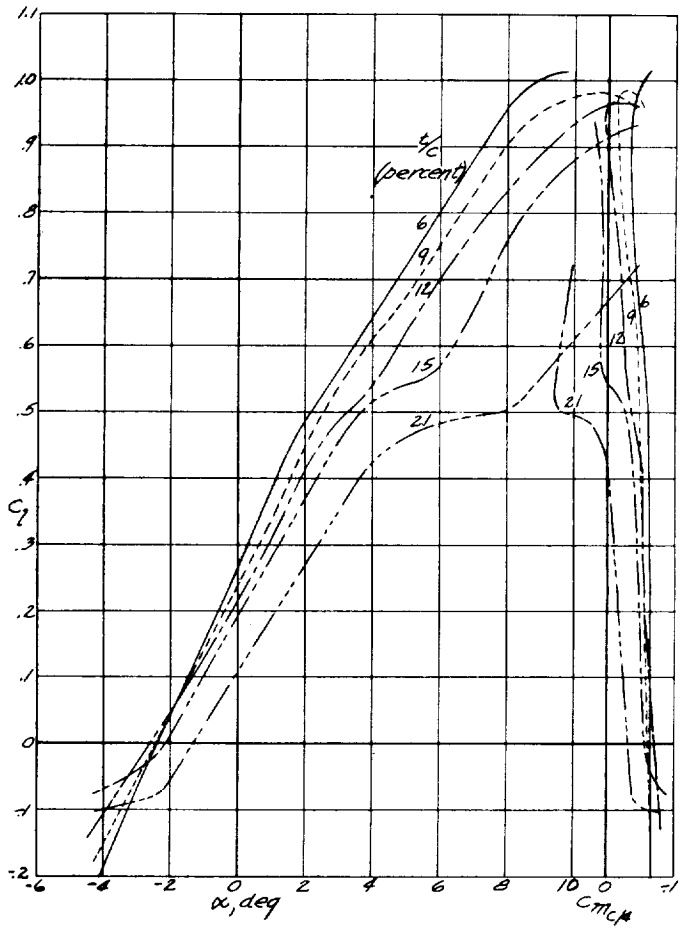

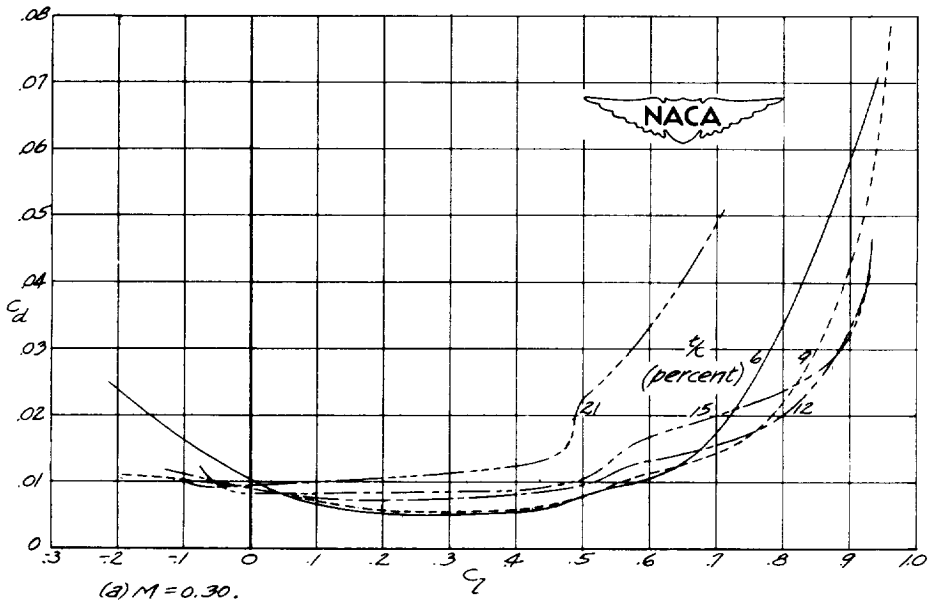

(a) M = 0.30.

Figure 8.- Aerodynamic characteristics of NACA 16-3XX airfoils.

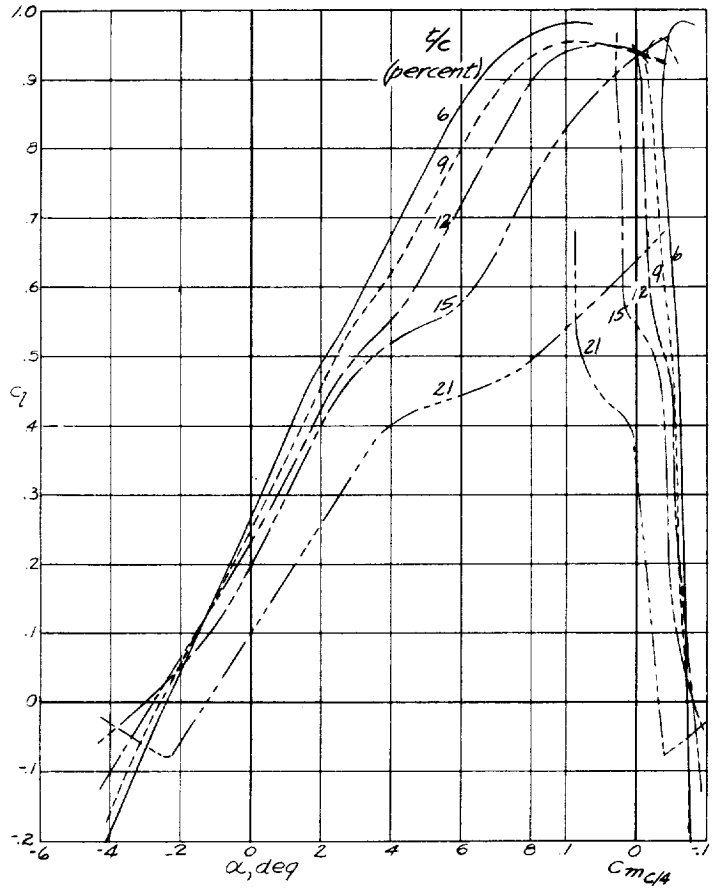

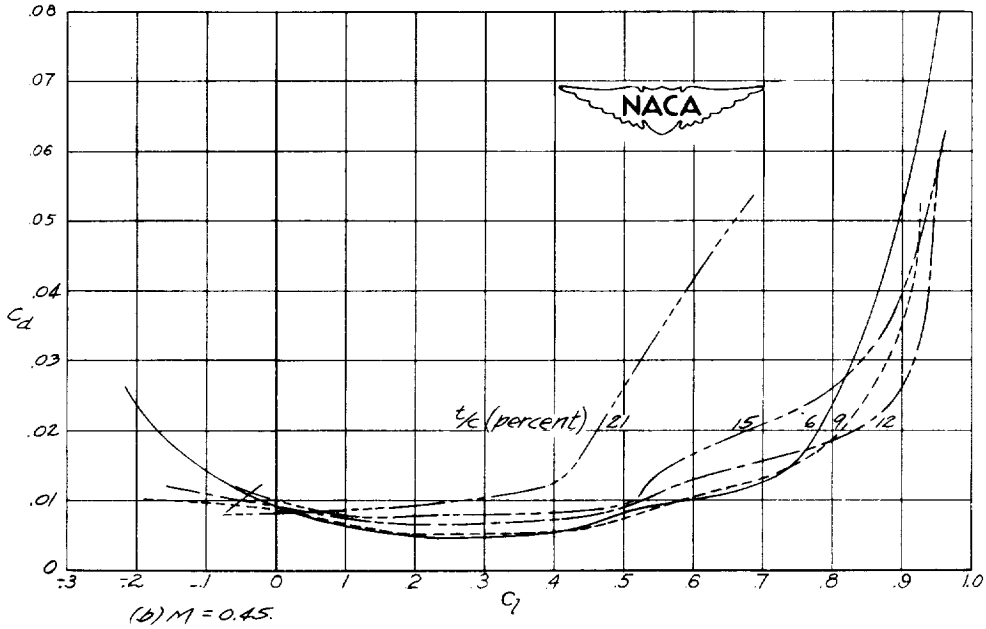

(b) $M = 0.45$.

Figure 8.– Continued.

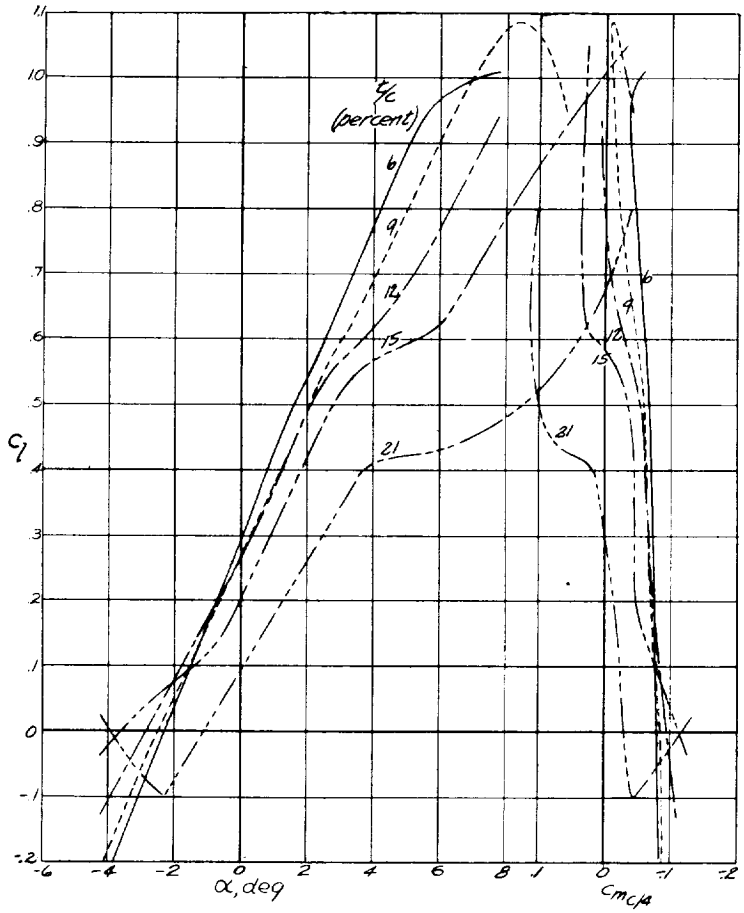

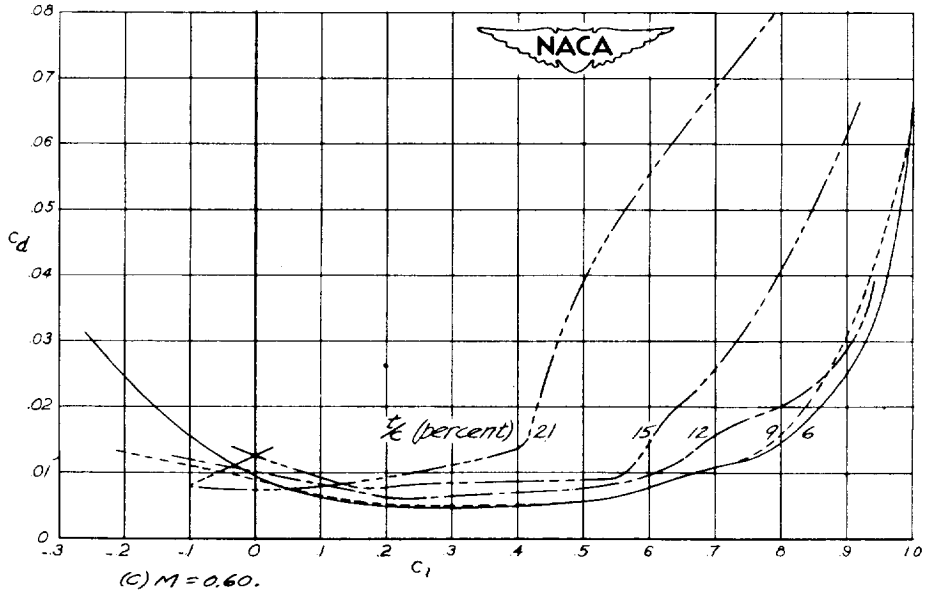

(c) M = 0.60.

Figure 8.- Continued.

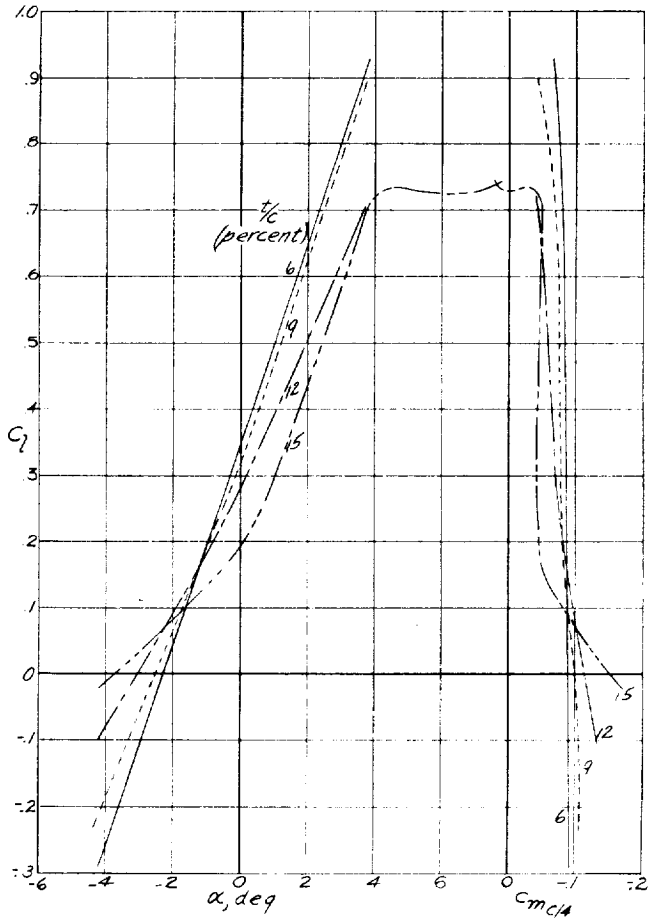

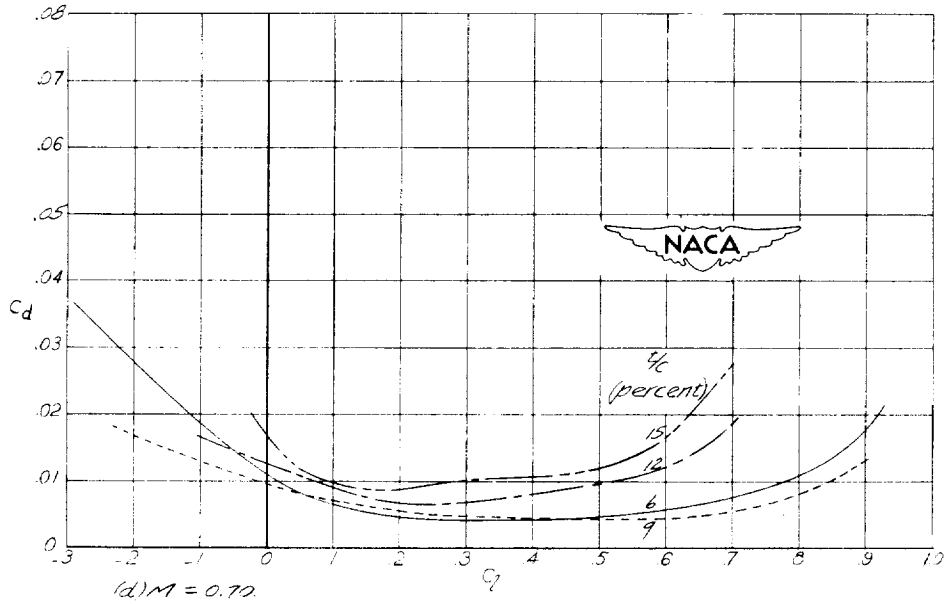

(d) $M = 0.70$.

Figure 8.— Continued.

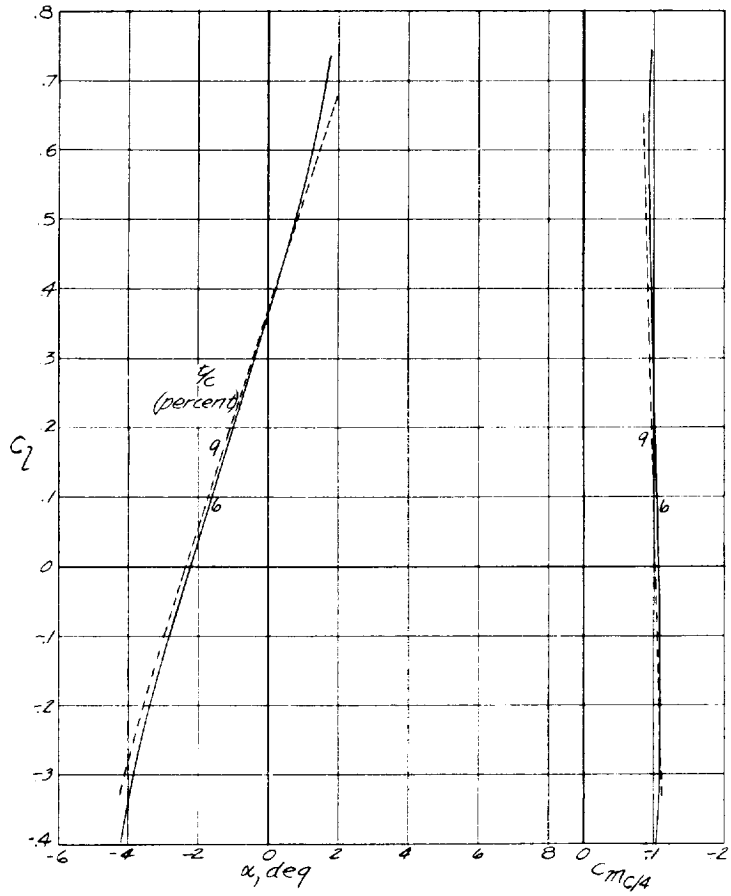

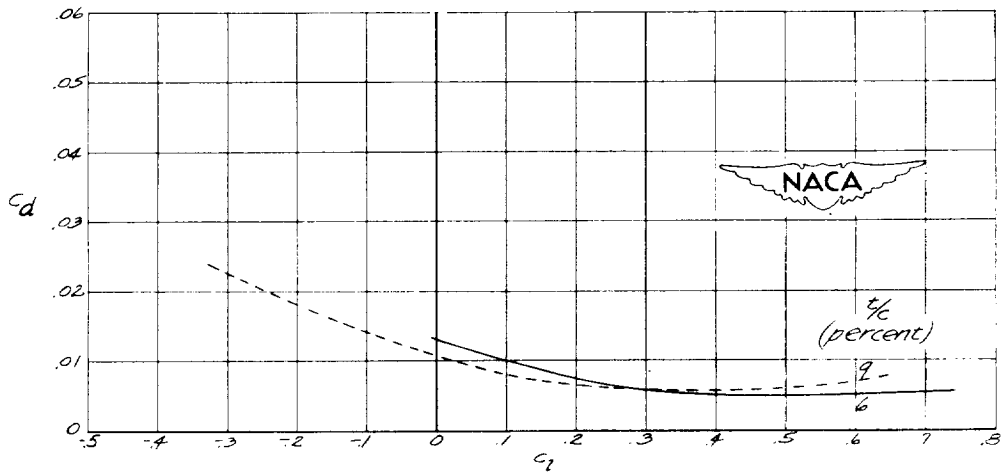

(e) $M = 0.75$.

Figure 8.- Concluded.

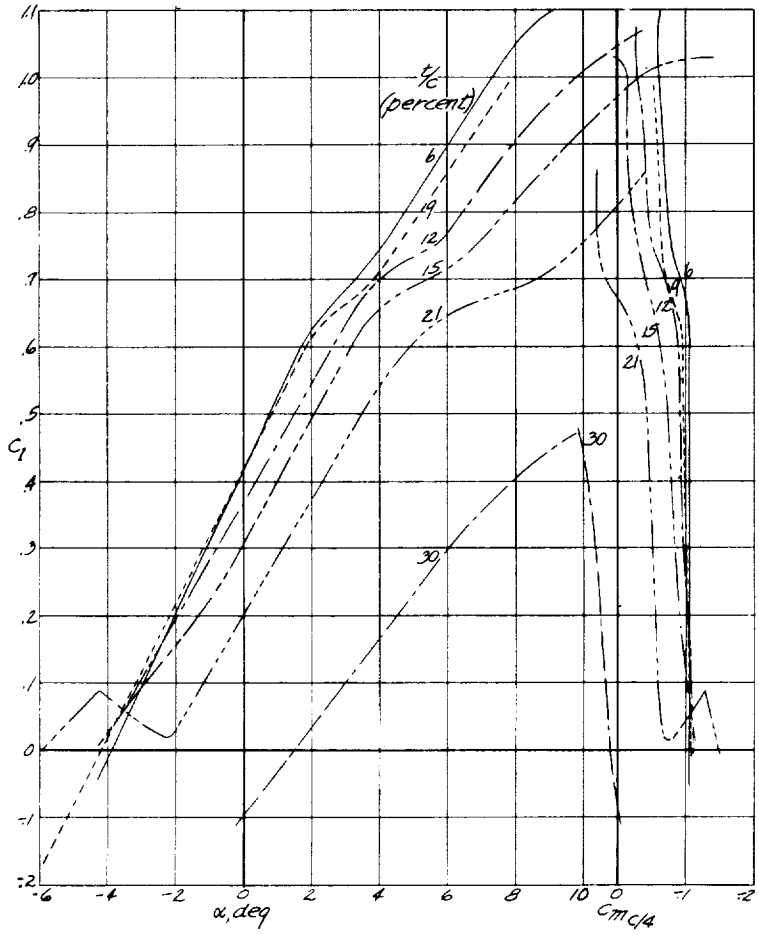

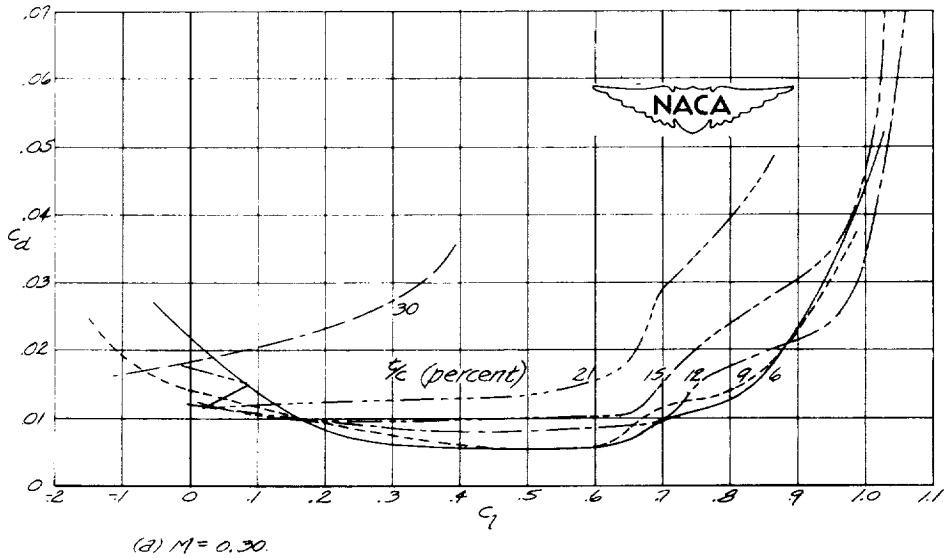

(a) M = 0.30.

Figure 9.- Aerodynamic characteristics of NACA 16-5XX airfoils.

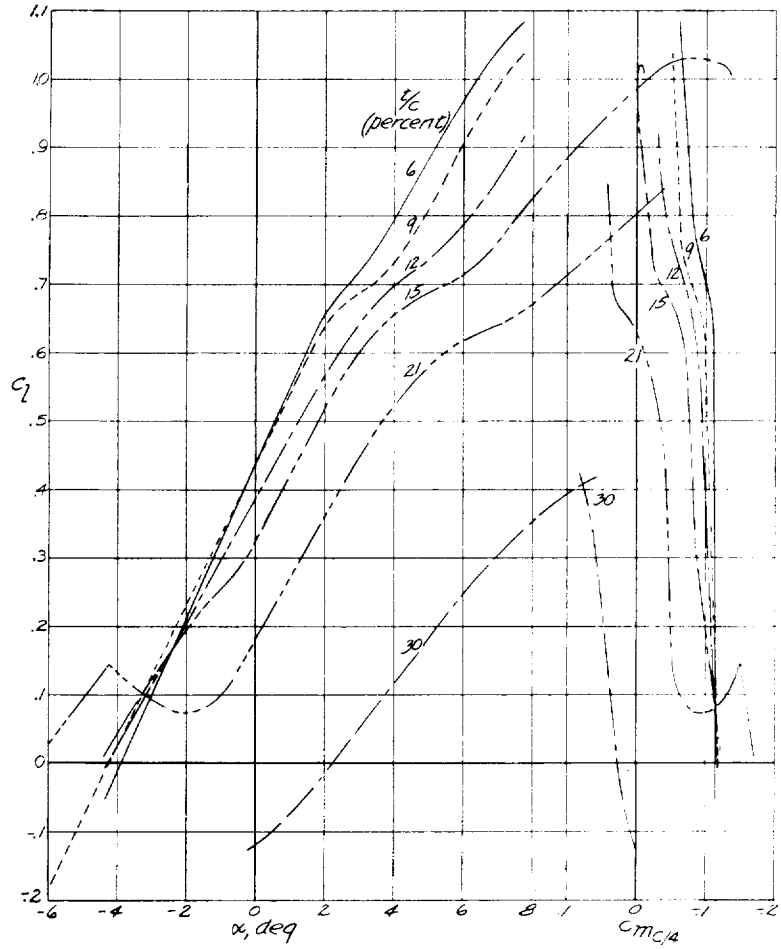

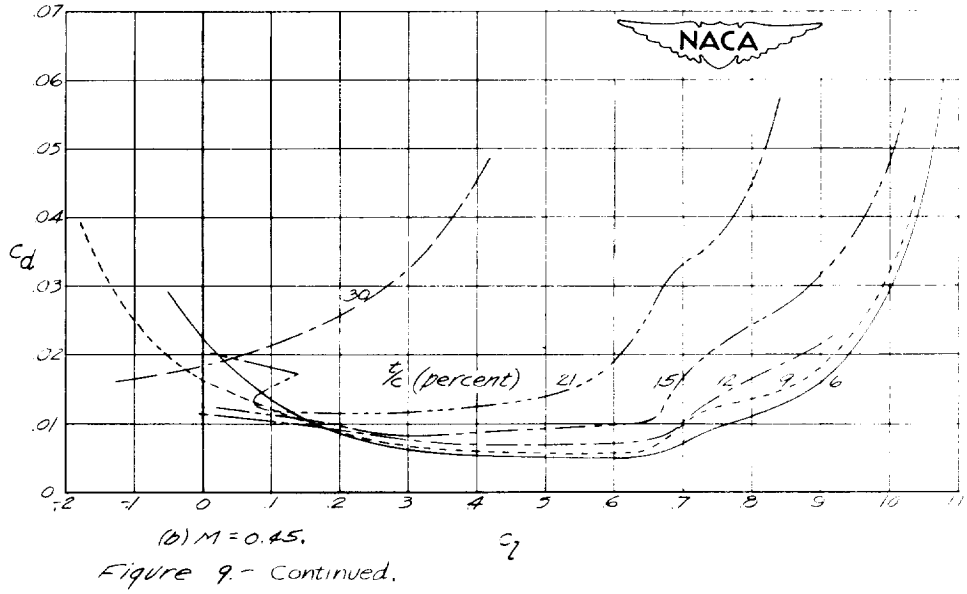

(b) $M = 0.45$.

Figure 9.- Continued.

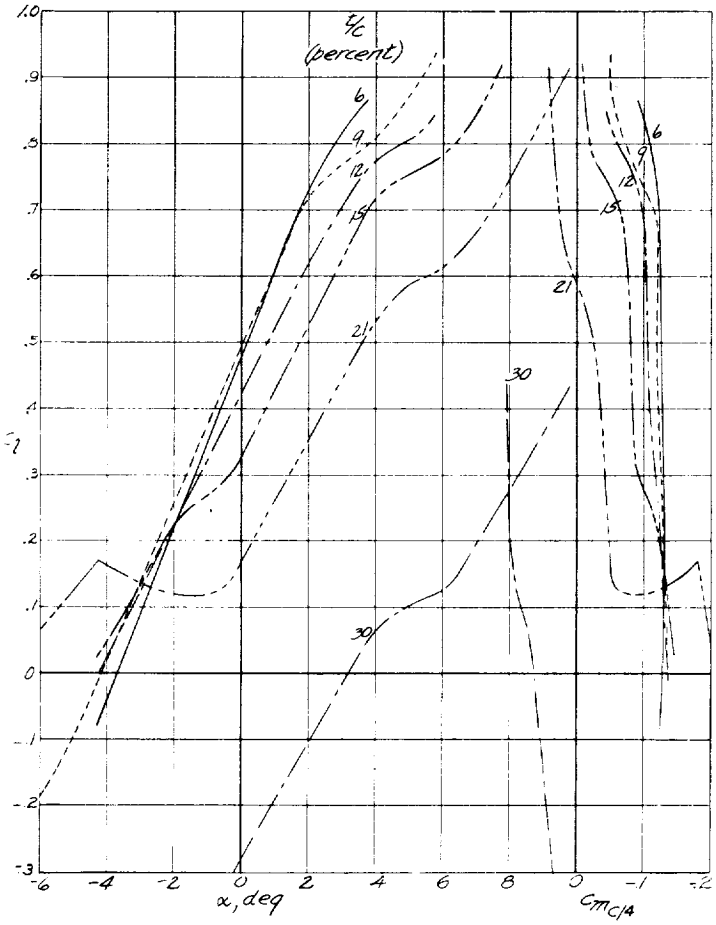

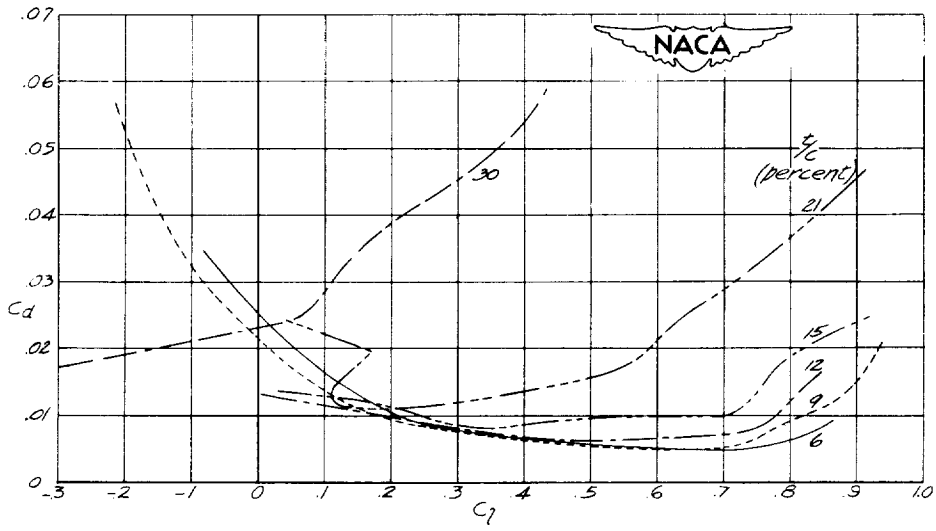

(c) M = 0.60

Figure 9.- Continued.

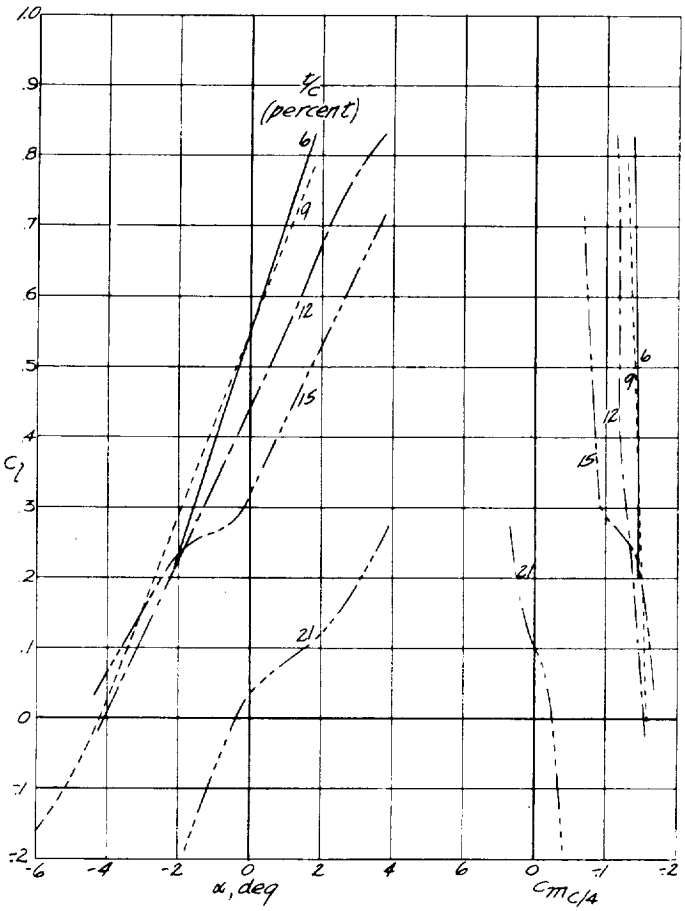

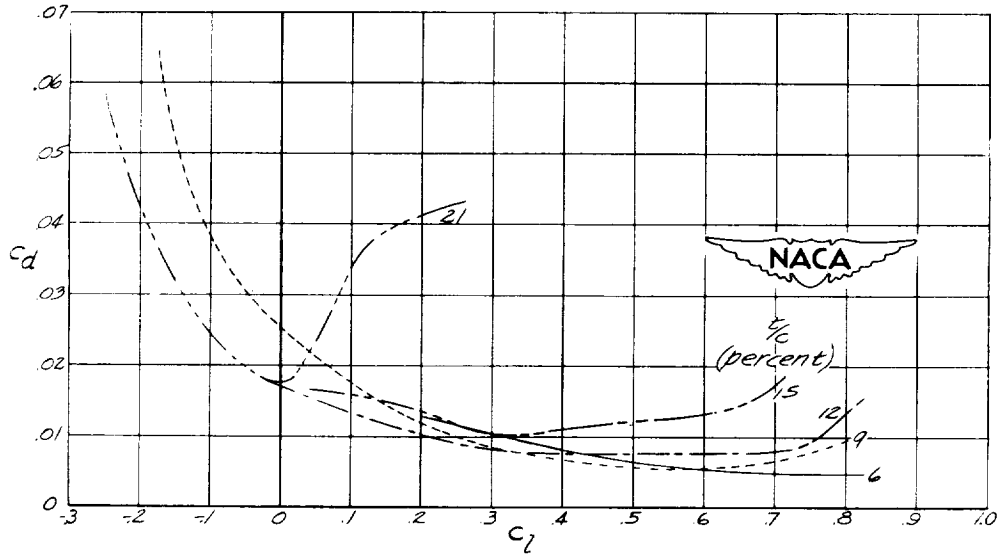

(d) M = 0.70.

Figure 9. – Continued.

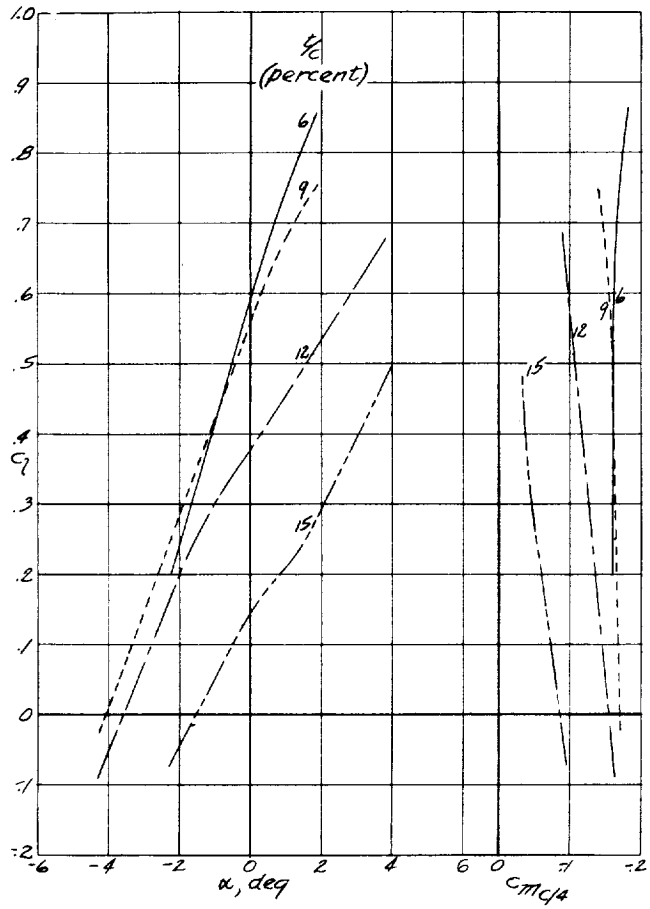

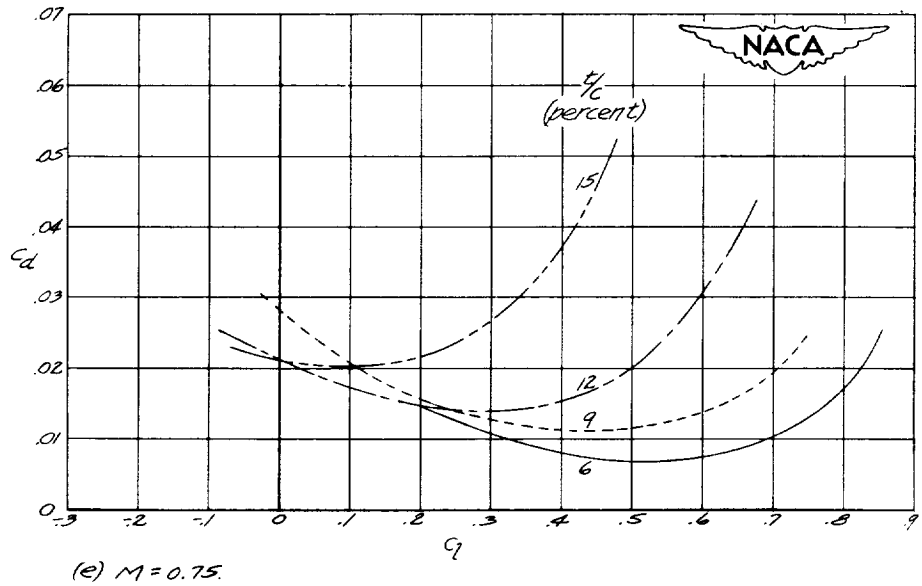

(e) $M = 0.75$.

Figure 9. – Concluded.

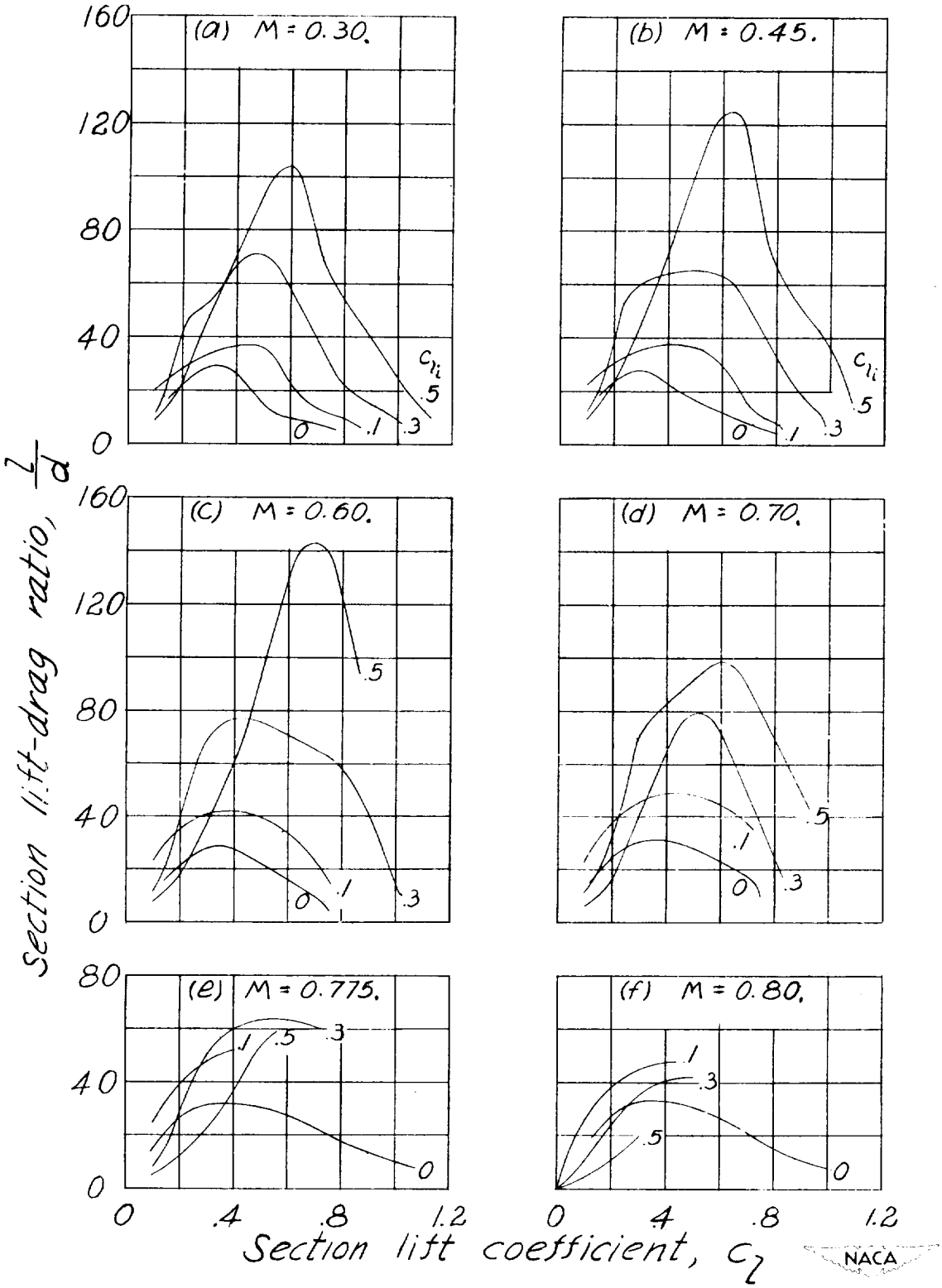

Figure 10.- Variation of section lift-drag ratio with section lift coefficient for NACA 16-X06 airfoils.

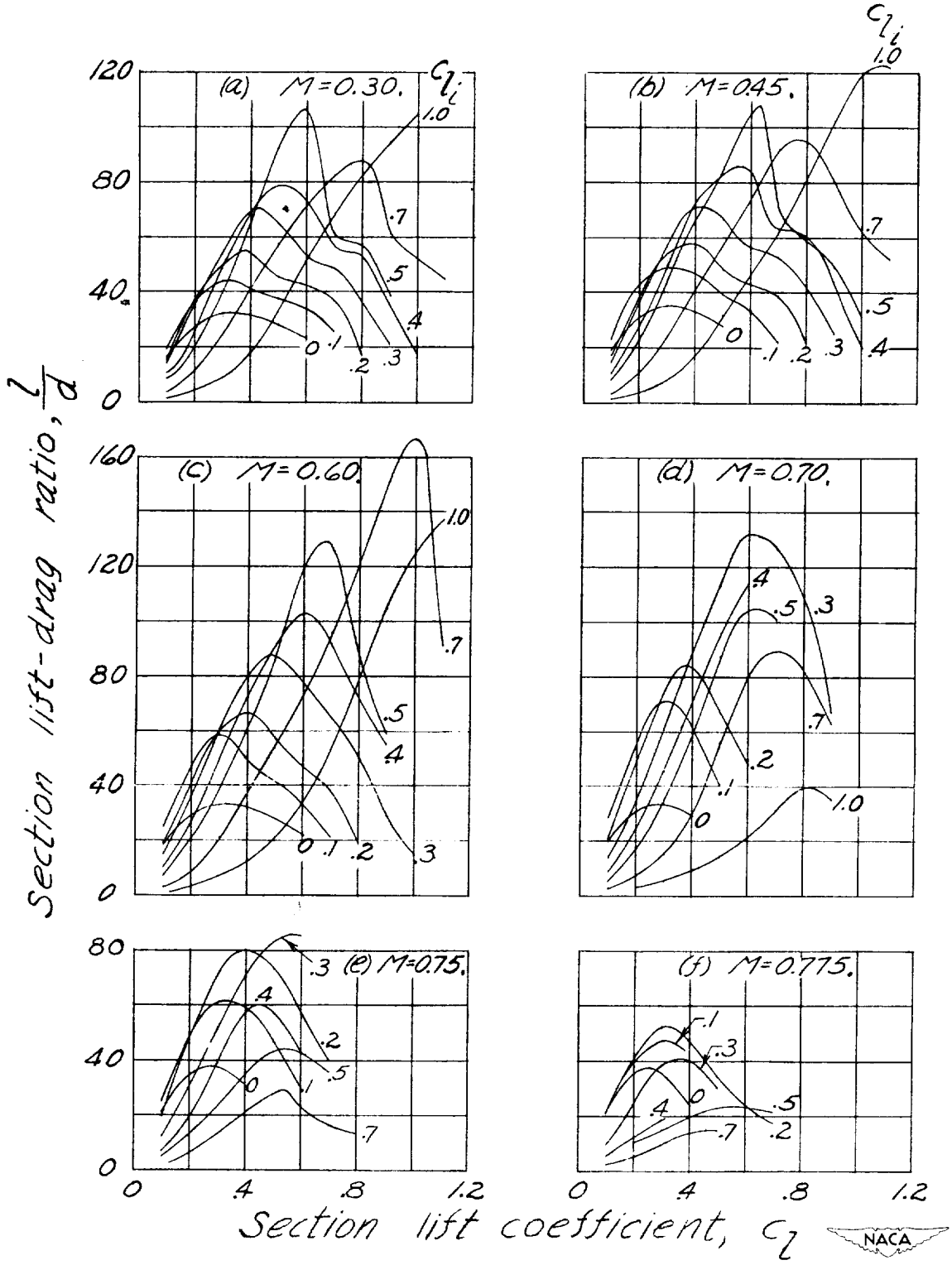

Figure 11.—Variation of section lift-drag ratio with section lift coefficient for NACA 16-X09 airfoils.

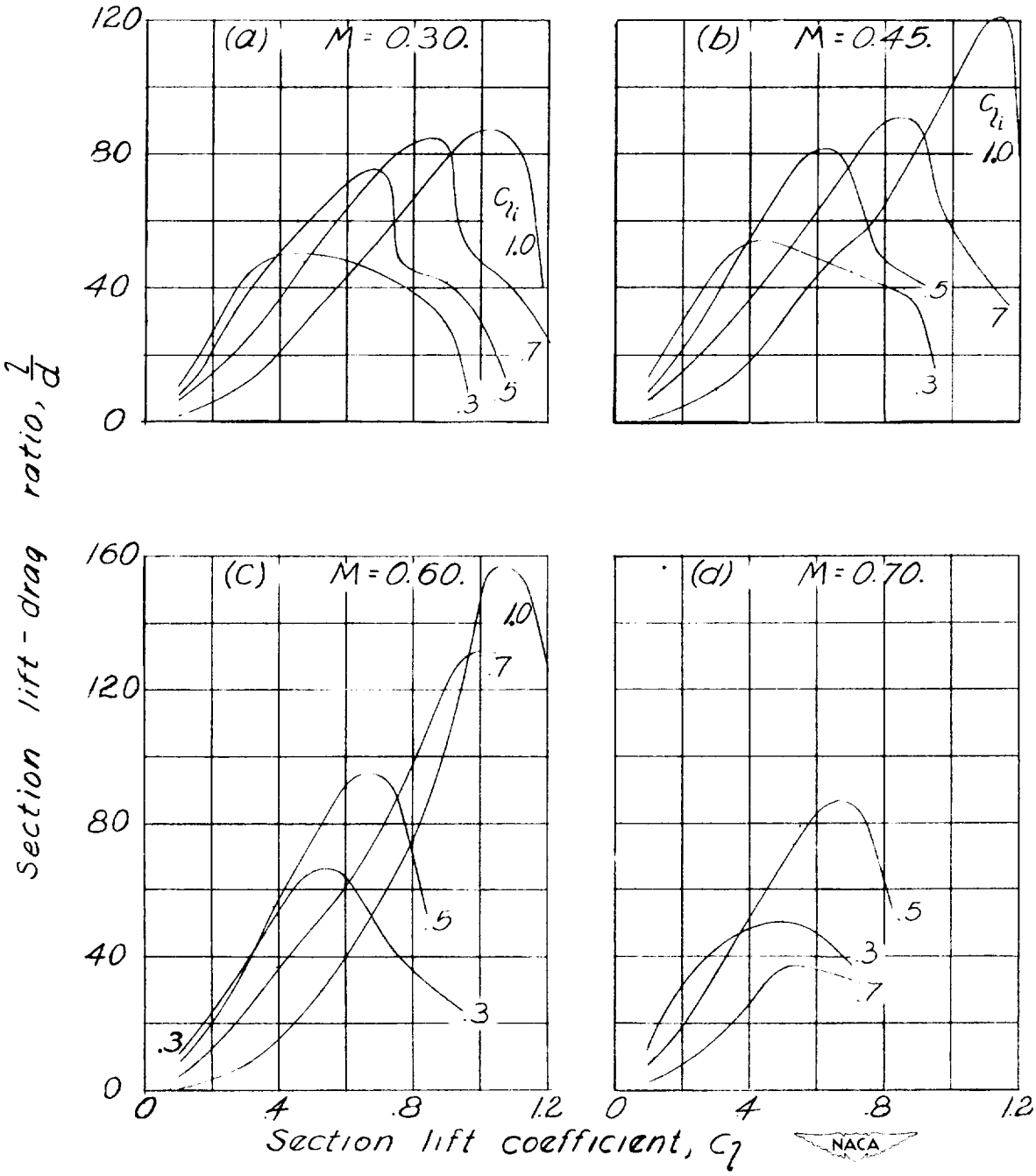

Figure 12.— Variation of section lift-drag ratio with section lift coefficient for NACA 16 - X12 airfoils

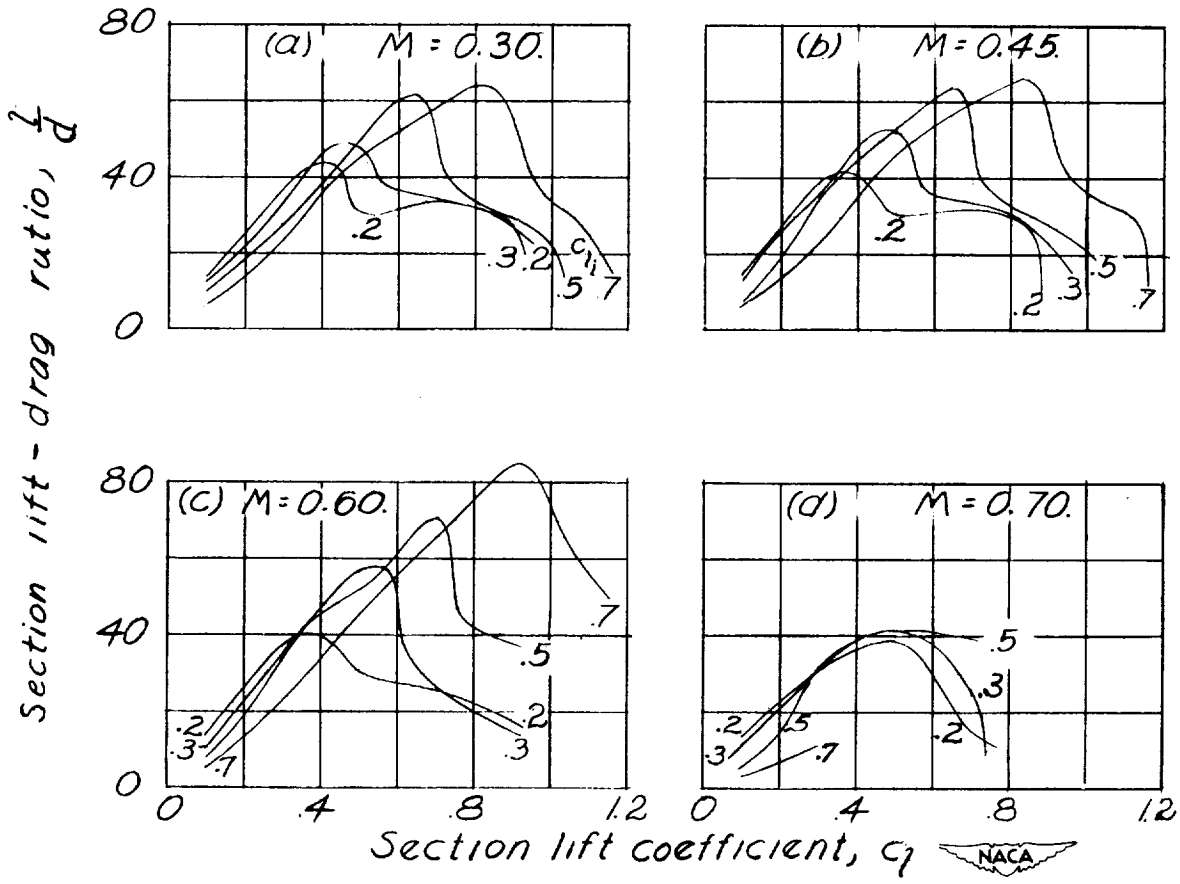

Figure 13.— Variation of section lift-drag ratio with section lift coefficient for NACA 16-X15 airfoils.

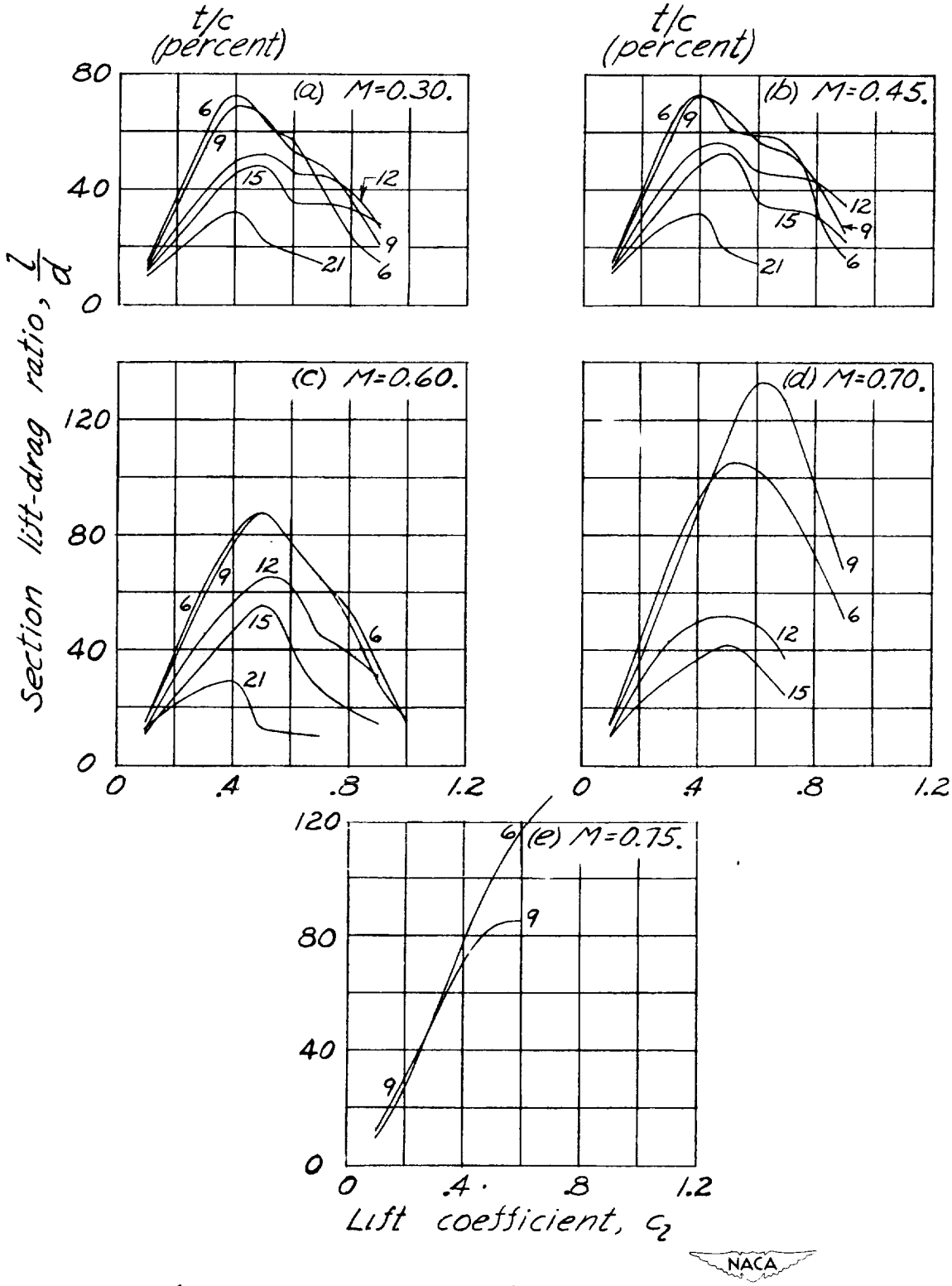

Figure 14.- Variation of section lift-drag ratio with section lift coefficient for NACA 16-3XX airfoils.

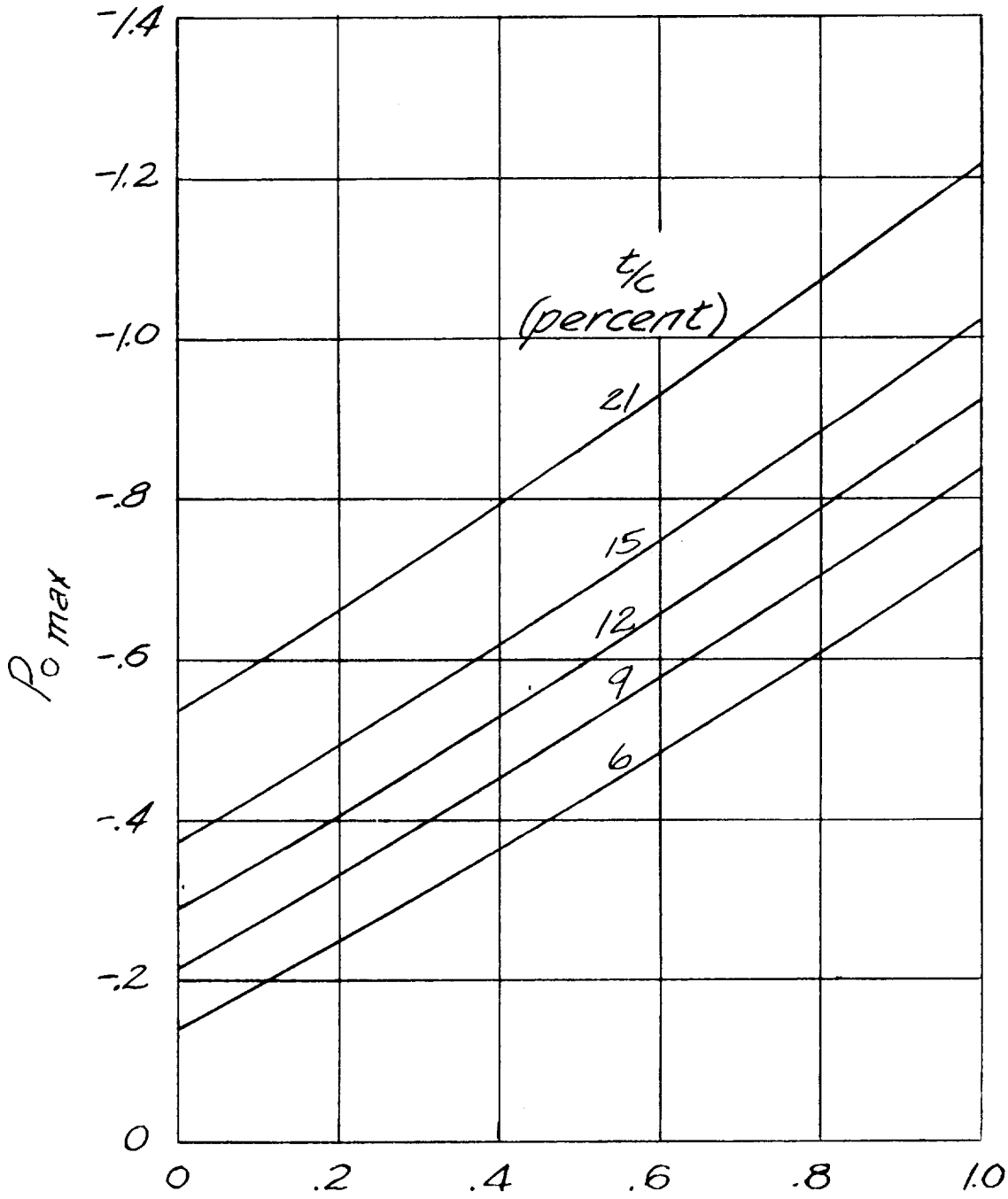

Figure 15.- Theoretical variation of $P_{o\,max}$ with c_{l_i}. $\alpha = 0°$.

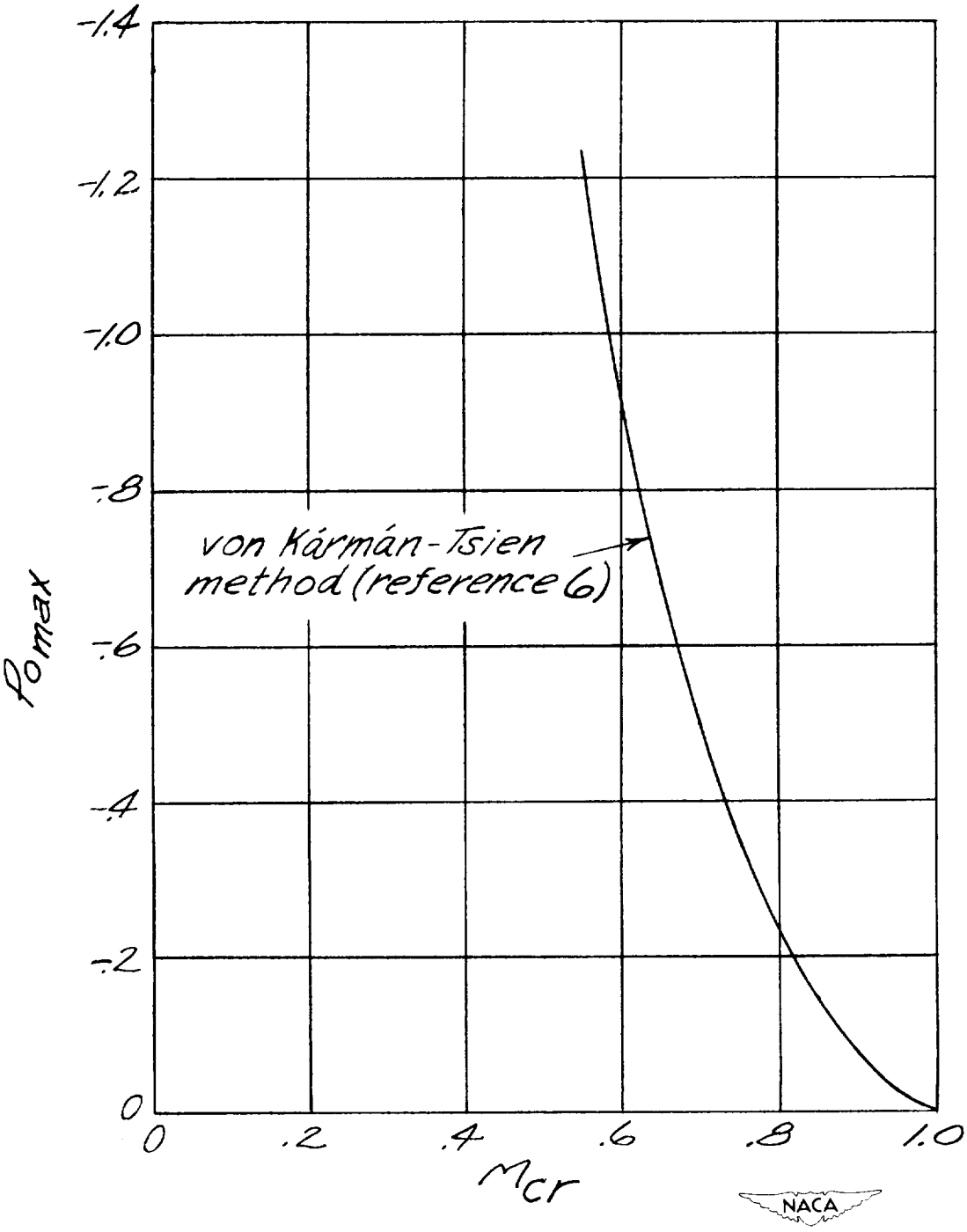

Figure 16.- Variation with critical Mach number of the maximum incompressible pressure coefficient.

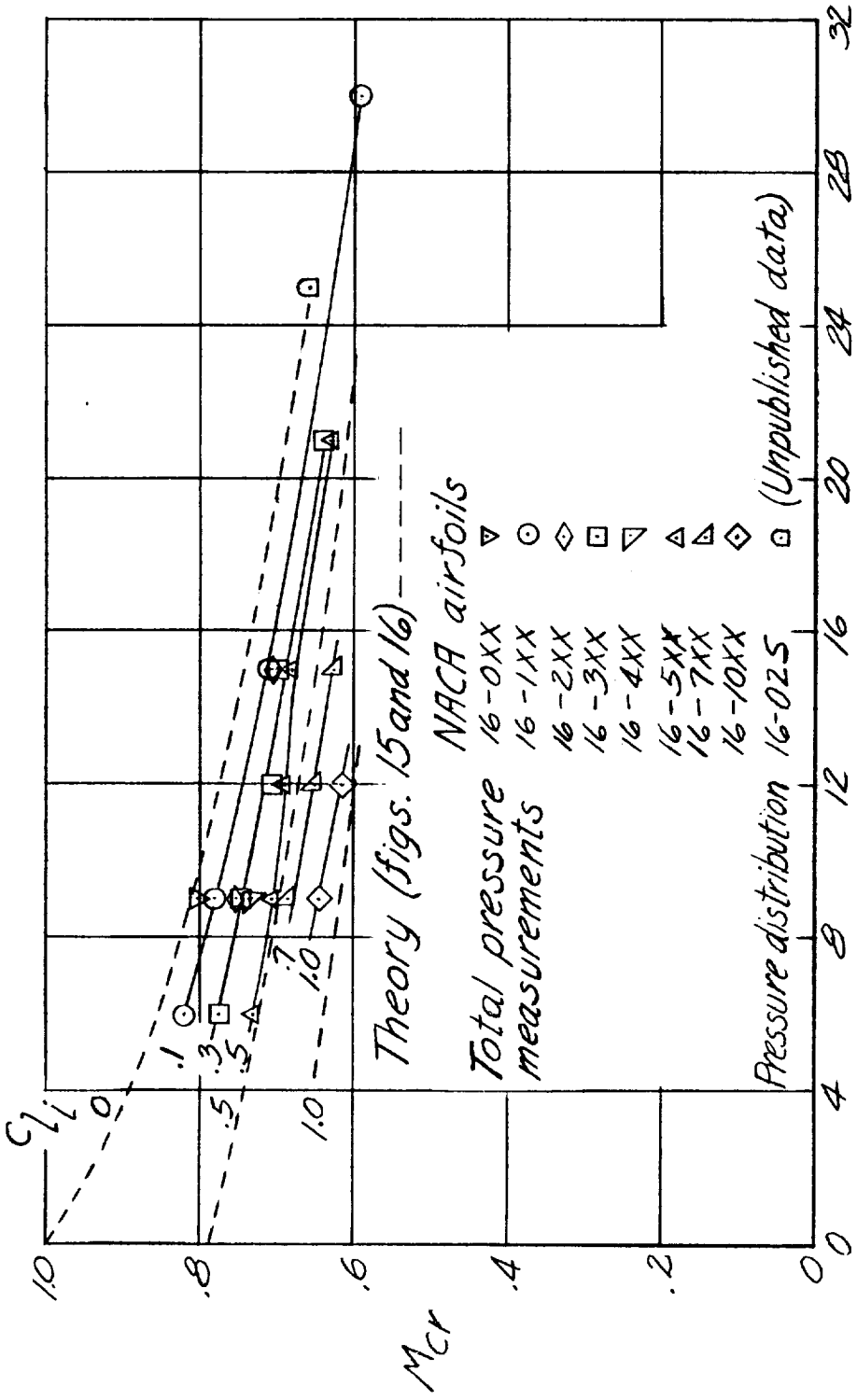

(a) Comparison between the critical Mach numbers obtained by theory and experiment. $\alpha = 0°$.

Figure 17.- Critical Mach number curves.

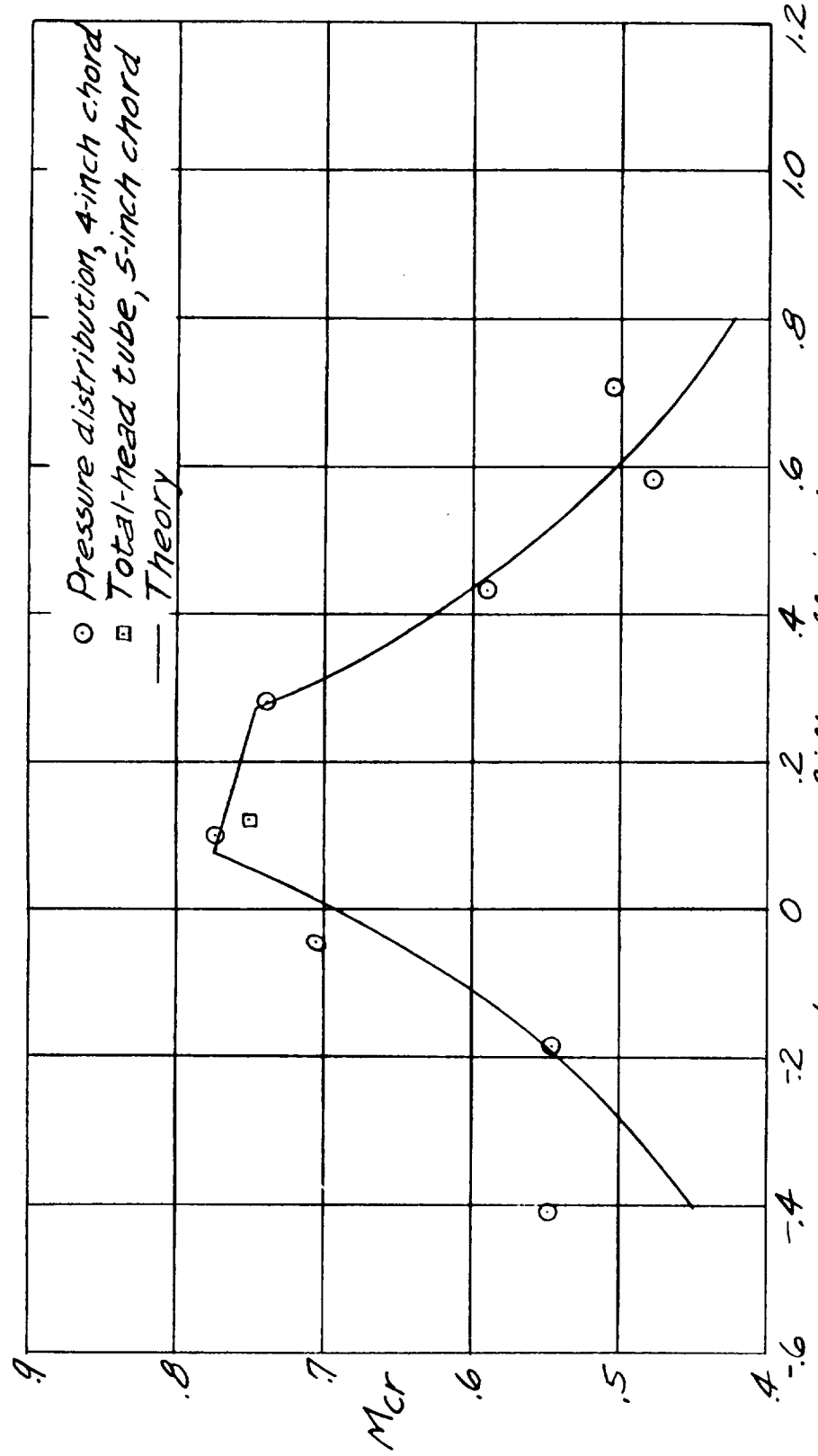

(b) Comparison between the critical Mach numbers obtained by theory and by experiment for the NACA 16-209 airfoil.

Figure 17.- Continued.

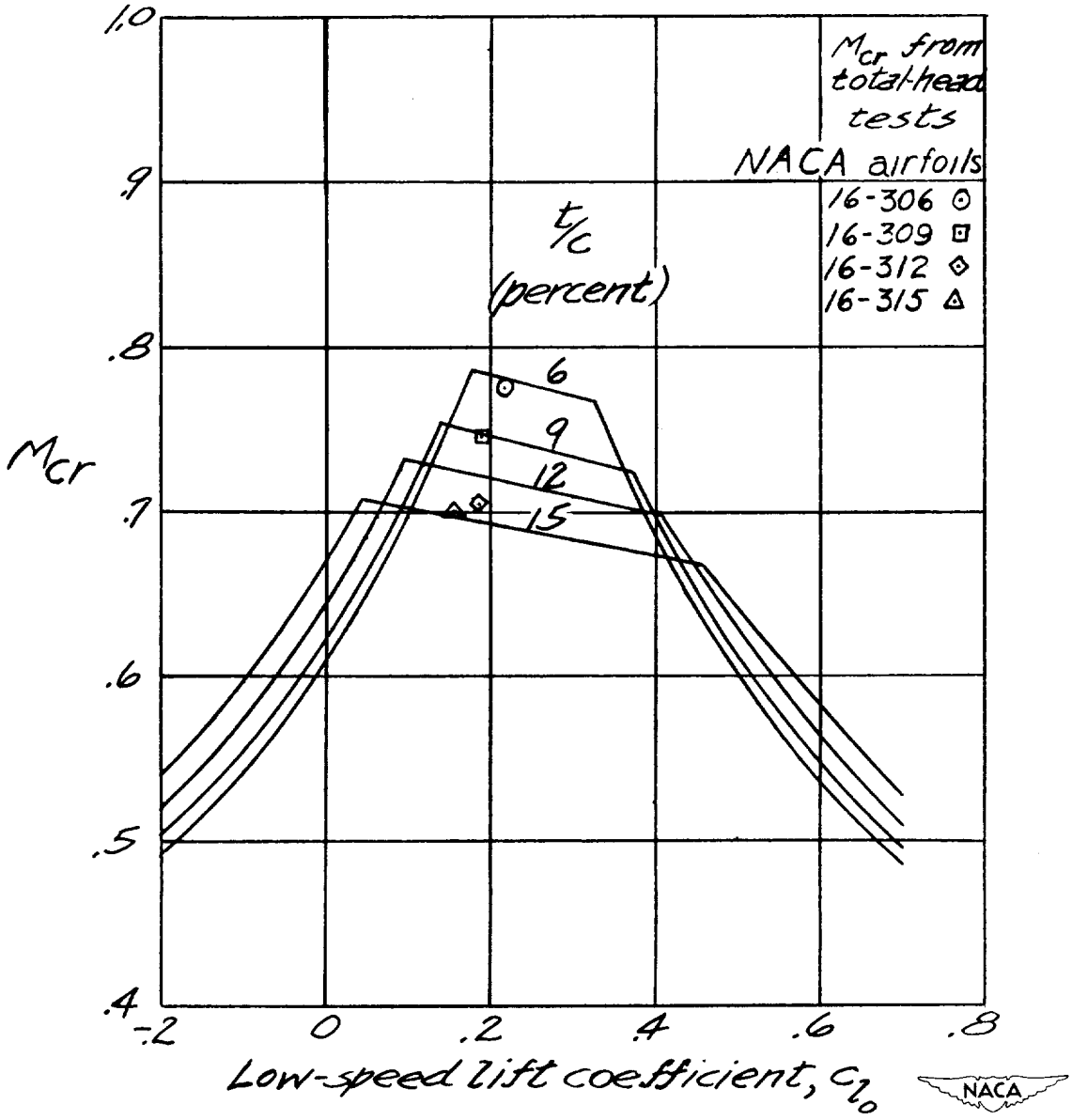

(c) Theoretical variation of critical Mach number with low-speed lift coefficient for NACA 16-3xx airfoils of various thickness – chord ratio.

Figure 17.– Continued.

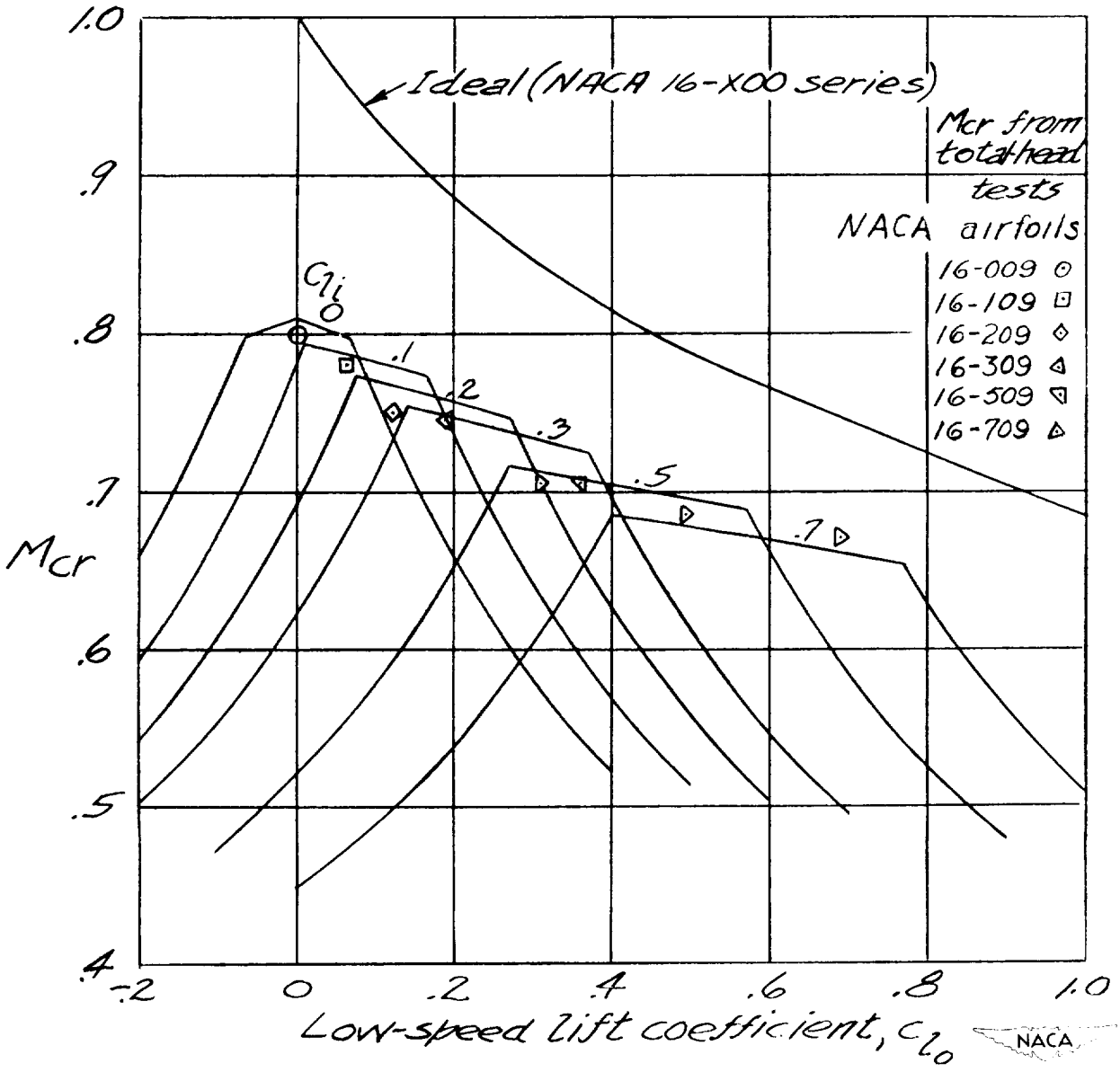

(d) Theoretical variation of critical Mach number with low-speed lift coefficient for NACA 16-X09 airfoils of various camber's.

Figure 17.- Concluded.

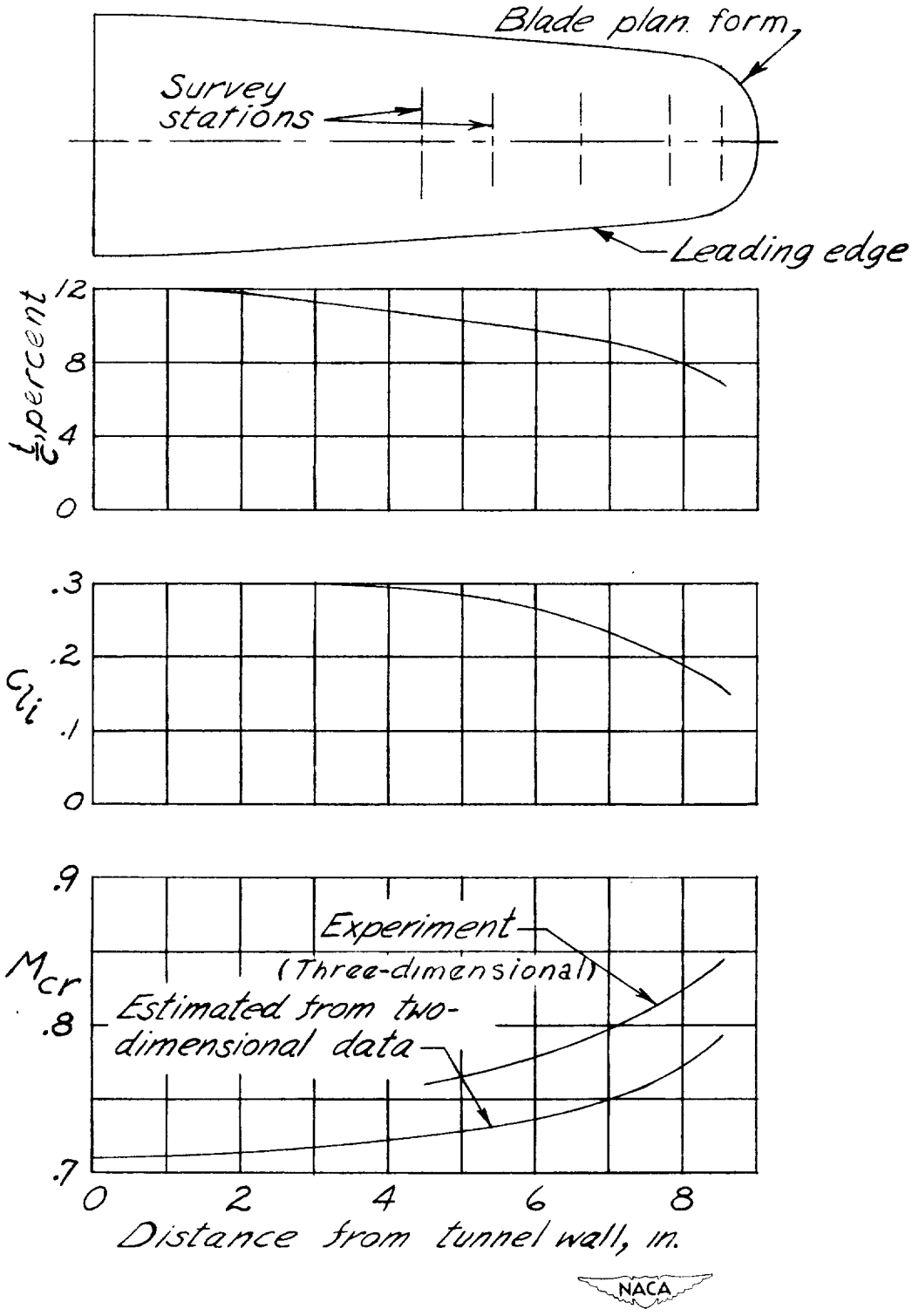

Figure 18.- Measurements near the tip of an untwisted propeller blade. $\alpha = 0°$.

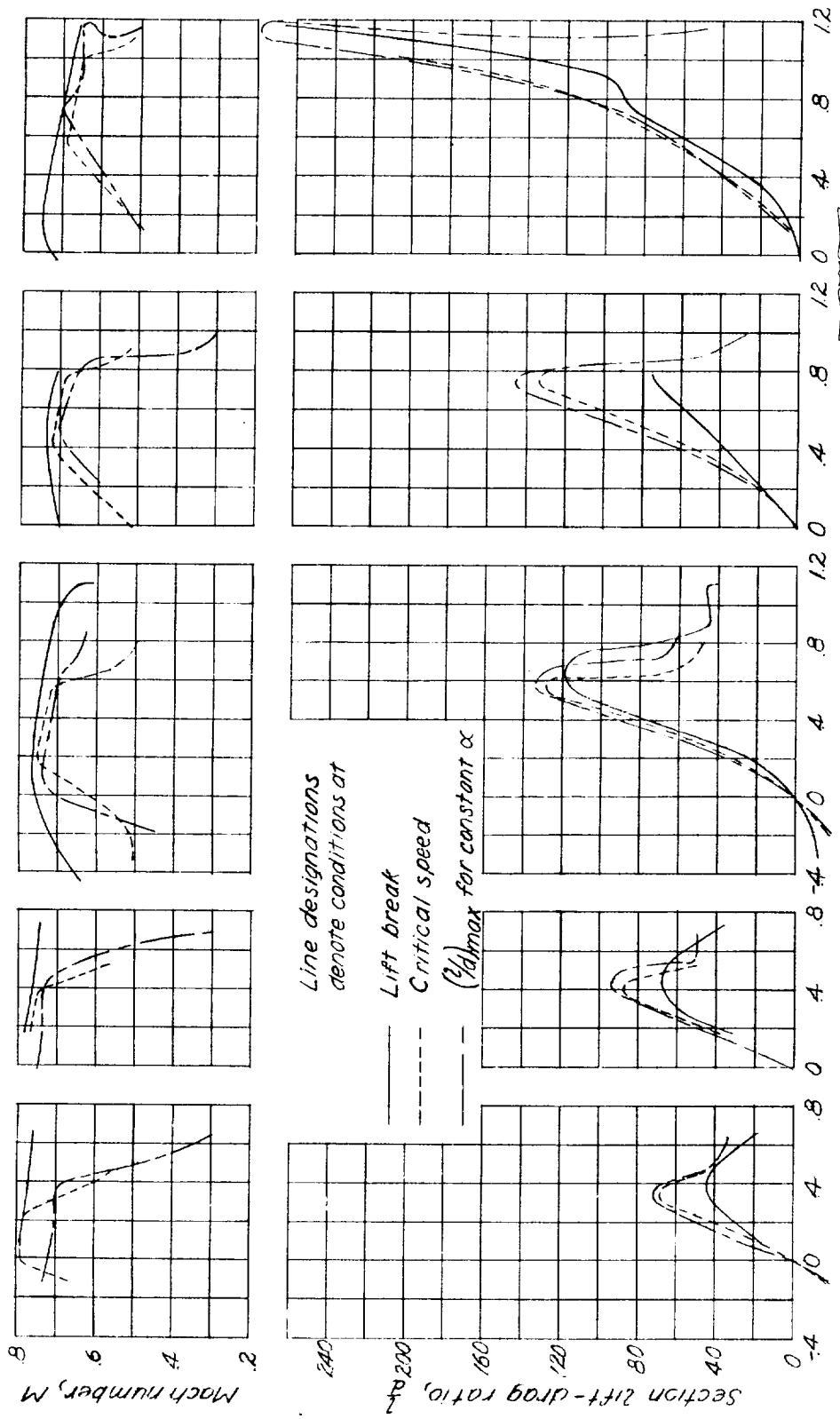

Figure 19.- Conditions for lift break, critical speed, and maximum lift-drag ratios for the NACA 16-X09 airfoils.

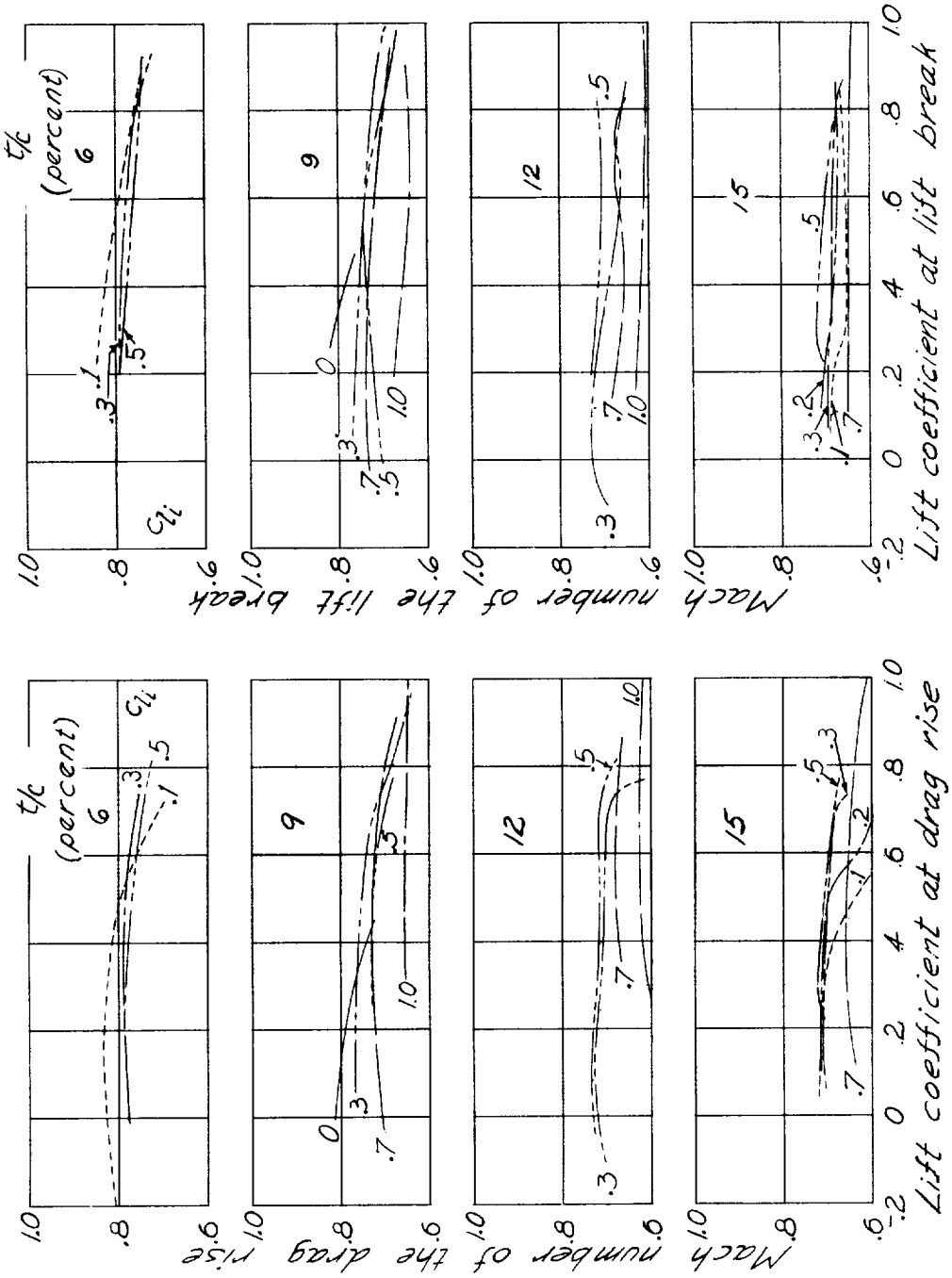

Figure 20.- Lift-break and drag-rise characteristics of various NACA 16-series airfoils.